Nishina Memorial Lecture

FROM X-RAY TO ELECTRON SPECTROSCOPY

Kai Siegbahn

Department of Physics
University of Uppsala

Sweden

April 4, 1988

Prof. Siegbahn giving Nishina Memorial Lecture at the Fuculty of Science, University of Tokyo on April 4, 1988.

FROM X-RAY TO ELECTRON SPECTROSCOPY

Kai Siegbahn

CONTENTS

1. Historic background

Röntgen's surprising discovery in November 1895 can be regarded as the great break-through from classical physics to a new era, which developed into modern atomic physics. Hittorf, Lenard and Crookes made important preliminary work in this field, a fact that Röntgen pointed out in his report on the discovery "Uber eine neue Art von Strahlen". He and many other scientists must have been strongly stimulated by the almost science-fiction like picture, that Crookes called forth at a meeting in Royal Society in London in 1878: "The phenomena in these exhausted tubes reveal to physical science a new world - a world where matter may exist in a fourth state, where the corpuscular theory of light may be true, and where light does not always move in straight lines, but where we can never enter, and with which we must be content to observe and experiment from the outside."

Many of the scientists at that time worked intensely in this field and had certainly also used fluorescence screens and had by those means the conditions for the discovery of the radiation. It is, however, interesting to note how Röntgen at his sensational discovery investigated with scientific thoroughness the properties of the new radiation. Quickly and with superior experimental skilfulness Röntgen attained order in a field, that before had been completely outside human experience. It would last almost 17 years until any essentially new properties of this radiation were being added to those which Röntgen himself had found. One of Röntgen's early observations, which would be significant in the medical use, was that when the cathode radiation in the tube scattered against platinum it appeared a harder radiation than when it scattered against aluminium, glass or other light materials. The most essential novelty for atomic physics in general was that one had found a radiation that could find its way through every kind of material and, in particular, could penetrate the before hidden interior part of the atom. In that way the necessary conditions had been created for a first analysis of the inner structure of the atom.

The next break-through in the scientific field came first with the discovery of the diffraction of this radiation in crystals by von Laue, Friedrich and Knipping in 1912. Somewhat before, however, Barkla and others had with simple means furnished proofs of some properties of the Röntgen radiation, which had significance for the further development of atomic physics. After the penetration of aluminium foils the "soft" part of the radiation was quickly absorbed. Left behind was a rather homogeneous radiation. Allowing this "hard" radiation to strike an arbitrary plate, one could in the scattered radiation find three different components (Fig.1). The first component consisted of scattered radiation of the same kind as the impinging

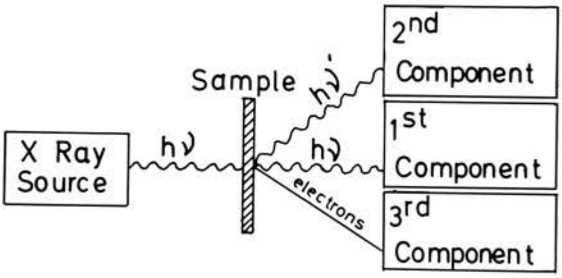

Fig. 1

The interaction of X-radiation with matter. One component is the scattered X-radiation with the same energy as the primary radiation from the X-ray tube. The second component is characteristic of the material being studied. In optical terminology this is the fluorescence radiation which developed into X-ray emission spectroscopy. The third component consists of electrons and is the basis for modern electron spectroscopy.

one. The second component was secondary X-radiation which was softer than the impinging one and characteristic of the irradiated material. From the study of this characteristic radiation Barkla could distinguish between two series of radiation, which he called K- and L-fluorescence radiation. For a certain element the penetration of the K-radiation was 300 times higher than for the L-radiation. From these early observations X-ray spectroscopy was generally developed by means of the more and more refined X-ray diffraction methods. X-ray spectroscopy made possible an atomic analysis of different materials and led to the discovery of new elements like hafnium and rhenium. The shell structure of the atoms (Fig.2) could be investigated by X-ray spectroscopy, a field in which my father was deeply involved /1/ and atomic physics was put on solid grounds.

The third component of the scattered radiation was found to consist of electrons, which were expelled from the irradiated material. What happened in this field of spectroscopy? For a very long time it was shadowed by the successful study of X-ray spectroscopy. In the twenties spectroscopic investigations of the secondary electrons, the "photoelectrons", were started by e.g. H. Robinson in England and M. de

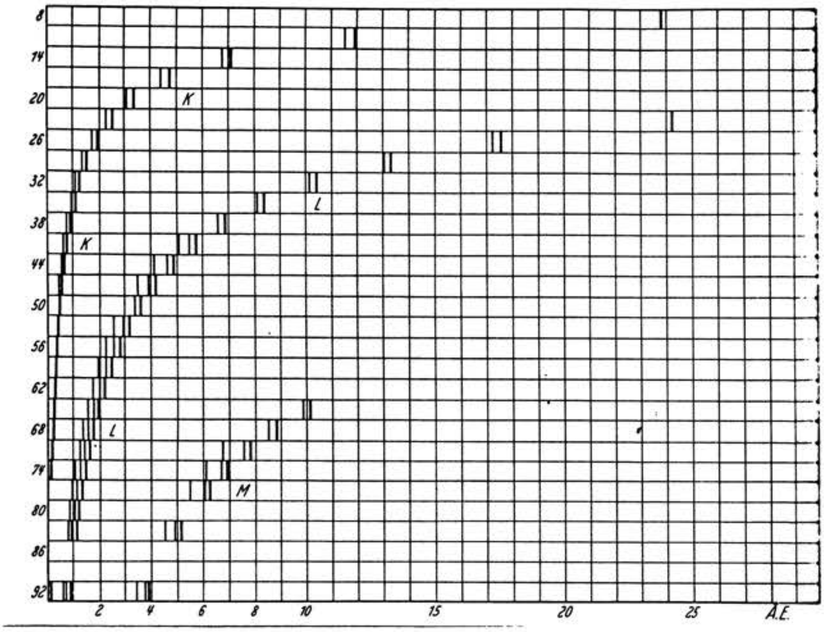

Fig. 2
X-ray emission spectrum (in Å) from the elements showing the three series K, L and M.

Broglie in France. They showed by means of magnetic deflection of the electrons, that also this component contained information on the shell structure of the atom and that one could obtain approximate values of the binding energies for the electrons in the different shells. This field turned out to be much more difficult to master and the accuracy was small.

My interest in this third component began early in the fifties. For some time I had been concerned with techniques to investigate electrons, emitted in radio-active β decay. A suitable way to investigate the γ radiation was to cover the radioactive sample by a thin lead foil and to record the expelled photoelectrons from the foil by an electron spectrometer. This work gradually led to improved resolution in nuclear spectroscopy /2/. I was finally able to observe and measure the inherent widths of conversion-electron lines due to the finite widths of the atomic levels involved in the internal conversion process during the nuclear decay. In order to observe such phenomena a resolution of 1:10^4 at these energies, around 100 keV, was required. The investigations were performed by means of a magnetic double focussing iron free spectrometer with large dispersion (R=30 cm). Fig.3 shows the different internal widths of the F- and I-conversion lines in the decay of radioactive ThB, the former line converted in the K shell the latter in the L_I shell.

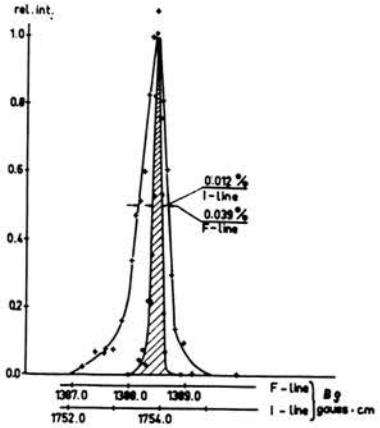

Fig. 3
ThB F- and I-lines. Internal conversion in the K and L_I shells, respectively. At this high resolution one can notice the different inherent widths of these β-lines.

Most of the high resolution work in my laboratory during that period of time was performed with a large double focussing magnetic spectrometer with iron yoke (R=50 cm) which was specially designed for studying complicated decay schemes of radioactive isotopes. The most complex of these was Au^{194}. It contained more than 100 γ-transitions, the conversion electron spectrum contained some 350 detectable lines. By means of a double counter operated in coincidence it was possible to detect lines of an intensity of 10^{-5} times that of the strongest lines. Fig.4 shows a limited part of that spectrum. In these investigations both internal and external photoelectron spectra were taken and the final decay scheme, further checked by coincidence studies from selected nuclear levels, is reproduced in Fig.5.

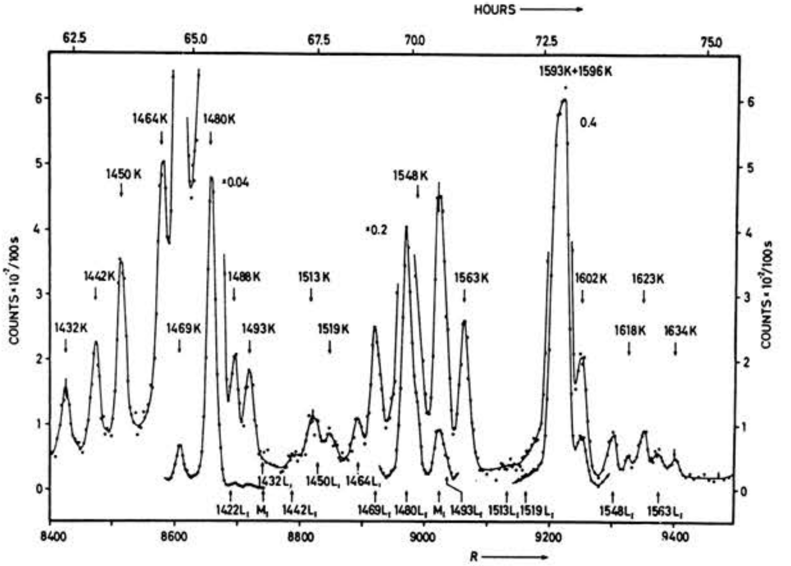

Fig. 4

Part of the internal conversion β spectrum of Au^{194}. There are altogether 350 observable β lines in this complex decay, with intensity variations of $1\text{-}10^{-5}$.

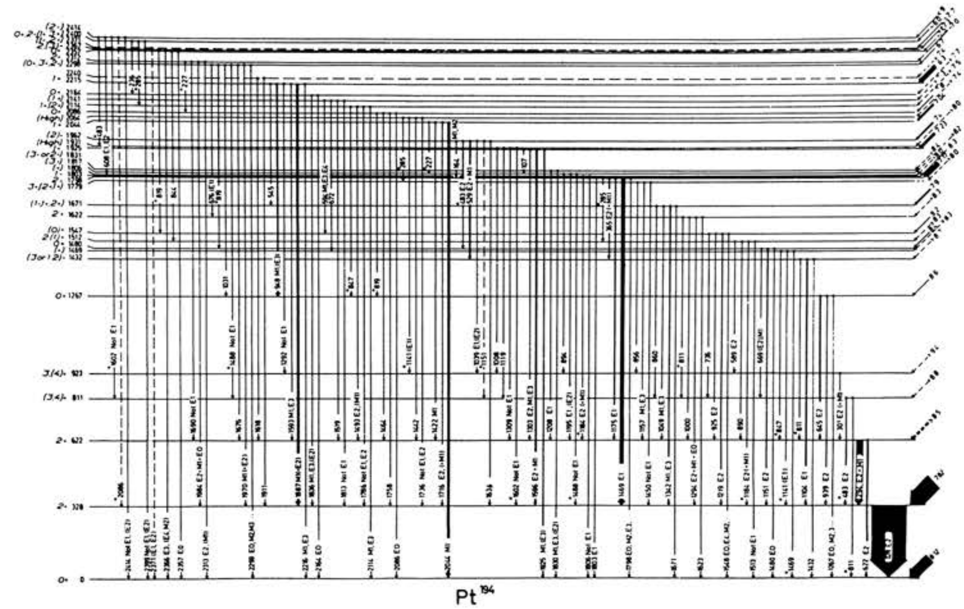

Fig. 5

Decay scheme of Au^{194} based on the internal conversion electron line and external photoelectron line spectra.

My interest to investigate finer details in nuclear spectra continuously tempted me to go back to Röntgen's original discovery and, more precisely, to the third component mentioned before and to see if new methods could be applied to atoms, molecules and solids using an X-ray tube instead of nuclear γ radiation. For this purpose the above mentioned iron free double focusing instrument was constructed and adopted to investigating electron energies some orders of magnitude less than in nuclear β decay. Robinson and some other sicentists around 1925 had been able to establish that electrons expelled from metals by means of the photoelectric effect exhibited an energy distribution that was consistent with the shell structure of atoms which had been studied in much more detail by X-ray emission and absorption spectroscopy. During the thirties and forties much of the interest in atomic physics shifted to nuclear physics. Partly because of this and partly because of the lack of adequate methods for handling the experimental problems associated with electron spectroscopy the field had waited for its development and exploration.

The mentioned early period is represented by the top of Fig.6 which shows a photographic recording of the photoelectron spectrum of gold by Robinson /3/ in 1925. The various levels in gold are distinguished in Robinson's spectrum and also in the corresponding photometric recording. The well-known N_{VI}, N_{VII} doublet, extensively used for calibrations in modern electron spectroscopy, is not observed in this early spectrum, however, and obviously the electron distributions rather resemble X-ray absorption distributions than true lines.

At the later part of the fifties the work in my laboratory had led to the development of an electron spectroscopy which was characterized by narrow electron lines from solid materials excited by X-radiation. The recorded electron lines were well defined by widths set by the inherent atomic widths themselves. The state of the art during this period is illustrated by the recordings of the gold spin doublet made during the early 60's in my laboratory (to the right of Robinson's spectrum). The same spectrum taken some years later is shown in the middle of the figure on an energy scale expanded by a factor 600 compared to Robinson's spectrum. The improvement in resolution

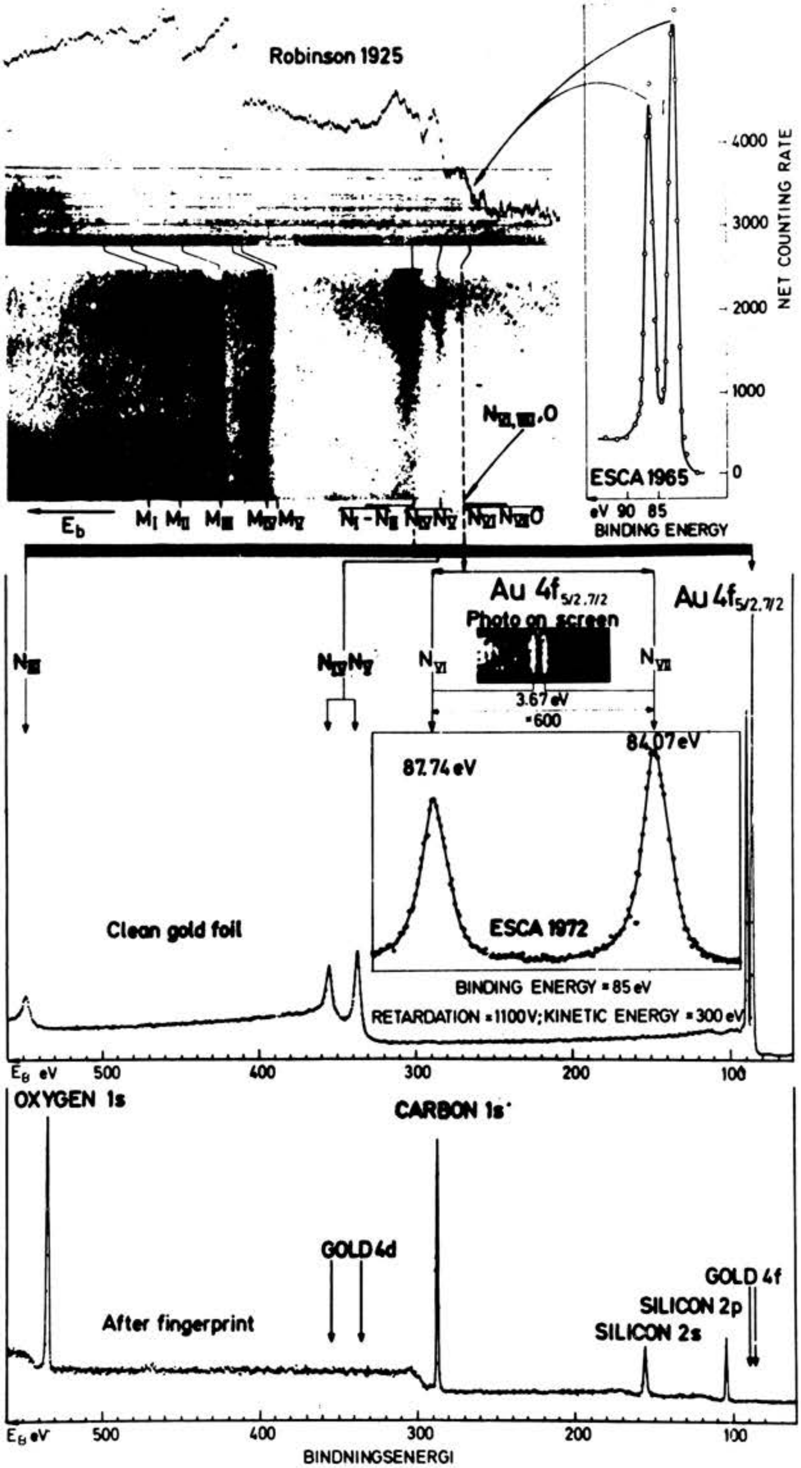
Robinson 1925
NET COUNTING RATE
4000
3000
2000
1000
0
ESCA 1965
eV 90 85
BINDING ENERGY
N_VI,VII,O
E_b
M_I M_II M_III M_IV M_V
N_I - N_III N_IV N_V N_VI N_VII O
Au 4f_5/2,7/2
Photo on screen
Au 4f_5/2,7/2
N_III
N_IV N_V
N_VI
N_VII
3.67 eV
=600
87.74 eV
84.07eV
ESCA 1972
Clean gold foil
BINDING ENERGY = 85 eV
RETARDATION = 1100V; KINETIC ENERGY = 300 eV
E_B eV
500
400
300
200
100
OXYGEN 1s
CARBON 1s
GOLD 4d
GOLD 4f
SILICON 2p
SILICON 2s
After fingerprint
E_B eV
500
400
300
200
100
BINDNINGSENERGI

Fig. 6

between the two later spectra is due to the introduction of X-ray monochromatization by means of crystal diffraction of the AlKα radiation. This made it possible to pass beyond the previous limit set by the inherent width of the X-ray line. The lowest part of the figure illustrates one particularly important feature of electron spectroscopy. The difference between the middle and the lowest part of the figure demonstrates the surface sensitivity of this spectroscopy. A fingerprint on the gold foil completely wipes out the gold lines and replaces them by other lines dependent on what elements happened to be on the surface layer of that finger.

Electron spectroscopy is nowadays an independent alternative to X-ray and other spectroscopies and contributes with much new information about the properties of matter. In particular surface science and technology makes use of electron spectroscopy as a convenient tool to characterize surface conditions and reactions. Applications are found in many other areas in the border lines between physics and chemistry. To emphasize these aspects the acronyme ESCA (electron spectroscopy for chemical analysis) was introduced /4,5/. The historical background is covered in several more recent works /6,7,8,9/.

Fig. 6

Some steps in the development of photoelectron spectroscopy excited by X- radiation. Upper figure to the left: the recording of gold as obtained by Robinson in 1925 with its photometer curve. To the right: the "gold doublet" photoelectron lines around electron binding energies of E_B~85 eV as observed after that photoelectron line spectroscopy had been developed at the end of the fifties. These and any of the other lines cannot be seen in the previous spectrum. The middle spectrum shows the same spectrum when X-ray monochromatization of AlKα at 1486.6 eV ($\Delta h\nu = 0.2$ eV) had been introduced. The gold doublet is inserted in this figure in an expanded scale ~600 times that of the Robinson spectrum. The lower figure shows the surface sensitivity of electron spectroscopy. A fingerprint has wiped out the gold lines and produced new lines.

2. Some basic features of electron spectroscopy

In photoelectron spectroscopy the sample is introduced into vacuum and radiated with soft X-rays, ultra-violet light or synchrotron radiation. In addition, an electron beam can supplementary be used to excite Auger electron spectra by electrons and, if properly monochromatized, for electron scattering spectroscopy. A certain number of the electrons which are expelled from their atomic bindings may leave the surface layer without energy losses, the scanning depth being set by the energy dependent mean free paths. An electrostatic lens system collects and focusses the electrons onto the slit of the electron analyser. An extended detector is situated in the focal plane where the different electrons are simultaneously being recorded. These events appear on the screen of a computer as a fence of separate electron lines (see Fig.7). These lines characterize the examined substance, the elemental composition and the chemical bindings.

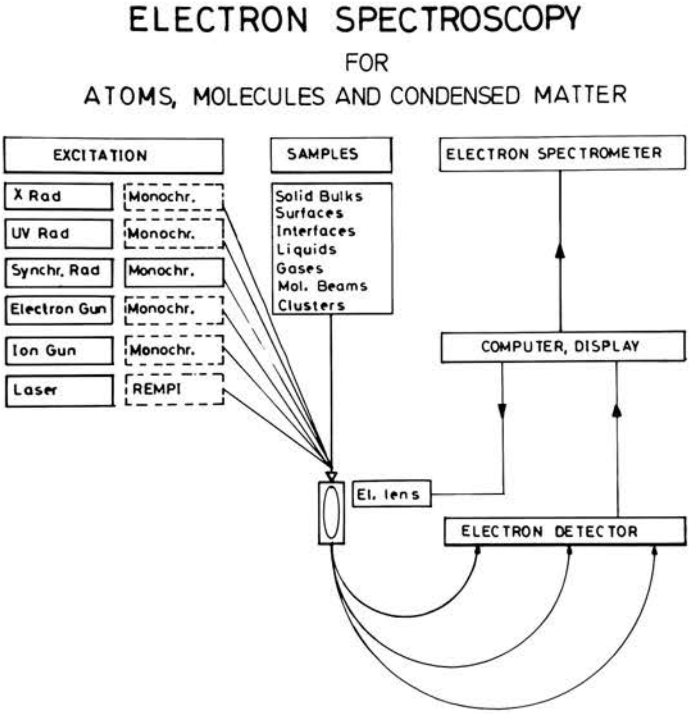

Fig. 7
Scope of electron spectroscopy.

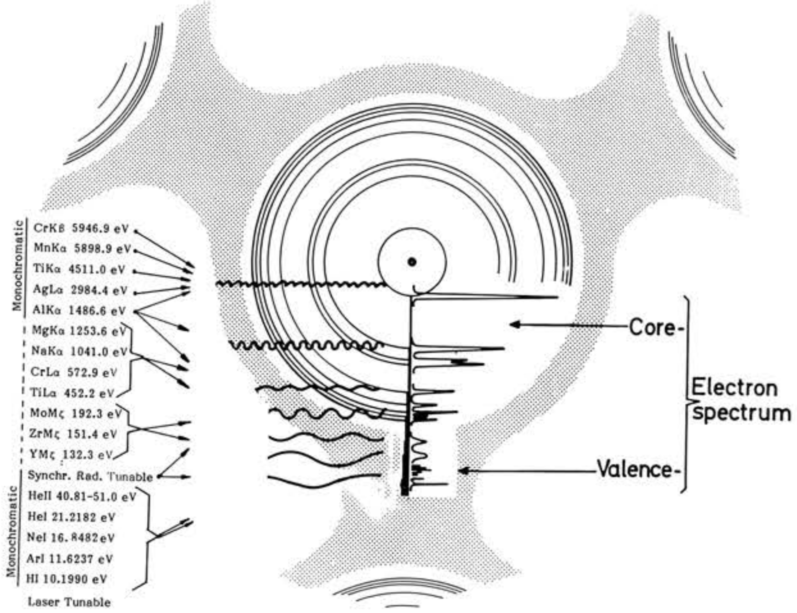

Fig. 8
Excitation of core and valence electron spectra.

Solid materials with elements over the whole periodic system can be examined and also gases down to low pressures ~1-10^{-5} torr. The spectroscopy has been applied also to liquids and solutions. Extensions of electron spectroscopy are under way by using LASER radiation for excitation (in particular resonance enhanced multiphoton ionization, REMPI).

Fig.8 illustrates an atom which is bound to other atoms in molecular valence bondings, alternatively adsorbed or chemically bound to a surface. In order to eject electrons from the inner part of an atom (the "core" region) harder radiation is required than for the external valence electron region. When an electron is emitted a hole is created in the electron shell. This is immediately followed by a relaxation of the other electrons which thereby adjust themselves to the new potential by means of a "shrinkage" and flow in the surrounding electron cloud. The hole has a certain very short lifetime ($<10^{-14}$Sec) before it is filled by an electron from some externally situated shell. The atom can dispose of the released energy either in the form of an X-ray photon or by emitting another (Auger) electron. In such a case three levels are involved (e.g. LMM etc.). Such electrons are recorded together with the primary emitted photoelectron spectrum. One advantage to excite Auger electrons by X-rays compared to electrons is the great improvement in signal to background. These conditions are further discussed later in this survey.

When a chemical compound between two or more atoms is formed a redistribution of the external valence electrons of the atoms occurs which are responsible for the chemical bonds. The electric potential around a certain atom in the molecule will then be changed, to an extent which is dependent on the specific nature of the chemical bond in the different cases (e.g. at different "states of oxidation"). This new electric potential influences the bond strength of the inner electrons which surrounds the atomic nucleus and the consequence of this is a "chemical shift" in the recorded electron spectrum. This information is exceedingly important in electron spectroscopy. One can for example easily distinguish, even at modest resolution, between metallic atoms and those which have been oxidized at the surface layer.

Fig.9 shows such a case /10/. It concerns the surface of a silicon crystal and one observes in the electron spectrum taken at modest resolution two main lines which are due to the electrons from the 2s and 2p levels, respectively, from silicon. The spectrum also contains some satellites which are due to discrete energy losses of electrons. The difference between the lower and upper figure is that the crystal surface has been tilted so that the electrons in the latter case leave the sample at a small angle from the surface. Those electrons which come from below, from the "bulk", are then absorbed to a larger extent than those from the outer surface layer. The surface layer is favoured. One can notice how the slightly oxidized silicon layer on the surface shows up strongly in the form of SiO_2 lines to the left of the Si lines. They were only barely visible in the other spectrum.

At improved resolution (Fig.10) much more detailed information is obtainable concerning the depth composition at the oxidation /11/.

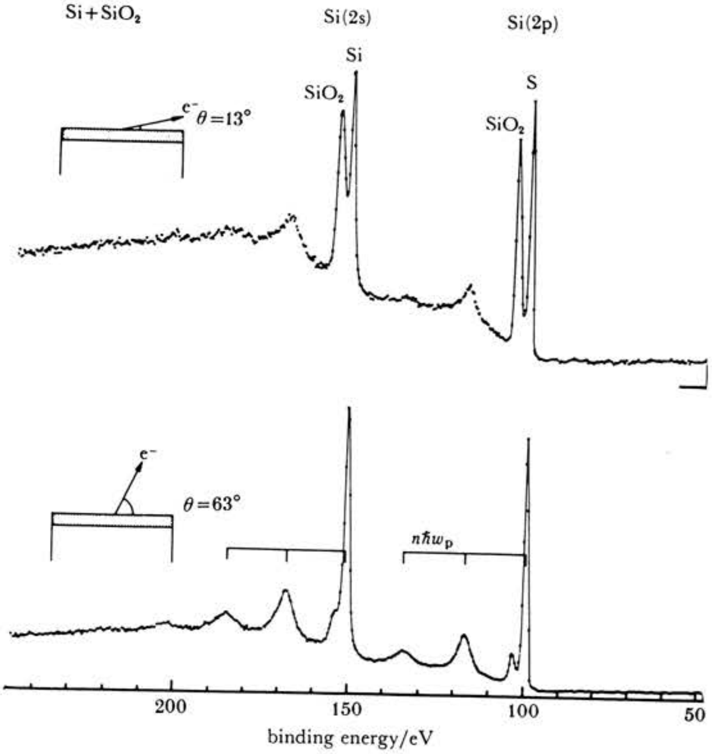

Fig. 9
Spectrum of a slightly oxidized silicon surface. By tilting the cryst
the oxide surface layer is emphasized. Plasmon lines are also observe

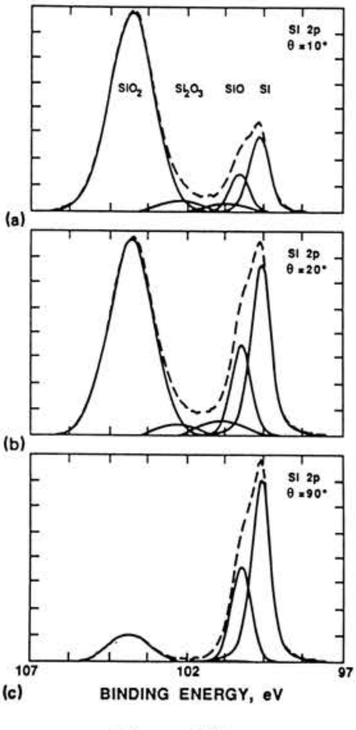

Fig. 10
A study of the oxidation of a silicon surface taken at higher resolution by means of the "tilting" method.

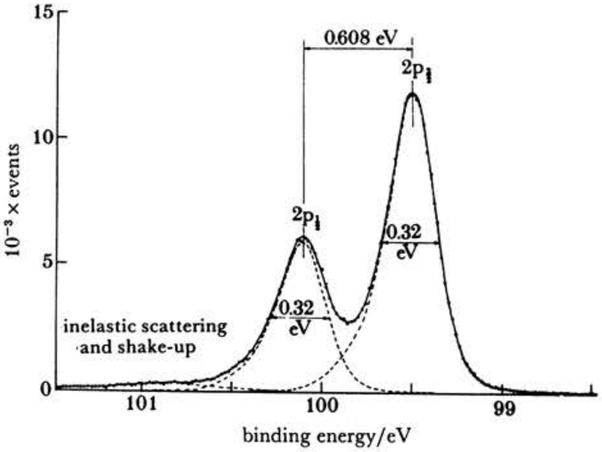

Fig. 11
Well resolved $2p_{1/2}$ and $2p_{3/2}$ core lines of Si(111) at T=300 K and $\theta=45^{\circ}$ by means of monochromatized AlKα 1486.6 eV ($\Delta h\nu=0.2$ eV) Observe the low background.

This is a simple and commonly used method to distinguish between bulk and surface. The surface sensitivity is a small fraction of a single atomic layer, under certain conditions less than a percent of an atomic layer.

The spectral resolution can be pushed much further than what is shown in Fig.9 and 10. Fig.11 gives a highly resolved spectrum of the $Si2p_{1/2,3/2}$ doublet excited by means of monochromatized AlKα rays /12/. Here the doublet is completely resolved in two components instead of the unresolved one in the previous figure. The background is also very small, essentially zero. Small intensity structures can then be observed slightly above background.

An increasing number of ESCA instruments are now in operation which are provided with X-ray monochromators for high resolution work. To a much less extent these are combined with a rotating anode. Still it is this combination which offers the best advantages for high resolution at high intensities. Ultimately, the recorded electron linewidths are set by the inherent levels widths. The use of an X-ray monochromator significantly improves the conditions for accurate deconvolutions at the analysis of the spectra, since the lines are getting narrower and the signal to background ratio is enhanced. The electron lines due to X-ray satellites situated close to the real line structures are elliminated and so is the background due to bremsstrahlung.

In photoelectron spectroscopy the recorded linewidths are lifetime and vibration limited. As an example carbon lines from polymers are usually rather broad by nature (>1 eV). If the sample is an insulator one always has to take precautions to avoid charging of the sample surface. Methods have been developed to elliminate or greatly reduce such artefacts in the spectra. Usually an electron flood gun with very low energy electrons is used to flooding the sample or one may simply use the degraded flux of electrons from the X-ray electron production at the sample by surrounding the sample by a cavity with two holes, one for the X-rays and one for the expelled photoelectrons in the direction of the slit of the analyzer. A more recent arrangement, is to use an unfocused electron gun with electrons in the 1 keV region. Another recently developed method is to use a wire net at a defined potential fairly closely situated to the sample surface. A further possibility which will be further studied would be to rotate the samples during the exposure. These methods are convenient to apply when the X-ray beam is strongly focussed onto the sample. As a general rule the samples should be made as thin as possible and be deposited on a conducting backing.

Some electron spectra will demonstrate the state of the art at good resolution /13/. Fig.12 shows the electron spectrum of copper. One observes the core levels with their different widths and intensities. Close to zero binding energy the conduction band (3d4s) is recorded. This structure and similar ones from metals and alloys etc. can be separately studied in much more detail at larger dispersion (see e.g. Figs.35 and 36). In the spectrum one also observes the Auger electron lines due to LMM transitions in the region excited by the same AlKα radiation.

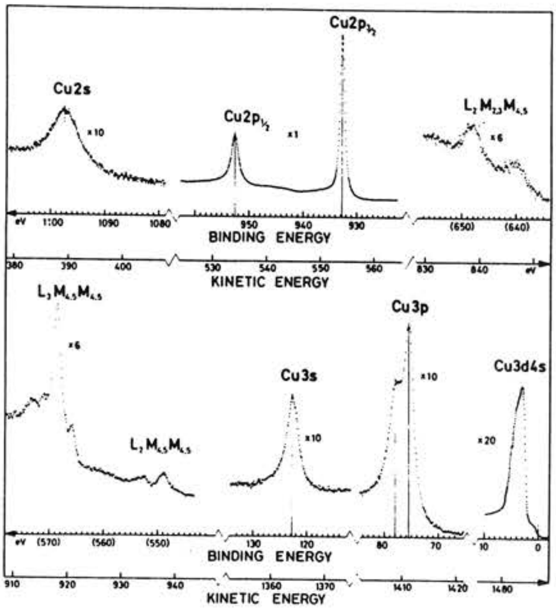

Fig. 12
The copper spectrum showing core photoelectron lines, Auger electron lines and the conduction band.

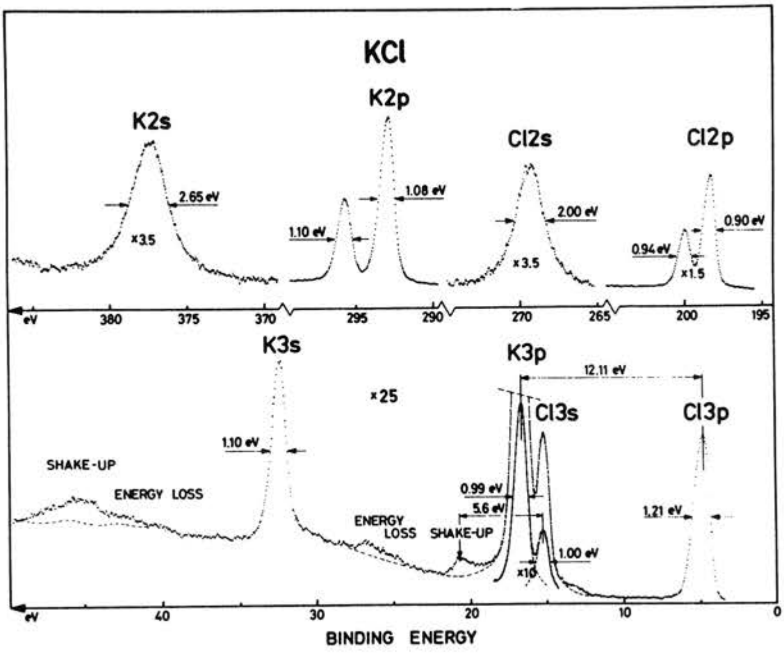

Fig. 13
The spectrum of an ionic crystal, KCl. The different linewidths for this insulator are given in the spectrum. The ionicity is related to the energy difference 12.11 eV.

Fig.13 shows the electron spectrum of an ionic crystal, KCl. The L and M sublevels for both elements are recorded and their linewidths are given in the figure. In the valence region (lower part) some energy loss and "shake-up" lines are shown. The shake-up line situated 5-6 eV from the Cl3s is due to a configurational interaction between the $3\underline{s}^2S$ ionic ground state and the $3\underline{p}^2 4s^*$, $3\underline{p}^2 4s^*$, $3\underline{p}^2 4p^*$ and $3\underline{p}^2 3d^{*2}S$ states. A strong shake-up structure situated 14 eV from the K3s is due to a configuration interaction between the $3\underline{s}^2S$ ionic ground state and the $3\underline{p}^2 4s^*$, $3\underline{p}^2 4p^*$ and $3\underline{p}^2 3d^{*2}S$ states. The energy difference between the two outer bands of the cation and the anion, K3p adn Cl3p, respectively, is according to the figure 12.11 eV. This can be used to assign an ionicity for such binary crystals.

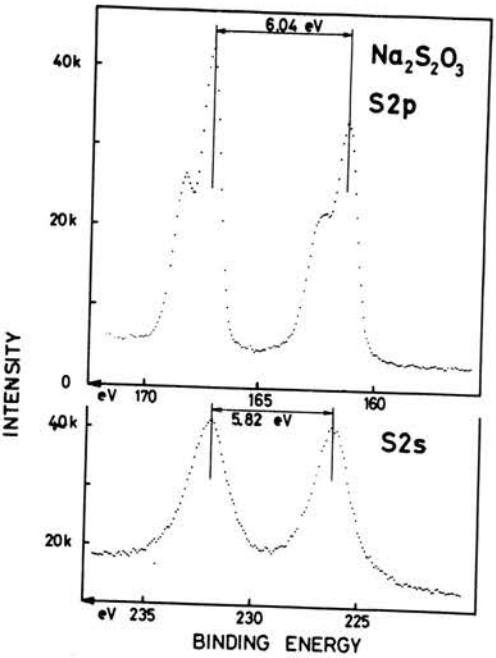

Fig. 14
ESCA chemical shifts for S2p and S2s in $Na_2S_2O_3$.

Some examples of ESCA chemical shifts will be given here. The first one concerns $Na_2S_2O_3$, Fig.14. There are two different sulphur atoms here which, according to classical chemical language, could be associated with oxidation numbers 6+ (central) and 2- (ligand). The ESCA chemical shift between the central S-atom (to the left) and the ligand S-atom (to the right) for the $2p_{1/2,3/2}$ doublet is 6.04 eV. This is

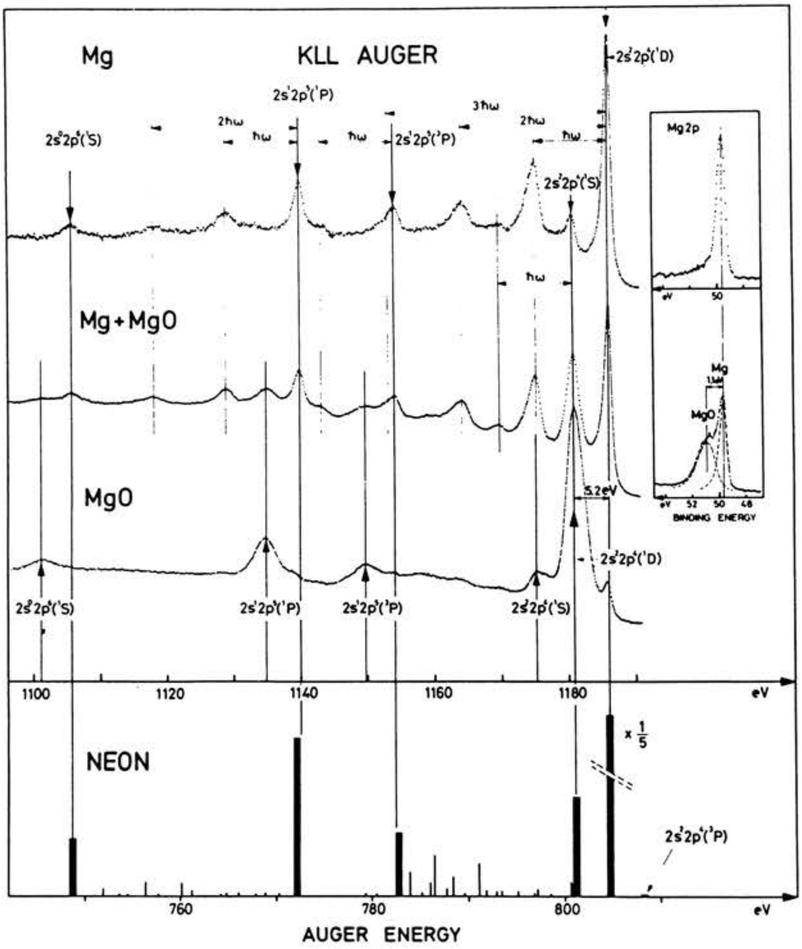

Fig. 15
MgKLL Auger electron lines at different stages of oxidation. Volume plasmons for each electron line are also observed. The chemical shift of the Mg2p line is inserted. The Ne Auger electron spectrum excited by electrons is inserted for comparison with Mg. This spectrum contains a great number of well resolved satellites /5/.

evidently a large chemical effect, even larger than the atomic spin-orbit splitting, which is just resolved in the spectrum. The lower part of the figure shows the corresponding shift between the 2s levels. One observes here the larger inherent linewidths of the s-levels. The chemical shift is almost the same, 5.82 eV, but may give room for a small second order effect.

The second example (Fig.15) concerns the MgKLL Auger electron spectrum excited with AlKα radiation at different stages of oxidation. The

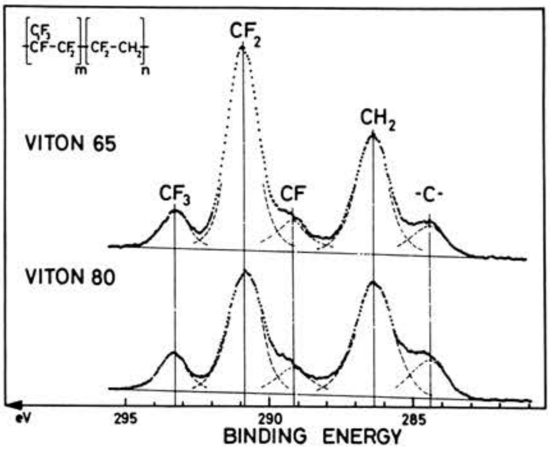

Fig. 16
ESCA spectra of the polymers Viton 65 and Viton 80 with different branchings in agreement with the measured intensities.

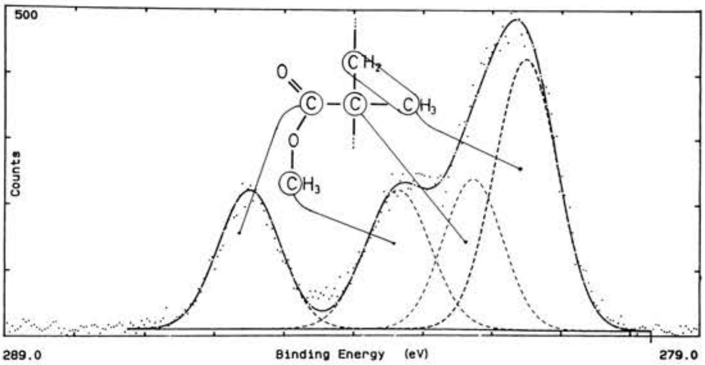

Fig. 17
ESCA spectrum of the polymer PMMA, polymethylmethacrylate. The deconvolution into components and their positions characterizes the polymer.

upper curve is a clean metal surface, the lower is the oxide (with only a trace of metal) and the middle at intermediate oxidation. Series of volume plasmons (metal plasma collective oscillations) for each Auger line are observed, some of which nearly coincide with other Auger electron lines. The MgO peak, when growing up, happens to coincide with the second Auger electron peak of the metal. For comparison, the NeKLL Auger electron spectrum is given below. This spectrum contains a great number of satellites, which can alternatively be recorded in separate experiments in the gas phase by means of electron excitation. Inserted in the figure is the Mg2p photoelectron line and the chemical shift of this during oxidation.

The chemical shift effect is frequently used in polymer technology for characterization of such materials. Fig.16 shows the C1s core line splitting in five components in the case of Viton. The relative intensities between the lines depend on the branching ratio in the polymer chain. From the spectrum in Fig.16 one can in this way distinguish between Viton 65 and Viton 80.

Fig.17 is a commonly used 'test' sample in ESCA, namely PMMA (polymethylmethacrylate). It is a polymer with wide-spread applications, e.g. in the production of semiconductor chips by means of lithography. The polymer chain consists of the group indicated in the figure. A good instrument, e.g. one with well focussed X-rays, should be able to resolve sufficiently well the different carbon atoms in this group /14/. It is an insulator and therefore subject to charging if not the correct precautions have been taken to eliminate this effect. The inherent widths of the photo lines are partly set by internal vibrations in this case. It is therefore not possible to distinguish all the lines completely. However, with good statistics (high intensity, low background and monochromatic X-radiation) a reliable deconvolution can be made showing four carbon components on the 'right' places, which is good enough for a characterization of this polymer.

3. Monochromatization of the exciting X-radiation. Instrumental arrangements.

An ultimate factor in reaching high resolution is the monochromacy of the exciting radiation. In the X-ray region one can use X-ray lines to confine much of the available X-radiation energy into a very narrow region defined by the inherent linewidth of the Kα line of the anode material (e.g. Al or Mg). For further improvements monochromatization by means of X-ray diffraction against a crystal (e.g.

quartz) is necessary. Regardless whether one starts with the discrete line spectrum of an anode material or the continuous spectrum of synchrotron radiation, which allows a continuously variable wavelength, it is the properties of the diffracting crystal which set the limit for the final resolution. Important factors here are the number of lattice planes in the crystal taking part in the diffraction and the suitable choice of crystal material to withstand radiation damage. Furthermore, mosaic structure of the crystal is a disadvantage for high resolution. Quartz is a particularly good choice for reaching highest resolution but is on the other hand fairly radiation sensitive and therefore not suitable in too high concentration of radiation, e.g. synchrotron radiation.

In the case of AlKα radiation the Bragg angle for quartz (010) is 78° which means that reflexion is almost at normal incidence. Under these conditions a spherically bent crystal will approximately achieve two directional focussing, i.e. point to point imaging. The reflectivity is quite high, around 50%. Using an array of such crystals (our recent design contains 19 crystals, each with a diameter of 6 cm) on the Rowland circle, or rather on a Rowland surface, one can collect and focus a substantial solid angle of monochromatized X-radiation with high intensity for the production of photoelectrons at the position of the sample.

In order to get a maximum of highly monochromatic X-radiation the primary radiation has to be emitted from as small a surface element as possible. The anode has to be watercooled and at the same time rotating in a good vacuum. In my most recent design the rotor will be magnetically suspended (see Fig.18) with an asynchronous elmotor between the 'active' magnetic bearings. By means of electronic sensors the rotating body is fixed (and adjustable) in both radial and axial directions. This is a stable and safe arrangement which does not require lubrication.

The design of a rotating anode is technically a demanding task. My laboratory has been dealing with such problems for a long period of time. The anode should be capable of very high speeds of rotation

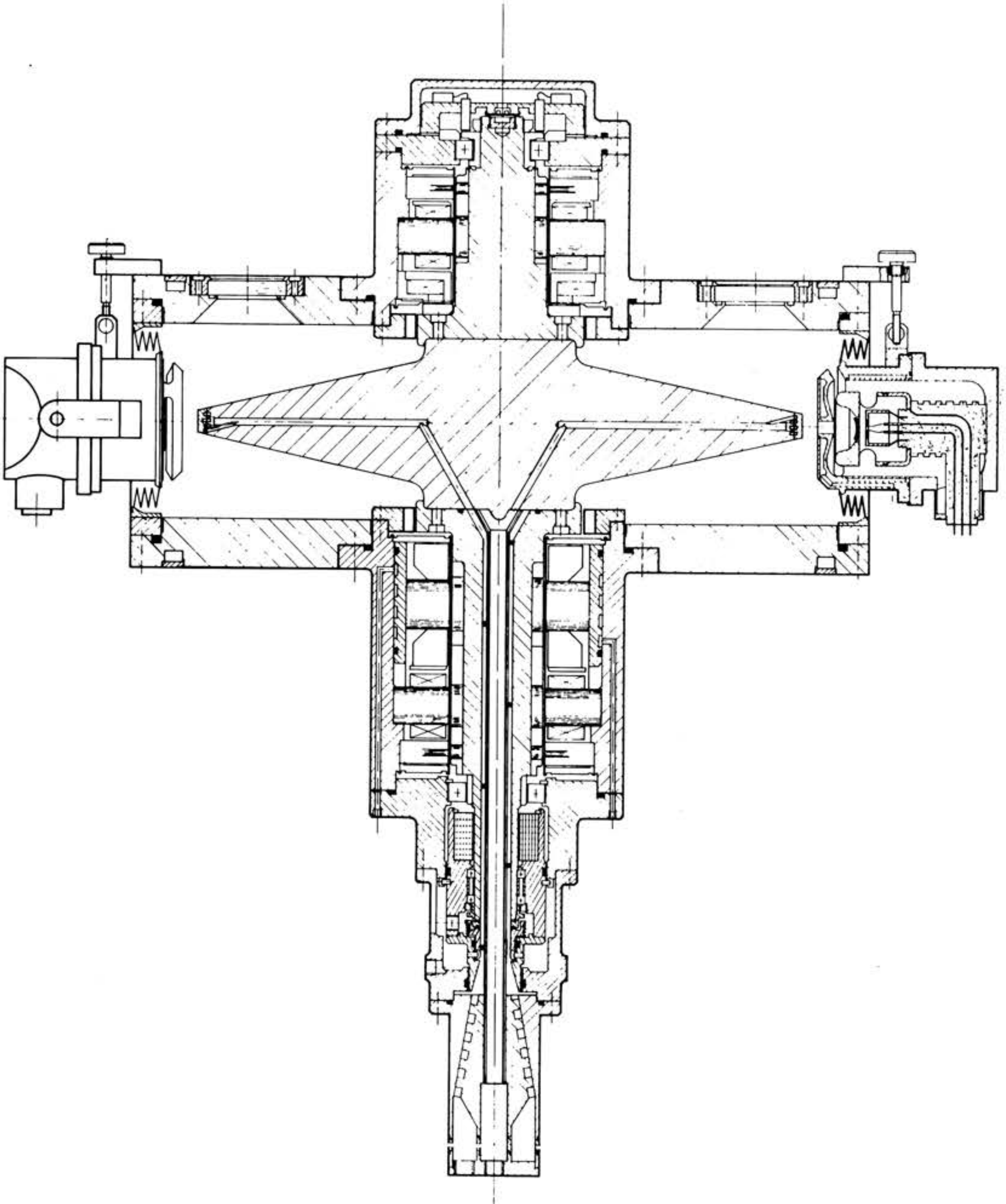

Fig. 18

The design of a new high speed, magnetically suspended, water cooled rotating anode. This high intensity X-ray generator is provided with two electron guns and several different anode materials along the rotor periphery to generate different X-ray wavelengths.

(>10 000 rpm) and strongly water cooled in order to be able to accept the high power levels required on a small area. With minor modifications the design according to Fig.18 can be made in any desired size. As an example, at 15 000 rpm and a diameter of 50 cm the rotor has a speed at the perifery of ~400 m/sec, i.e. well above the velocity of sound. For even higher speeds the strengths of the rotor itself, if necessary, can be further improved in the future by using composite materials. Dependent on the chosen spot size of the electron gun and the particular anode material one might be able to dissipate a power of ~50 kW due to an efficient water cooling of the rotor perifery. The heat generated at the surface of the rotor is distributed over the whole perifery but on top of that a quickly decaying transient temperature spike is developed each time a certain surface element is passing the electron beam spot. Because of this the very high rotor speeds are required. Other precautions have to be taken to create, preserve and to continuously inspect the surface conditions necessary to achieve high X-ray emission intensities. For this purpose the rotor house is provided with appropriate arrangements. On the external part at the perifery of the rotor, which is being exposed to the focussed electron beam, different anode materials can be deposited, in particular aluminium.

Since AlKα radiation is focussed at an angle of 78° in the first order of diffraction it is interesting to see what other X-ray lines of other materials could be used which have approximately the same Bragg angle at higher orders. Going from one anode material to another at multiples of 1486.65 eV, the energy of the AlKα line, requires then only minor mechanical adjustments from the standard position.

Doubling the X-ray energy results in a larger escape depth of the produced photoelectrons in the sample. The cross section for photoelectron production in the sample is getting down, unfortunately, but of some particular interest is the fact that the number of planes involved in the diffraction in the quartz is increasing. This has as a consequence that the theoretically attainable resolution is increasing. By means of the detailed dynamical theory of X-ray diffraction the rocking curves for quartz (010) (and other crystals) can be calcu-

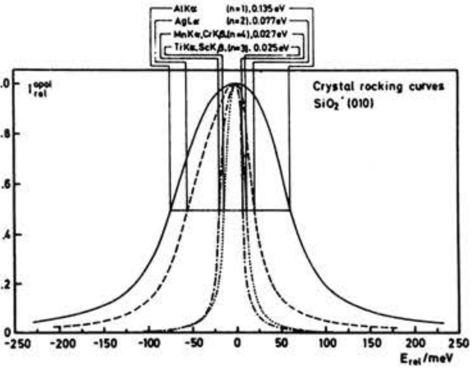

Fig. 19
Calculated rocking curves for several X-rays reflected against quartz (010) near 78° at different orders. The width of the rocking curve narrows at increasing energy.

lated for different wavelengths. Fig.19 summarizes the results /15/. Possible anode materials having approximately the same Bragg angle (78°) in different orders are: AlKα (first order), AgLα (second order), TiKα, ScKβ (third order) and MnKα, CrKβ (fourth order). According to Fig.19 the widths of the theoretical rocking curves are: 135 meV, 77 meV, 25 meV and 27 meV, respectively. As pointed out above the photoelectron intensities are decreasing and, furthermore, since the energies of the photoelectrons are increased the demands put on the resolving power of the electron spectrometer is correspondingly increased. Full use of the theoretically attainable higher resolution at higher orders according to Fig.19 will be at the expense of a great reduction in intensity. How far one can really reach the theoretical limit remains to be seen. For the case of AlKα the theoretical limit of 135 meV is almost reached by the actually obtained value of 0.21 eV according to Fig.20.

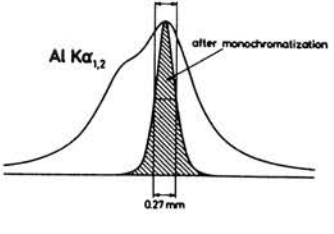

Fig. 20
Achieved monochromatization of the AlKα doublet reflected near 78° against a set of spherically bent thin quartz wafer crystals (010).

Instruments in electron spectroscopy can be constructed in a great variety of different ways, dependent on the modes of excitation, types of samples, research problems etc. On the market there are presently a number of designs available. They are usually tailor made for surface studies under ultrahigh vacuum conditions to be used on a routine basis. A typical trend today is to simultaneously make use of complementary multipurpose techniques for surface characterization like LEED, SIMS, TDS etc. Handling of gases or liquids requires efficient differential pumping and special designs. Synchrotron radiation, when available, is particularly well suited for excitation of photoelectron spectra and necessary when complete tunability is required. Commercial instruments take advantage of devoted laboratory sources like soft X-ray anodes adopted to photoelectron spectroscopy, ultra-violet discharge lamps and monochromatized and focussed electron beams. Tunable laser sources will provide new possibilities for investigations by means of multiphoton ionization and tunability in the valence region.

High spectral resolution is important in all cases. In the soft X-ray region the monochromatization can be achieved in its lower part by means of optical grating techniques as is done at synchrotron storage rings and in its higher part (>1 keV) by means of crystal diffraction. A recent laboratory design in my laboratory for this purpose is shown in Fig.21. It consists of the previously mentioned water cooled swiftly rotating anode (Fig.18) with two electron guns, the X-radiation produced by one of them being directed into an X-ray monochromator. The purpose of the other one is to enable other X-ray experiments to be done.

The spherically bent thin quartz crystals are mounted on a common zerodur block which can be moved in the horizontal direction around a vertical axis situated at the side of the block. Such a movement changes the Bragg angle and adjusts the crystal surfaces to stay on the Rowland circle (R=100 cm) when the house of the rotating anode is correspondingly moved along a prescribed curve on the rotor table.

The different anode materials are deposited as 3-6 mm wide strips aside of each other along the perifery of the rotor. The electron

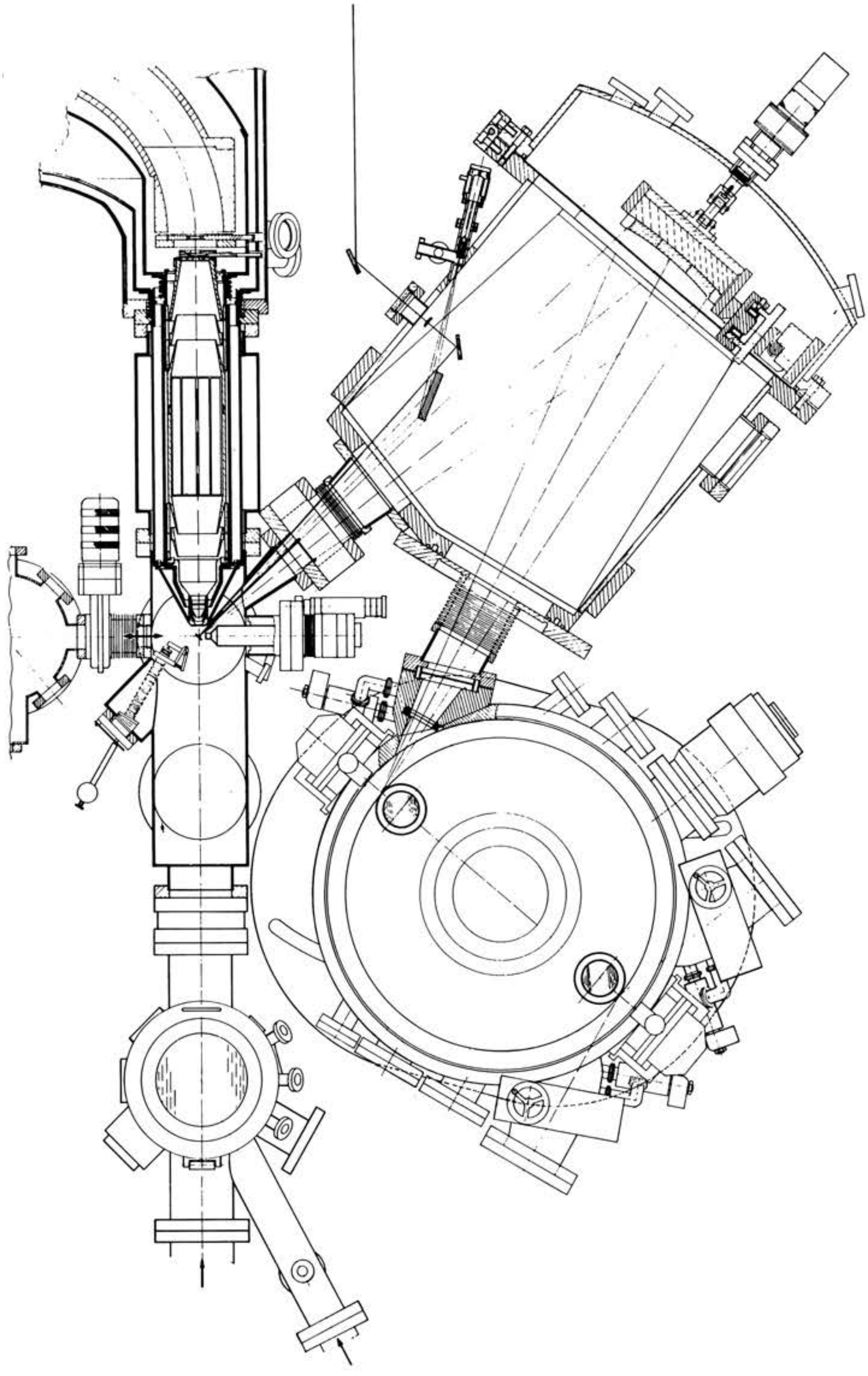

Fig. 21

gun can be tilted from outside to direct the electron beam towards the different anode materials. In accordance to the position of the electron beam spot on the anode the crystal block is simultaneously slightly tilted around a horizontal axis supported by a strong ball bearing.

By these arrangements the focussed and diffracted X-ray beam for different wavelengths will always hit the sample on the same spot in front of the electrostatic lens system. The movements can automatically be performed by step motors. The construction admits the use of the five anode materials Al, Ag, Ti, Cr and Mn in different orders as discussed above. The use of further auxiliary anode materials like Y, Zr or Mo to produce ultrasoft $M\zeta$ X-radiation in the 130-190 eV region can in principle be arranged within the same scheme. In that case a separate concave mirror or grating could be introduced in front of the crystal assembly. One should then make use of the presently quickly developing multilayer techniques which, at nearly normal reflexion, may enhance the intensity by some orders of magnitude due to a much increased reflectivity and also solid angle. This technique still waits for its full exploration.

The monochromator house is provided with further arrangements for UV and laser light which can be directed onto the same spot on the sample as do the X-rays. Other external radiation sources, inclusively synchrotron radiation, can also be handled in the monochromator house.

The lens system is a five-component system provided with an exchangeable auxiliary einzel-lens close to the lens entrance slit. In order to direct the beam accurately to a given small entrance slit at the analyzer an octopole electric deflector is mounted inside the long

Fig. 21
The rotating anode-monochromator (RAMON) arrangement and the lens system of the electron analyzer. The monochromator provides additional radiation sources for UV and laser excitation focussed at the same spot on the sample. There is a fine-focus electron gun for additional Auger electron excitation and microscopic scanning of the sample. Samples can be introduced either from two sample preparation systems from the back side or via a vacuum lock devise joining this part of the instrument with the other part of the total instrument.

central section of the lens system. The lens system is surrounded by two concentric μ metal shields, as is the analyzer.

This einzel-lens is not always required for ordinary spectroscopic work. It is provided with a collimating slit to achieve a magnified real electron optical image at the entrance slit to the analyzer. This is to achieve lateral resolution. Developments in order to realize high lateral resolution (<100 μm) combined with good energy resolution are presently under way in several laboratories. Arrangements for this purpose can be made in many different ways. In the present case the magnification achieved by the einzel-lens may be about 10-20 times, dependent on the chosen geometry. If the X-ray spot on the sample surface is concentrated to be 0.2x1 mm^2, which is feasible with the present high intensity X-ray generator combined with the focussing monochromator, this small spot will emit photoelectrons at a very high intensity. The conditions are therefore ideal for achieving high lateral resolution. To achieve this one can choose a suitable magnification by means of the magnifying electron optical lens system. The simplest case is shown by the arrangement in Fig.21. Additional lenses would give higher magnification at the expense of intensity. It is therefore of prime importance to start with a high brilliance at the sample spot to be investigated. A swiftly rotating anode as in Fig.18 is particularly well suited for this purpose. With 20 times magnification the electron image at the entrance slit of the analyzer would become 20 mm x 4 mm^2. If the analyzer is accurately adjusted it will produce a real image in the focal plane of the same dimensions. There are several ways to proceed from here. For example, one can use a slit at the entrance of the analyzer which has a width of 0.1 mm. Then the analyzer will accept electrons only coming from a 5 μm wide strip of the sample. With a perfectly chosen optical system with negligible aberration errors in regard to both lens system and analyzer a point to point image is produced in the focal plane of the analyzer which has simultaneously dispersed the energy spectrum from each point on the sample. By means of the electric octopole deflector the illuminated sample surface can be scanned. In such a deflector the two ortogonal deflections are completely independent of each other /16/. If the sample has a large area the region corresponding to the X-ray spot is being selected by means of the sample manipulator. The position sensitive multichannel-plate detector is in this "photoelectron microscope" electronically an integrated part of the total system.

Obviously, the high lateral resolution mode of operation is realized only at a great expense of intensity. If this is not required, the lens system can be used under much more relaxed conditions, the main purposes being a high collection efficiency and good optical retardation properties for achieving high intensity and high energy resolution, respectively.

A view of the total ESCA instrument with its accessories is shown in Fig.22. The spherical analyzer (R=30 cm) is provided with two separate lens and detector systems, one for electrons being bent in the horizontal plane and the other in the vertical plane. Two separate experimental sets up are then available and samples can be studied in anyone of them. There is a connection between the two through a valve.

There are several different modes of excitations within the system and also complementary techniques, in particular for surface studies. Since differential pumping has been introduced in the sample houses the instrument is also equipped for studying gases and liquids as well as solids.

In the sample chamber which analyzes the electrons in the vertical plane there are provisions for UV excitation by means of a set of one toroidal mirror and four toroidal gratings adjustable from outside which covers the energy range between 10-51 eV. In the same chamber there is a two-stage high resolution electron monochromator, variable between ~1 eV - 6 keV for electron scattering in the 90° direction, an Auger gun and an ion gun with a Wien selective filter. Provisions for electron flooding for electric neutralization of surfaces are included. Laser radiation can be introduced.

Samples can be introduced into the chamber through different ways. One introduction port is connected to a preparation chamber which in

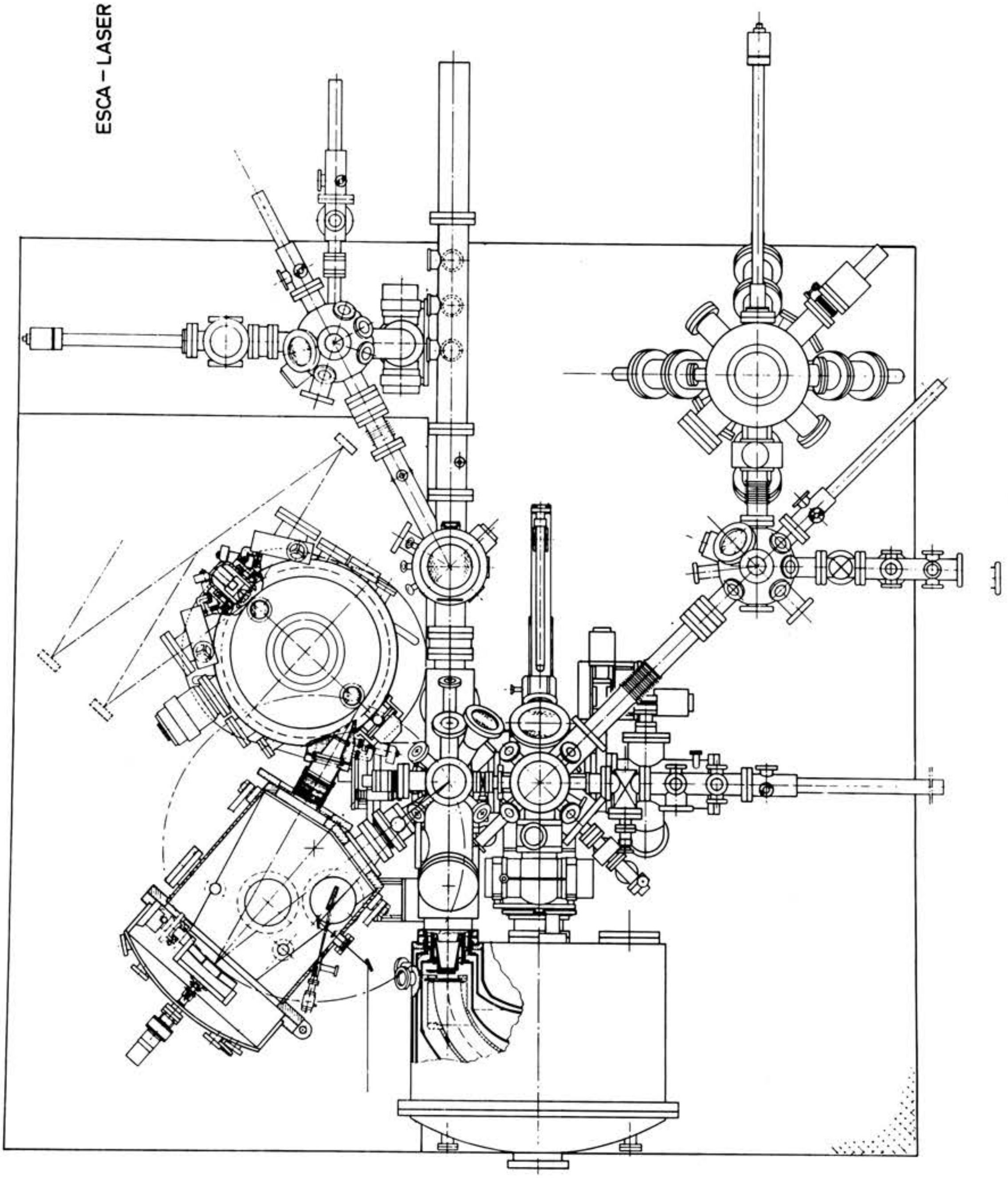

Fig. 22

turn communicates with an MBE system. The other port is a fast sample inlet directly into the measuring position of the analyzer through a vacuum lock devise. This sample chamber is connected through a valve on top of the sample chamber to a further apartment, containing facilities for complementary surface techniques, like LEED etc.

A long range manipulator carries the sample into different measuring positions and provides the means for angular studies and temperature regulation. A horizontal rod brings the sample into the second part of the instrument where the electrons are analyzed in the horizontal plane.

The primary mode of excitation here is the monochromatic X-radiation and the other radiation facilities previously described in Fig.20. There is a further focussed scanning Auger gun situated close to the sample. The latter is transferred from the introduction rod to a manipulator in front of the lens slit.

This sample house communicates with a chamber which branches into two directions backwards. One is a separate preparation chamber (with its own sample inlet devise) for the normally occurring sample preparations like evaporation, sputtering, CVD etc, the other is a specially designed inlet system for liquids and solutions, which admits direct communication "on line" between the liquid sample in the spectrometer and chemical experiments to be performed in the laboratory.

Fig. 22

A total view of the ESCA-LASER instrument. There are several separate preparation facilities "on line" of the instrument. One is for ordinary chemical and adsorption operations and the other is for the preparation and introduction of liquid samples. These facilities concern the first part of the instrument as shown in the previous figure.

The sample house for the second part of the instrument is shown in the figure in front of the analyzer with its various sources of excitation. It communicates with an UHV preparation chamber connected to a molecular beam epitaxi (MBE) apparatus. This sample house is furthermore provided with a fast inlet for samples of different kinds carrying them directly into measuring position in front of the lens slit. There are altogether five different ways to introduce samples into different parts of the instrument.

The pump system consists of several turbo pumps arranged to achieve differential pumping in various parts of the instrument and a cryopump with high pump capacity (1500 ℓ/sec). For liquid studies of water solutions a special cool trap is justified.

Fig.23 shows a vertical view of another and smaller apparatus which is mainly designed for studying gases (gas cells) and molecular beams (supersonic jets). Since it is constructed for UHV performance surface studies can, however, also be performed. The cross section in Fig.23 shows an energy variable electron monochromator, in two subsequent steps (to avoid space charge limitation). This is identical to the one in the bigger instrument. The electron beam is crossing the vertical molecular beam. The inelastic scattered electron beam is analyzed, after passing the lens system, by a spherical analyzer with a radius of curvature of 36 cm.

Other radiation sources are situated around the sample house. There is polarized laser radiation (from two tunable lasers) pumped by an excimer laser crossing the molecular beam. The photoelectrons being produced by two-coulours resonance enhanced multi-photon ionization (REMPI) are directed into the same analyzer.

One can either use the analyzer or a time-of-flight arrangement which is attached to the back side of the analyzer. This is primarily intended for mass analysis of ionic fragments and for this purpose it is provided with a mass reflector to achieve high mass resolution /17/. For electrons, the reflector electrodes are adjusted from outside to be symmetrically located around the electron beam and used for additional focussing. The electron detector is then located further away along the tube.

Fig. 23

Side view of the second and smaller instrument. In this section one notices the analyzer with its lens system and a two-stage electron monochromator on the other side. At the back side of the analyzer an ion reflector is mounted for TOF mass spectrometry. It can be used also for TOF electron spectroscopy without the reflector. The laser beam is directed normally to the plane of the figure, crossing the molecular beam coming from a pulsed gas nozzle on top of the sample chamber. A UV polarizer is situated on the back side of the chamber along the direction of the laser beam.

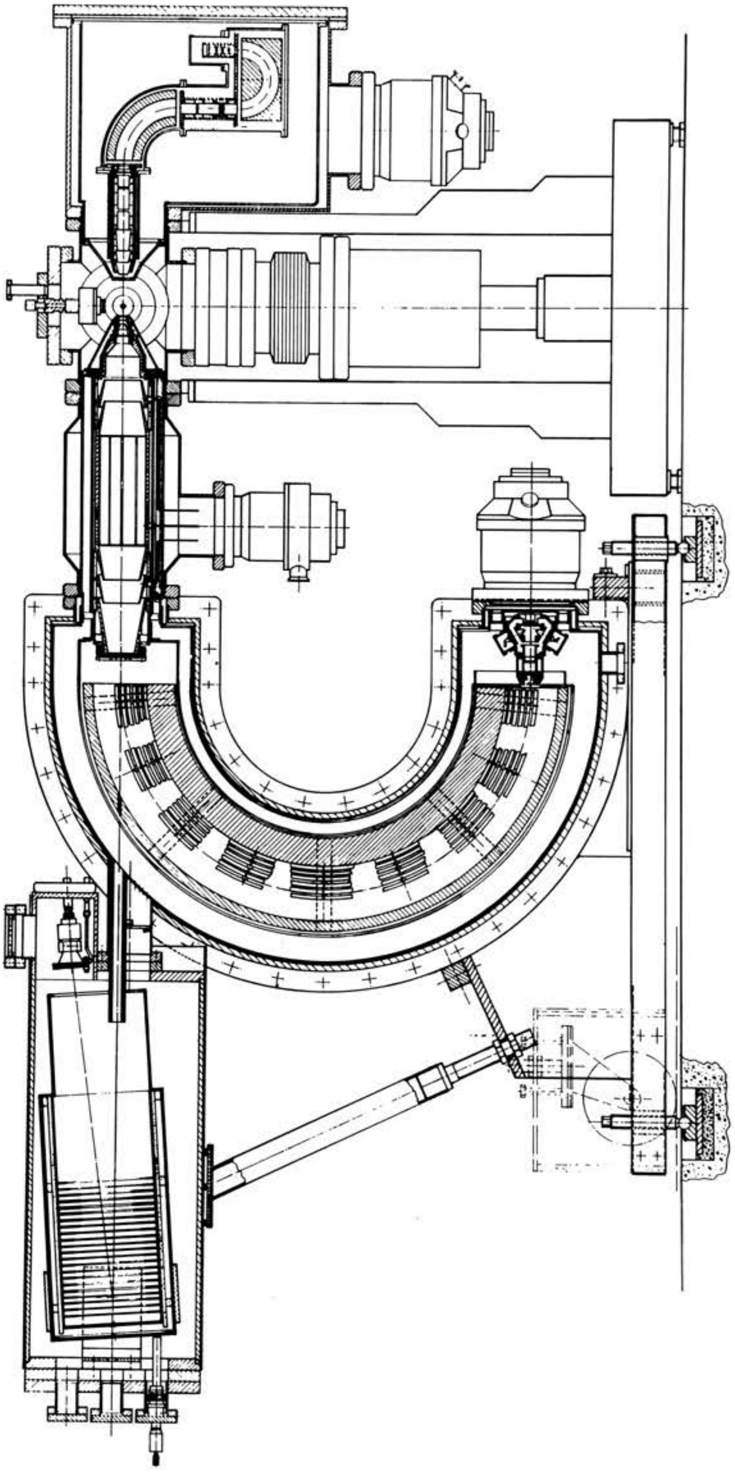

Fig. 23

The electron detector in the focal plane of the analyzer is normally an extended 6 cm long multichannel plate detector. It can be replaced by a Mott scattering detector (with an accelerating voltage of 20kV) to record the polarization of the electrons /18/. The intensity is then reduced by a factor of 1000. This alternative is shown in the figure.

Opposite to the laser beam entrance in the sample house there is a four-component UV polarizer which induces photoelectrons either in the molecular beam or in a gas cell. This polarizer can also be attached to the big instrument because of the adopted modular design concept. By rotating the polarizer around its axis the electric vector of the photons can be automatically turned around.

There are four further directions available for excitation or spectral studies around the sample house, one being e.g. an Auger electron gun, another an ion gun. A third flange can be used for optical fluorescence spectroscopy and a fourth for high intensity UV excitation close to the magic angle.

The system is flexible enough to enable other types of experiments to be performed. For gas or molecular beam experiments the top of the sample house is used for a pulsed gas nozzle inlet or gas cell introduction. For surface studies this space is available for an additional chamber including LEED etc. plus a sample manipulator. The main pump which accepts the molecular beam is a 1500ℓ cryopump.

An alternative to the above described experimental arrangement is shown in Fig.24, this time as a horizontal section. Here the instrument has been combined with a conveniently sized version of the previously described X-ray generator and monochromator or an external radiation source, such as synchrotron radiation. Again there are several alternative ports available for different sources of excitation and sample introduction.

Fig. 24

Top view of the instrument shown in Fig.23. This is an alternative mounting, where the same analyzer as in the previous figure is turned 90° to be in the horizontal plane. It can then be provided with a rotating anode and monochromator (RAMON). The UV polarizer is shown in this section.

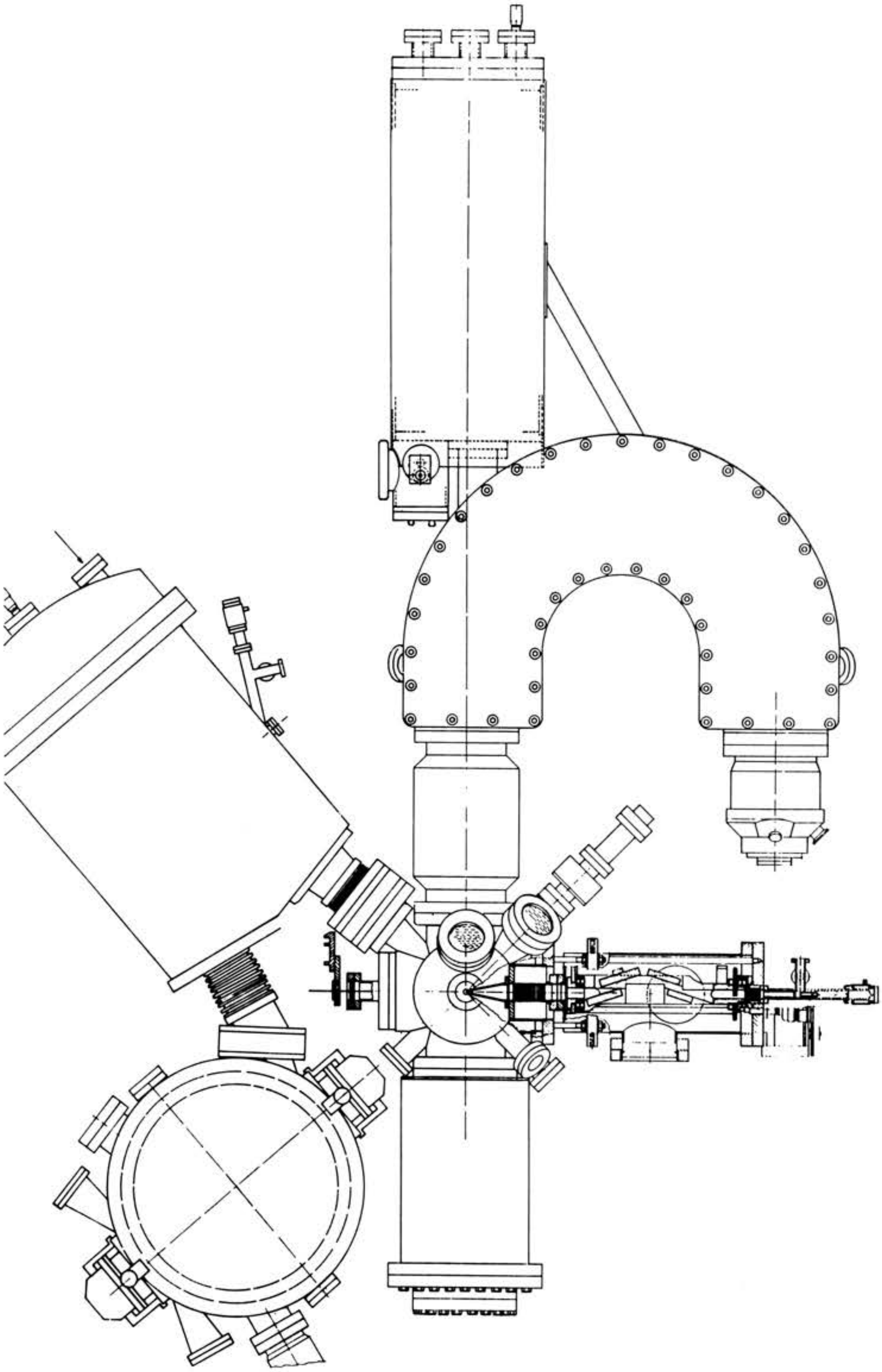

Fig. 24

4. Surface and interface shifts

In some cases the electron binding energy difference between the surface and bulk is sufficiently big so that, at high resolution, one obtains, for each level, two separate lines. Such shifts are not due to ordinary chemical shifts, e.g. due to oxidation as in Fig.9, but to the fact that the uppermost surface atoms do not have any neighbour atoms at the vacuum side, whereas the bulk atoms have neighbours on both sides. In the example given in Fig.25 /19/ the surface-bulk shift for Yb metal is 0.55 eV.

An application of this phenomenon can be found in the study of the diffusion of a surface layer into the bulk of a substrate. Fig.26 shows how this diffusion can be followed as a function of time in the case of a surface layer of gold being deposited on a bulk substrate of Zn, Cd and In /20/. The upper curves show the well-known gold doublet discussed before in Fig.6. After a while the intensities of

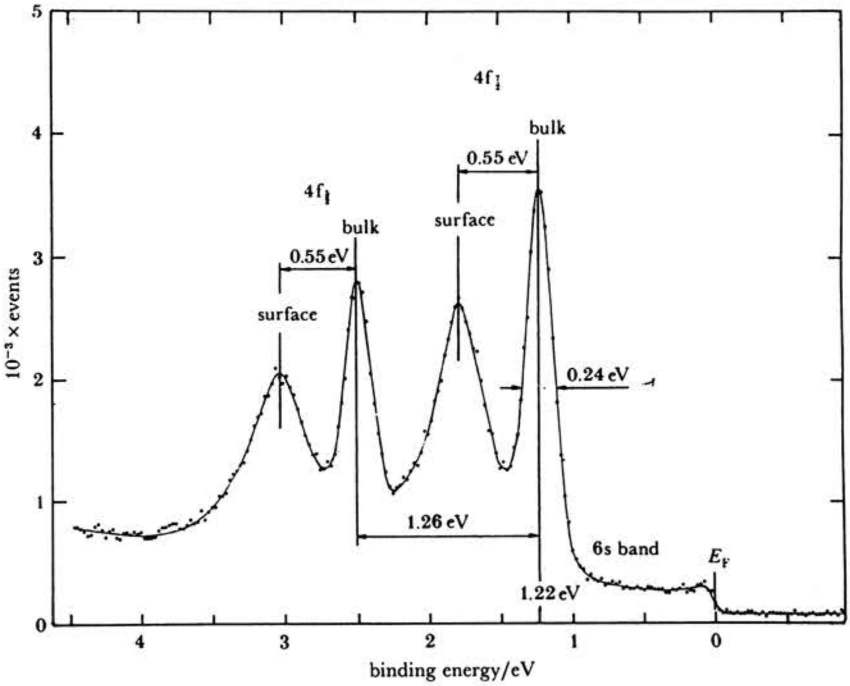

Fig. 25
Core level shifts between surface and bulk of the 4f levels in ytterbium at 300 K excited at hν=40.81 eV.

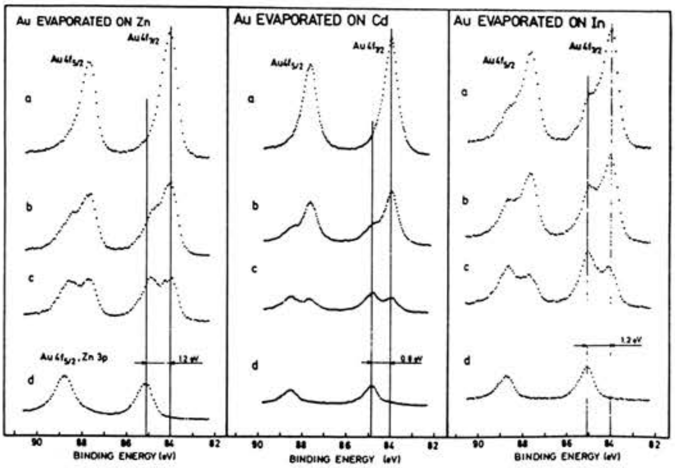

Fig. 26
Diffusion of evaporated Au into Zn, Cd and In as a function of time.

these lines decrease and two new lines appear somewhat shifted relative to the original ones. Finally, the original lines have disappeared and left room for a shifted doublet. The gold atoms are now situated in the bulk of the substrate metal.

As we shall see it is possible to reach interfaces slightly below the surface layer of a compound for inspection. In the cases when the top layer of interest consists of only a few atomic layers one can use the very soft X-radiation which can be conveniently handled and monochromatized by optical gratings (say <500 eV). In the more general case, when also the bulk composition is of interest, one example being an interface which is situated somewhat deeper in the bulk (>10Å), one should use harder X-radiation in order to increase the mean free path of the produced photoelectrons. This is a normal situation in practice and is usually encountered in semi-conductor investigations and studies of layered compounds. The relative surface sensitivity is then reduced but instead the depth sensitivity is increased. Alternatively, one has to remove by various means (e.g. ion bombardment) successively the outer atomic layers in order to reach the material in the bulk, e.g. an interface. This is a commonly used procedure but is also wellknown to present some problems which can cause interpretational complications. From this point of view it is useful to have access to harder, well monochromatized X-radiation

($\geq$1.5 keV) which was discussed in the previous section and to make use of the sample "tilting" method for depth composition scanning.

The experimental accuracy in the determination of electron peak positions have gradually improved to such an extent that the binding energies that can be extracted from electron spectra often can be given with errors in the 0.1 eV range and even less for metals and much less (1 meV) for gases. It is then of importance to carefully consider problems related to the choice of reference levels to connect electron spectroscopic data with other data. Core electron binding energies for a metal are measured relative to the Fermi level. In order to relate this binding energy to that referred to the vacuum level of the free atoms one should add a metallic work function ϕ.

One can also proceed by means of a thermochemical approach. One then assumes a complete screening of the positive hole left behind in the metal lattice at the photoelectron emission due to the good mobility of the conduction electrons. This is a generally accepted assumption in electron spectroscopy to treat the relaxation in metals. The 'equivalent core' model is extensively used. It states that the core ionized atom is treated as an impurity atom with nuclear charge Z+1. With these assumptions a Born-Haber cycle can be performed in accordance to a treatment by B. Johansson and N. Mårtensson /20-26/. One then connects the binding energy shift ΔE_C to macroscopically measurable quantities like the cohesive energies and solution energies in metals. ΔE_C is the shift between the metal core level referred to the Fermi level $E^M_{C,F}$ and the corresponding free atom referred to the vacuum level E^A_C according to (see Fig.27):

$$\Delta E_C = E^A_C - E^M_{C,F} \qquad (1)$$

The Born-Haber cycle gives the relation

$$\Delta E_C = I^{Z+1}_{(Z)} + E^{Z+1}_{coh} - E^{Z}_{coh} - E^{imp}_{Z+1}(Z) \qquad (2)$$

Here M denotes the metal, A the atom, C the core, F the Fermi level, Z the atomic number and I the appropriate valence ionization energy

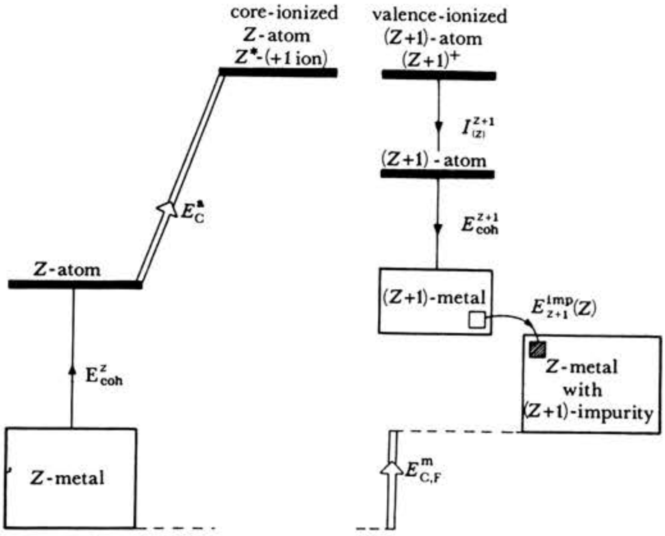

Fig. 27
The Born-Haber cycle for a metal connecting the binding energy shift between a metal core level referred to the Fermi level and the corresponding free atom referred to the vacuum level.

(usually the first ionization energy). E_{coh} is the cohesive energy and $E_{Z+1}^{imp}(Z)$ is the solution energy of the impurity atom (Z+1) in (Z) metal. The dominating contributions to the shifts are the difference in cohesive energy between the (Z+1) and Z metal and the ionization energy of the (Z+1) atom.

The same treatment as for metallic bulk can also be applied to surface core-level shifts. The surface atoms experience a different potential compared to the layers below because of the lower coordination number. This results in somewhat different core level binding energies. One can extend the previous Born-Haber cycle model to account for the surface-bulk core level shift. Empirically, the surface cohesive energy is approximately 80% of the bulk value. The result is then:

$$\Delta E_C^{S,B} = E_C^{surf} - E_C^{bulk} = 0.2\left(E_{coh}^{Z+1} - E_{coh}^{Z} - E_{Z+1}^{imp}(Z)\right) \qquad (3)$$

This equation obviously relates the surface chemical shift and the heat of surface segregation of a (Z+1) substitutional impurity in the Z metal.

In a recent investigation performed by N. Mårtensson et al. /27/ a quantitative study of metal-metal adhesion and interface segregation energies by means of electron spectroscopy was made. They were able to study layer dependent core level shifts for Yb epitaxially grown on Mo(110) for the first three layers. They used the surface sensitive 100 eV radiation from the MAX synchrotron. Well resolved Yb 4f lines could be recorded simultaneously for the interface layer between Yb/Mo, for the nearest bulk Yb and for the free Yb surface according to Fig.28.

These measured shifts provide new quantitative information on the energetics of adhesion and interface segregation which would be very difficult to obtain by other means. When making similar assumptions as above concerning screening etc. one arrives to an expression for the shift between the interface and the surface which reflects the effect of a free Yb surface when a Mo surface is adhered to it. This shift is denoted the "adhesion" shift ΔE_B^{Adh}. The shift between the interface and the bulk is denoted similarly the "interface" ΔE_B^{Int}. One finds that

$$\Delta E_B^{Adh} = \varepsilon_{Adh}^{Z^*,M} - \varepsilon_{Adh}^{Z,M} \qquad (4)$$

i.e. the adhesion shift is the difference in adhesion energy/atom of Z and Z* to the substrate. The appropriate quantitative comparison between experiment and theoretical treatment is performed in the above quoted paper.

Using Eq.(4) an adhesion energy difference of 1.15 eV/Yb atom is obtained which should be compared to the measured shift ΔE_B^{Adh}=1.19 eV.

The fact that at high resolution the various shifts between the surface layer, the bulk and the interface layer can be observed so distinctly as in Fig.28 is gratifying. Hopefully, the techniques may be applicable over other areas of the Periodic System even when the shifts are smaller. A necessary condition for this is that the required high spectral resolution can be achieved.

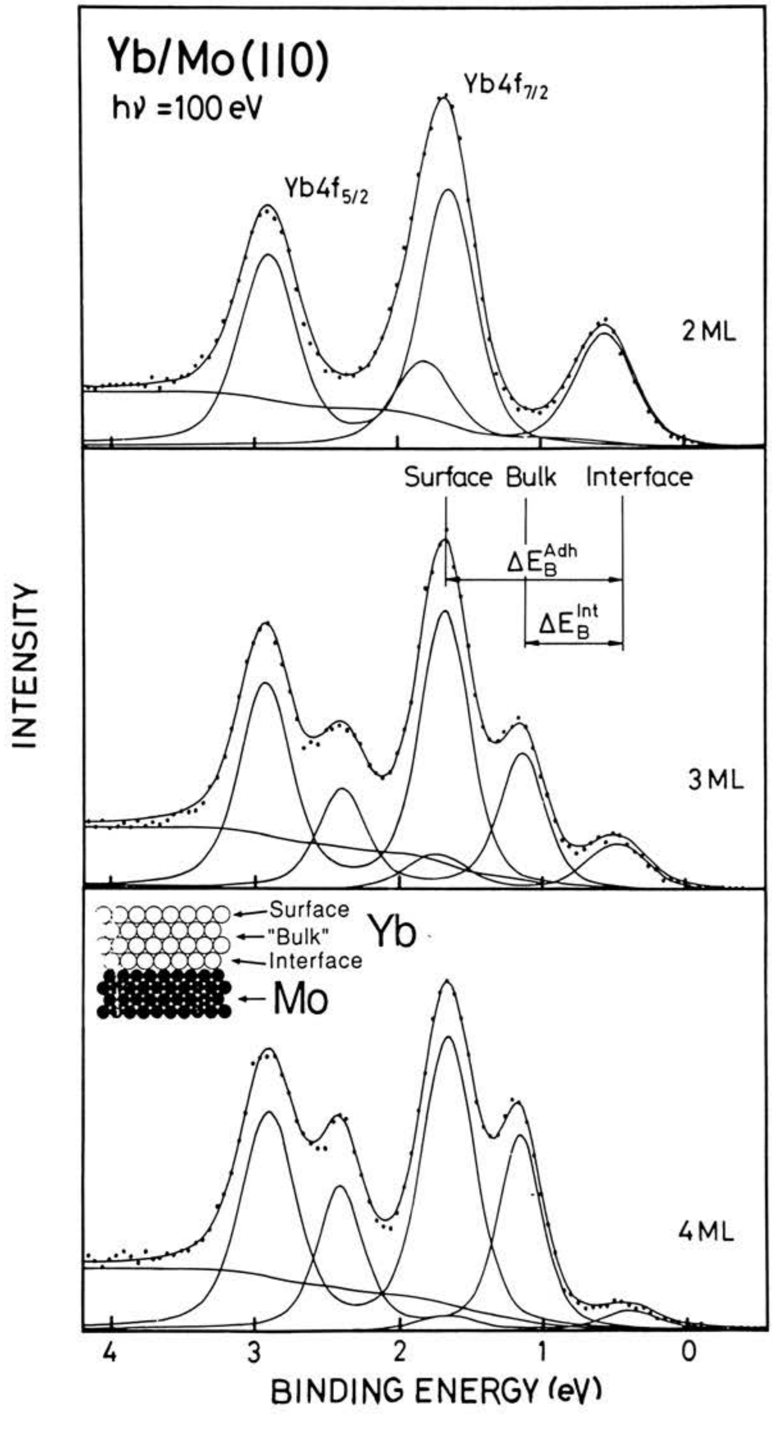

Fig. 28
Yb 4f electron spectra for 2, 3 and 4 monolayers of Yb deposited on Mo(110). Excitation at hν=100 eV synchrotron radiation.

A further interesting illustration of this quality is a recent finding by A. Nilsson and N. Mårtensson /28/. A closer inspection of the line forms (and also positions) at high resolution (AlKα, $\Delta h\nu=0.2$ eV) of adsorbates reveals temperature dependent vibrational effects which can be correlated to the actual sites of the adsorbed molecules on the substrate surface. They observe extra line broadenings on the "wrong" sides of the core lines (i.e. on the high energy side) of oxygen and carbon, when CO is adsorbed on a clean N(100) surface.

This phenomenon corresponds to hot bands in UV excited free molecules and is consequently temperature dependent. The magnitude of this broadening can be explained as due to strongly site dependent vibrational effects which are coupled to the final state energies of the adsorbate through vertical transitions at the ionization. Other possible effects for line broadenings have previously been discussed as results of soft electron-hole pairs emission within a $2\pi^*$-derived resonance at the sudden perturbation of the core hole. The effects observed by Nilsson and Mårtensson seem to be of a different origin and if so could have interesting implications not only for detailed surface studies by means of photoelectron spectroscopy but also for other surface methods like NEXAFS and photon induced desorption.

Recently, a new and faster alternative to the conventional all semiconductor npn transistor has been proposed. This substitutes a very thin layer of metal for the base of a standard transistor, thereby strongly reducing the transit time for electrons from collector to emitter. For such an optimized SMS transistor the theoretical cut-off frequency could be as high as 30 GHz instead of 4 GHz for a GaAs transistor. This SMS transistor consists of a thin layer of cobalt disilicide sandwiched between two thicker layers of silicon, serving as emitter and collector enclosing the $CoSi_2$ base.

Another possible choice is to use a platinum silicide. Previously the metal-GaAs interface has been studied by electron spectroscopy /29-32/ with the localized core levels used to trace the band bending of the valence band at the interface. For a silicon-silicide interface, however, the problem presented is more difficult because the metal phase itself, which is the platinum silicide, contains silicon that has to be distinguished from the semiconductor silicon. A high resolution is then necessary.

In an investigation in our laboratory /33/ this problem was studied at a resolution of the monochromatized AlKα line (1487 eV) of ca 0.23 eV. It was then possible to resolve the semiconductor $Si2p_{3/2}$ core line from the silicide Si2p lines of the Si-Pt silicide sample. In this way a direct determination of the Schottky barrier could be made. At this resolution the electron spectrum revealed that the silicide consisted of two chemically different forms, namely PtSi and $PtSi_2$. The spectra showed that on top of the silicide there was a layer of mixed silicon oxides. It was also found that this oxidation took place more easily than for clean Si surfaces, indicating that the presence of metal atoms in the underlying silicide layer might have a certain catalytic promoting influence on the oxidation of silicon.

The ESCA shifts can to a first approximation be interpreted as corresponding to the potential shift connected with the rearrangement of the valence electron density. In this way one can by means of ESCA trace the potential distribution that causes the Schottky barrier for a particular metal-semiconductor interface and one can actually measure its value, which in this case was found to be 0.82±0.05 eV. This fits neatly to what has been found by others for PtSi-Si junctions with other methods.

The principle of the measurement of the Schottky barrier is illustrated by Fig.29. The barrier height ϕ_B is obtained by subtracting the distance between the Fermi level and the silicon valence band from the band gap. From the figure,

$$\phi_B = E_g - E_B^{INT}(Si2p) - \Delta E \qquad (5)$$

From an experimental point of view it is necessary that the silicide film is thin enough and that the excitation radiation is hard enough so that the Si bulk line is still observed. The energy resolution at

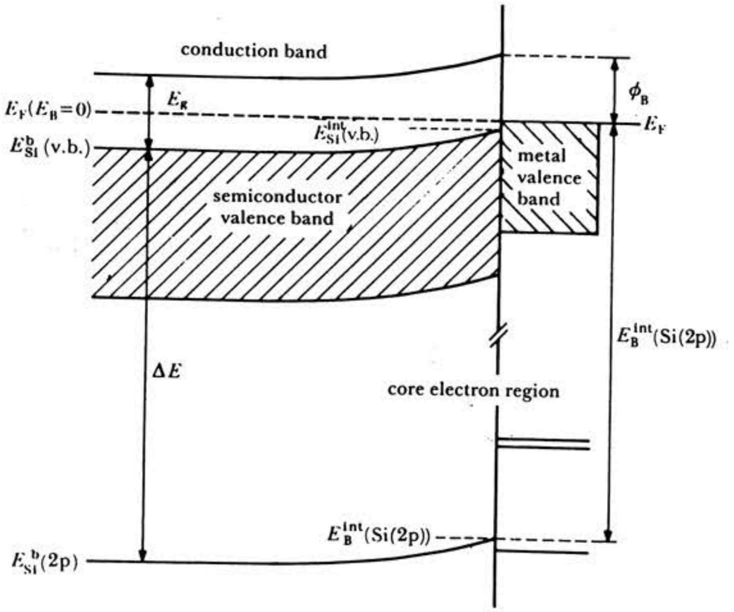

Fig. 29
Principle of ESCA measurement of a Schottky barrier ϕ_B. The abbreviation v.b. is for valence band;
subscripts F, b and g are for Fermi, bulk and gap, respectively;
superscript int is for interface.

the required fairly high photon energies (in this case 1487 eV) is sufficiently high to resolve the Si bulk line from the other Si2p lines and to allow the observation of the sharp Fermi edge.

As emphasized above in surface science not only the top layer but also the composition and the chemical bonds between atoms close to and below the top surface layer are of importance. When some element has a concentration profile within the electron escape depth, i.e. when there are surface layers of different composition with a thickness less than the escape depth, the peak amplitude of that element shows a dependence of the exit angle. The surface concentration profile, in accordance with the previous example can then be investigated.

Another such a study which was of medical interest dealt with blood-compatible surfaces /34,35/. The systems studied were colloidal heparin, or dextran sulphate stabilized with hexadecyl ammonium chloride, deposited onto steel substrates, and chemically related substances. By using the mentioned angular dependence (tilting) techniques, it was found that the intensity ratio for the S2p peaks from disulfide and sulphate exhibit angular dependence for albumin-covered heparin-glutar and dextran sulphate-glutar surfaces. This indicate that the disulfide groups are positioned closer to the external surface than the sulphate groups.

In a series of experiments on a similar problem cationic polyethyleneimine was adsorbed on sulphated polyethylen surfaces at different pH, varying from 4.0 to 9.0. From the angular dependence of the amine:protonated amine peak ratio (see Fig.30) it was possible to conclude that there was an accumulation of charged amine groups towards the sulphate surface at high pH. The angular dependence of the intensity ratio N/N^+ (neutral amine:protonated amine) furthermore showed that adsorption at pH 4.0 gave a higher relative amount of charged

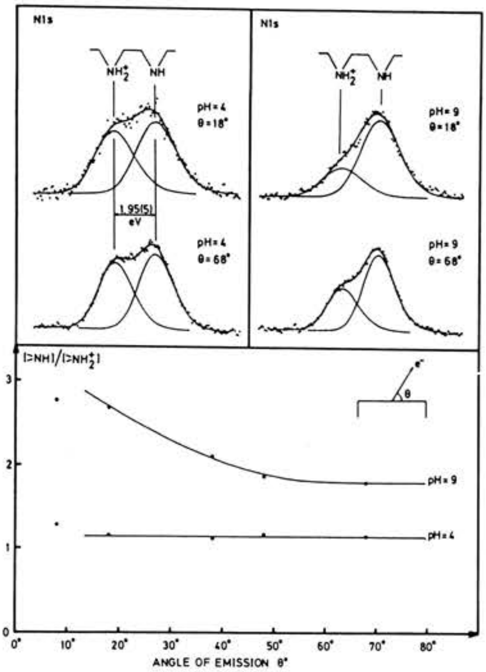

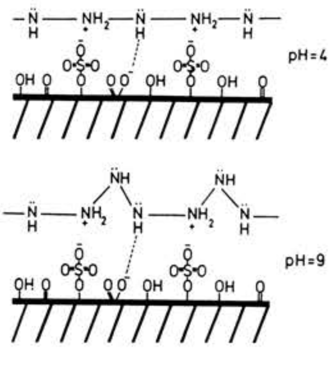

Left: Angular dependence of surface layer lines.
Above: Construction of surface composition.

Fig. 30
Angular dependence of a surface layer of amino-protonated-amine and the resulting surface construction.

groups and that this amount was independent of the exit angle. Adsorption at pH 9.0 gave a relatively larger amount of neutral amine groups and a N/N^+ ratio that was dependent on the exit angle.

A straightforward interpretation of these results is that the configuration of PEI when adsorbed at pH 4 is essentially flat on the surface while adsorption at pH 9.0 gives a 'layered' configuration with the charged groups (N^+) closer to the sulphated surface and the neutral groups further out according to the right part of Fig.30. The fact that the number of charged amino groups remains constant leads to the conclusion that the adsorption could be considered as an ion exchange reaction. The results also imply that polymer surfaces with different densities of sulphate groups would adsorb different amounts of PEI. So it would be possible to make polymer surfaces with different densities of amine groups not only by adsorption at different pH but also by varying the sulphate group density.

Core-level binding-energy shifts at surfaces and in solids have been reviewed by W.F. Egelhoff Jr. /36/.

5. Studies of gases by monochromatic X-radiation

Electron spectra of gaseous molecules are favourable to study at good resolution since the usually occurring additional solid state broadenings in bulk matter is absent. Furthermore, the energy calibration procedure is simplified by the possibilities of mixing the sample gas with conveniently chosen standard calibration gases. Fig.31 is an example of how this is performed /37/. It is an aromatic molecule with a fluorine and an amino group attached to the benzene ring in para position, para-aminofluorobenzene. In order to study the chemical shifts in this compound CF_4, N_2 and CO_2 were mixed with the sample gas. In the spectrum one can determine the chemical shifts accurately. Even the different carbons in the benzene ring can be distinguished, namely those which are neighbours to the substituents.

As an example of an electron spectrum of a gaseous phase and how it changes at condensation we take mercury /13/. If a droplet is intro-

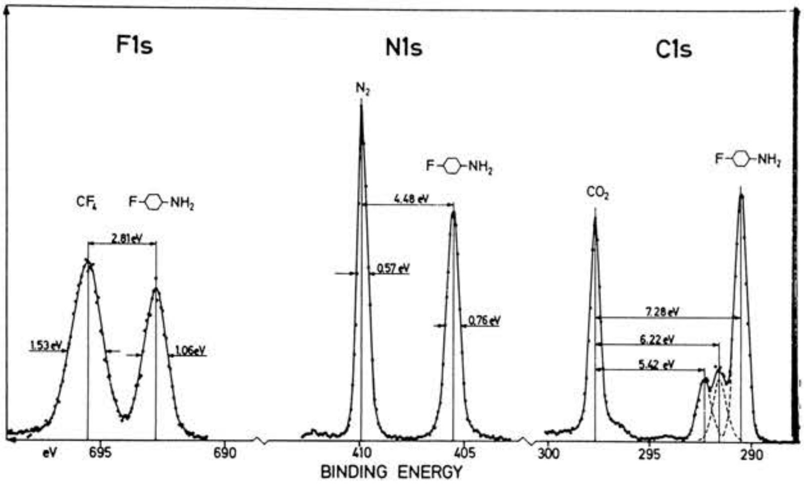

Fig. 31
The core electron spectrum of gaseous para-aminofluorobenzene. CF_4, N_2 and CO_2 have been used as calibration gases mixed with the gas sample under study.

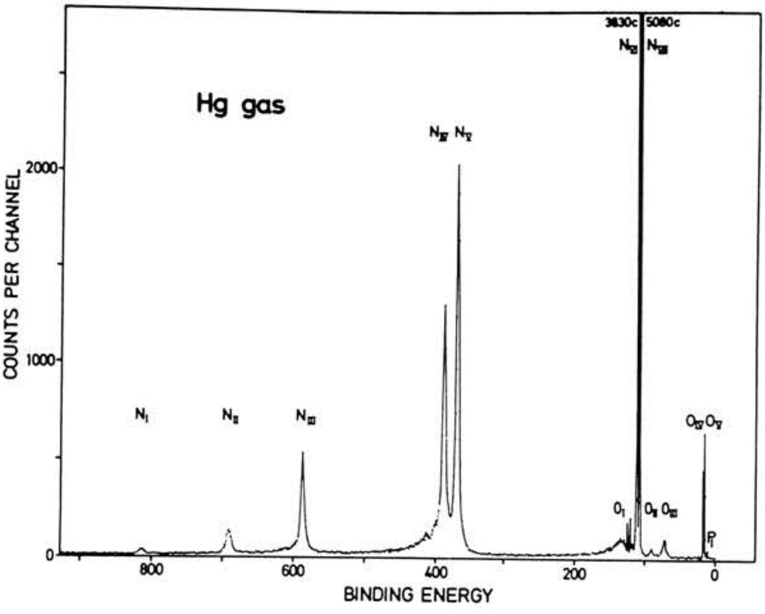

Fig. 32
Electron spectrum of Hg vapour by means of AlKα excitation.

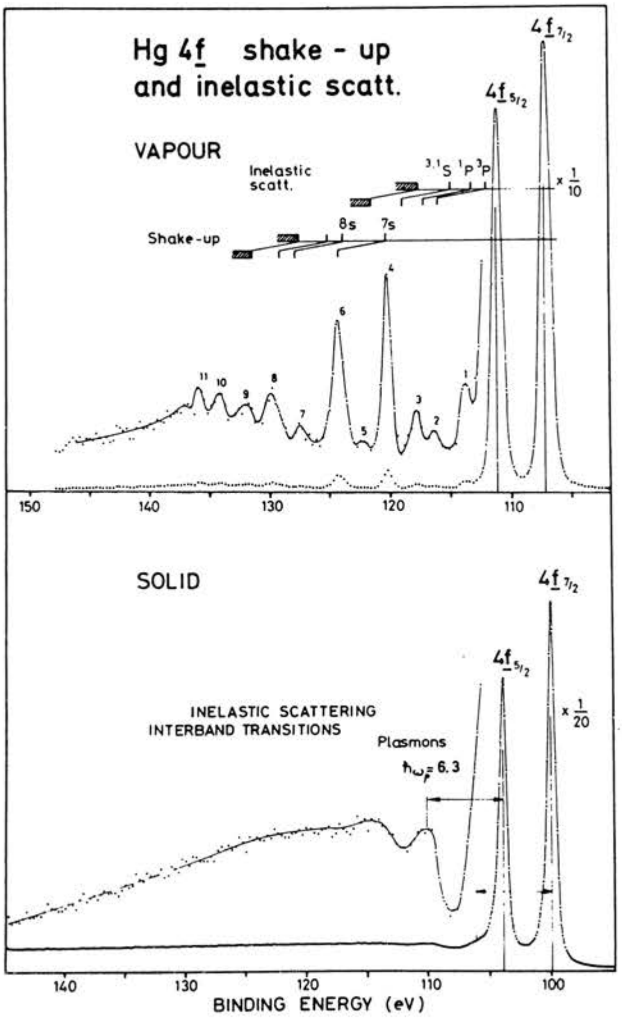

Fig. 33

Shake-up spectrum of Hg N_{VI}, N_{VII}. The first few lines are due to inelastic scattering (pressure dependent) in the mercury gas. Remaining lines are due to the internal excitation of the mercury ion (shake-up). Lower figure shows the same part of the spectrum after condensation.

duced into the electron spectrometer the vapour pressure at room temperature, ca 10^{-3} torr, is sufficient to produce a spectrum. This is shown in Fig.32. All levels in the Hg atom which can be reached by the AlKα radiation are recorded. The line widths in the spectrum are the inherent atomic widths.

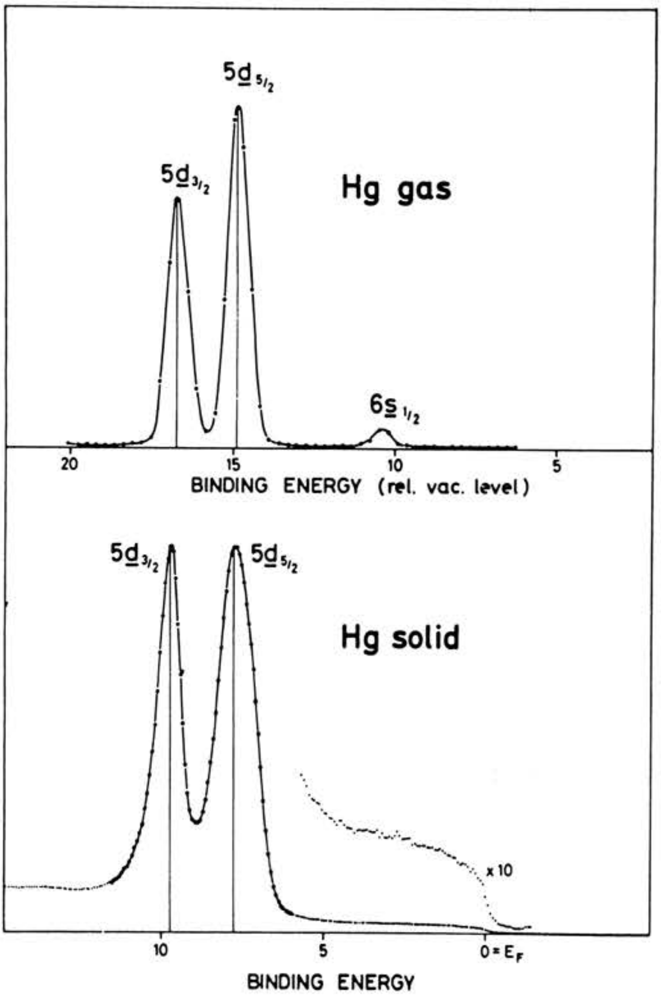

Fig. 34
The effect of condensation on electron lines close to zero binding energies. Upper spectrum from Hg vapour, lower spectrum from solid Hg.

Many of the lines are followed by more or less observable satellites. These are due to "shake-up" phenomena during the photoelectron emission process /38/ or to inelastic sattering of electrons. A typical example is given in Fig.33 for two of the main lines in the mercury spectrum /13/.

Close to zero binding energy one observes a group of lines denoted by O_{IV}, O_{V}, P_{I}. Fig.34 shows an enlargement of this group, in the gaseous phase (upper figure) and when the Hg vapour has been condensed on a "cold finger". One observes a broadening of the lines in the condensed phase. This is due to the "solid state broadening" caused by the mutual influence of the closely spaced atoms. A particularly dramatic effect is observed for the P_{I} (or 6$\underline{s}$) level which experiences a continuous spreading with a well defined edge on the high energy side. This is the Fermi edge of the conduction band of mercury which consequently is due to the seemingly unimportant atomic P_{I} line in the gas phase spectrum.

6. Conduction and valence bands

The previous example directs our attention to the valence region. This can be studied at different excitation energies. It is usually advisable to use fairly high excitation energy to avoid possible mixing with states close to the band edge. At sufficiently high excitation energy the shape of the band electron spectrum starts to converge. At low excitation energies the shapes reflect interesting phenomena which are indeed important. There exists a lot of information from such studies /39-42/ but we will not discuss these here. We will only give some typical examples of bands obtained at high excitation energy, namely with AlKα at 1487 eV ($\Delta h\nu$=0.2 eV. Fig.35 shows the conduction band of gold taken at high resolution and Fig.36 the corresponding band of silver. Both show characteristic structures which reasonably well can be reproduced by density of states calculations.

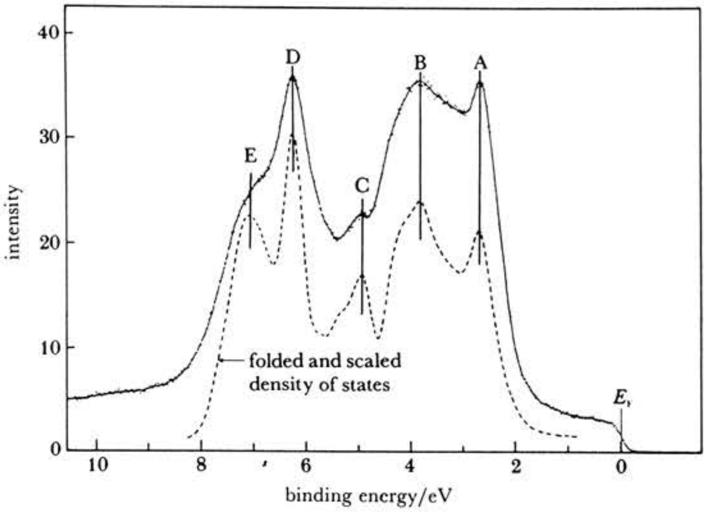

Fig. 35

The conduction electron band of gold. Monochromatic AlKα excitation ($\Delta h\nu = 0.2$ eV).

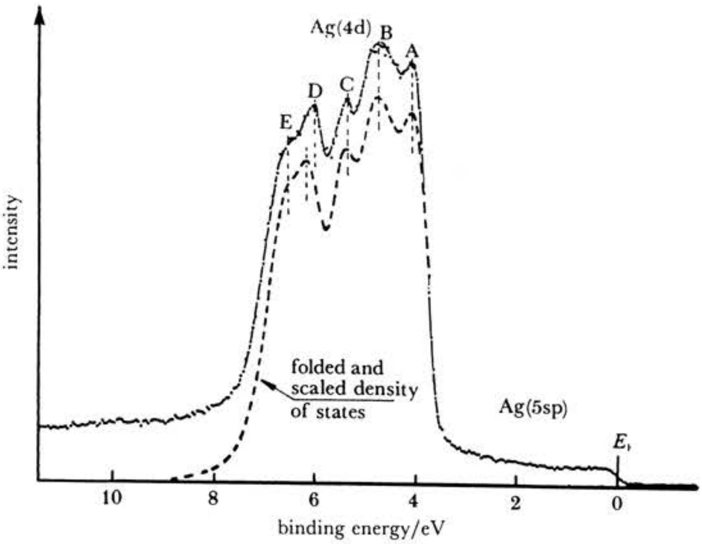

Fig. 36

The conduction electron band of silver. Monochromatic AlKα excitation ($\Delta h\nu = 0.2$ eV).

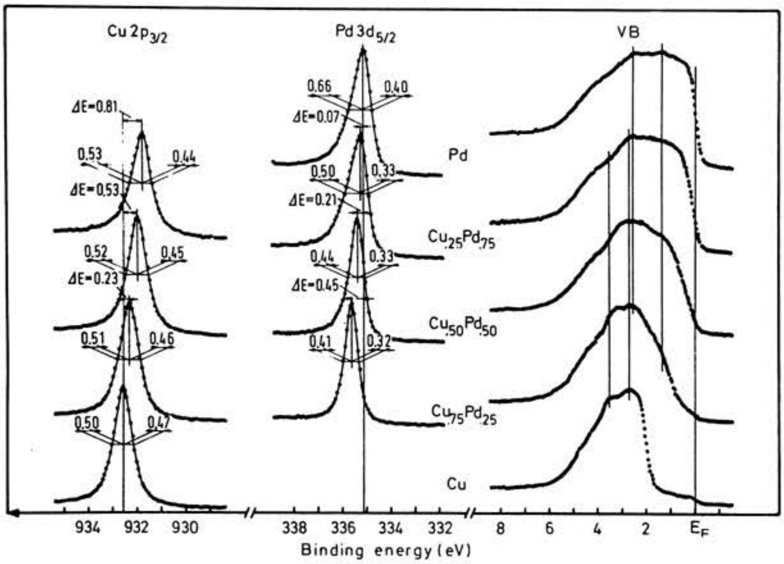

Fig. 37
$Cu2p_{3/2}$ and $Pd3d_{5/2}$ and the conduction bands for the pure metals and for different compositions of these alloys. The Pd core lines are asymmetric due to excitation of electron-hole pairs in the conduction band. The Cu core lines are almost symmetric. The conduction bands as well as the core lines are changing at alloying.

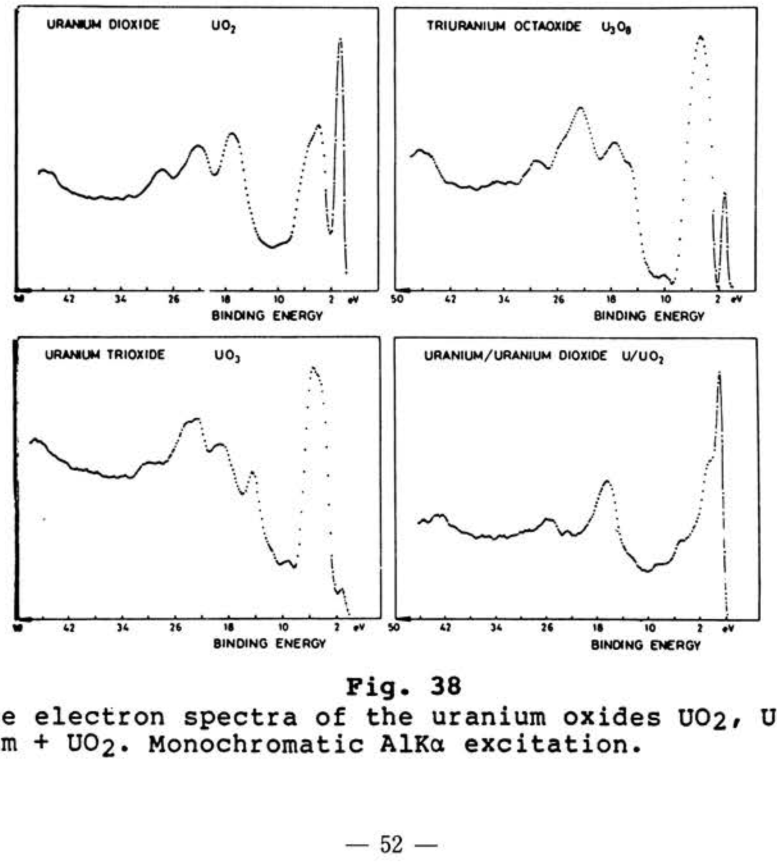

Fig. 38
The valence electron spectra of the uranium oxides UO_2, UO_3, U_3O_8 and uranium + UO_2. Monochromatic AlKα excitation.

Electron spectroscopy has been applied also to alloys, semiconductors and insulators. Fig.37 is an example of the conduction bands of palladium and copper and their alloys at different compositions /13,43/. One observes the shifts of the core levels at alloying and also changes in level widths and line asymmetries. The conduction band gradually changes from one pure metal to the other.

The valence spectrum of the different uranium oxides UO_2, UO_3, U_3O_8 and uranium + UO_2 are shown in Fig.38. They are examples of semiconductors and insulators and exhibit quite different spectra /44/.

Empty bands can be studied by the techniques mainly developed by V. Dose. One then makes use of the reverse photoelectron effect, i.e. an impinging electron beam is varied in energy until photons of a certain energy is appearing in a detector. We refer here to recent accounts due to V. Dose /45/, N.V. Smith /39/ and F.J. Himpsel /46/.

7. Excitation of gases with UV radiation

It is particularly advantageous to use VUV radiation from rare gas discharge lamps which contain a large number of sharp and intense UV lines for excitation of electron spectra from the valence regions of molecules /47/. Fig.39 shows the valence electron spectrum of CO_2 /42,43/. One can notice the vibrational structure of the molecular ion. In favourable cases even the rotational fine structures are visible.

In order to observe such finer details one has to go to the very limit of resolution. This limit is set by several independent factors, both due to the lamp conditions and the sample gas itself. In the lamp the most important contributions are due to Doppler broadening, self-reversal and self-absorption. The lamp gas and the interior of the lamp has to be very clean. It is advantageous if a discharge can be maintained at very low gas pressures, for example by means of a magnetically confined microwave discharge tuned to the electron cyclotron resonance condition. In the sample gas the main contributions come from the space charge caused by the produced ions and furthermore

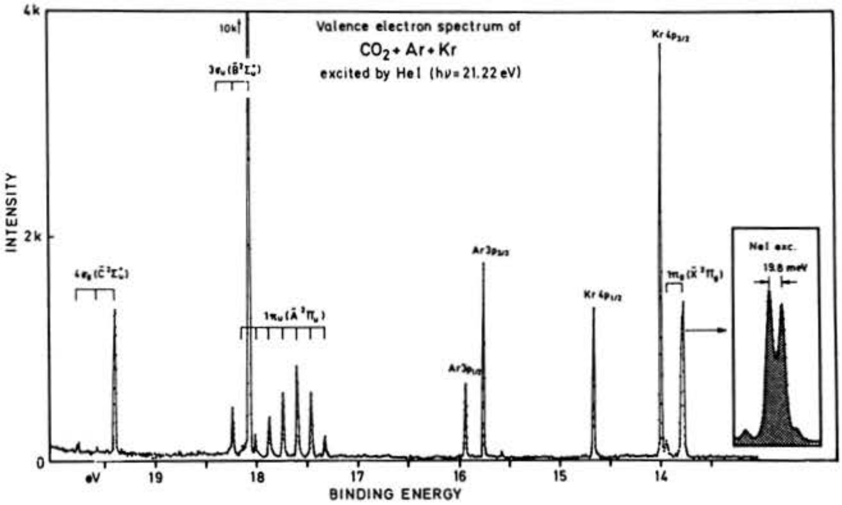

Fig. 39
HeI at 21.2182 eV (and NeI) excited valence electron spectrum of CO_2.

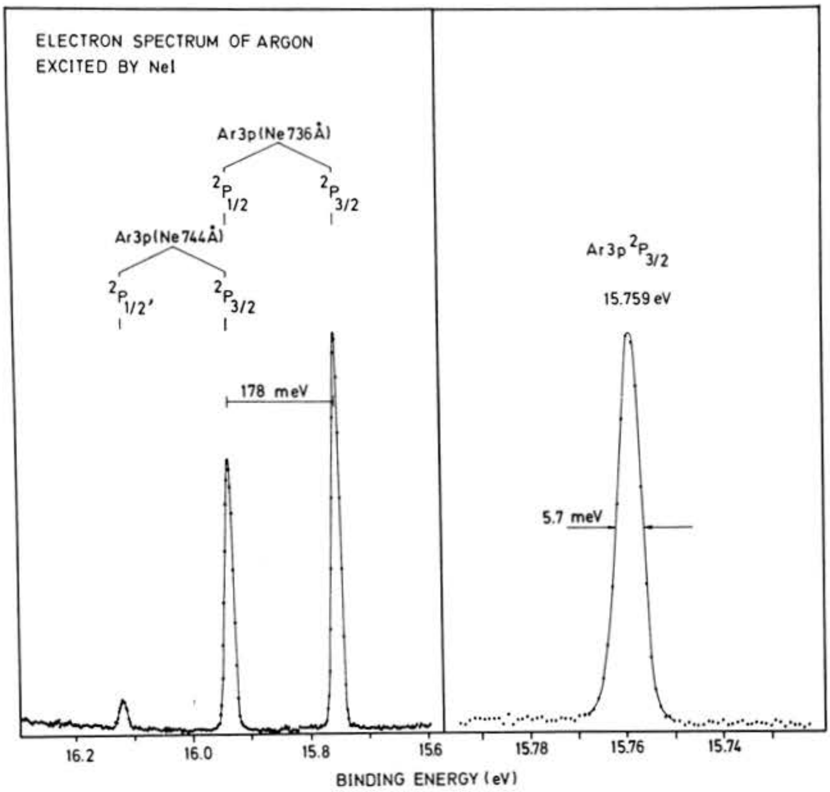

Fig. 40
3p doublet electron lines from Ar gas excited by NeI ($h\nu = 16.8483$ and 16.6710 eV). To the right: Light source and spectrometer adjusted for max resolving power of 5.7 meV.

from external electric gradients over the sample. Rotational fine structures usually result in unresolved line envelopes. The space charge effect is a main obstacle particularly in the case of pulsed laser excitation but also in other cases and special schemes have to be used to minimize these effects. The spectrometer resolution itself is naturally a further limiting factor.

Presently, the resolution for UV excitation is normally not much better than 10 meV but can be improved to around 5 meV. Fig.40 shows an example of the latter case for argon when NeI has been used for excitation /15/. It is likely that this limit can be improved further by using supersonic jet beams, better light sources, precautions as to the sample conditions and the surroundings etc.

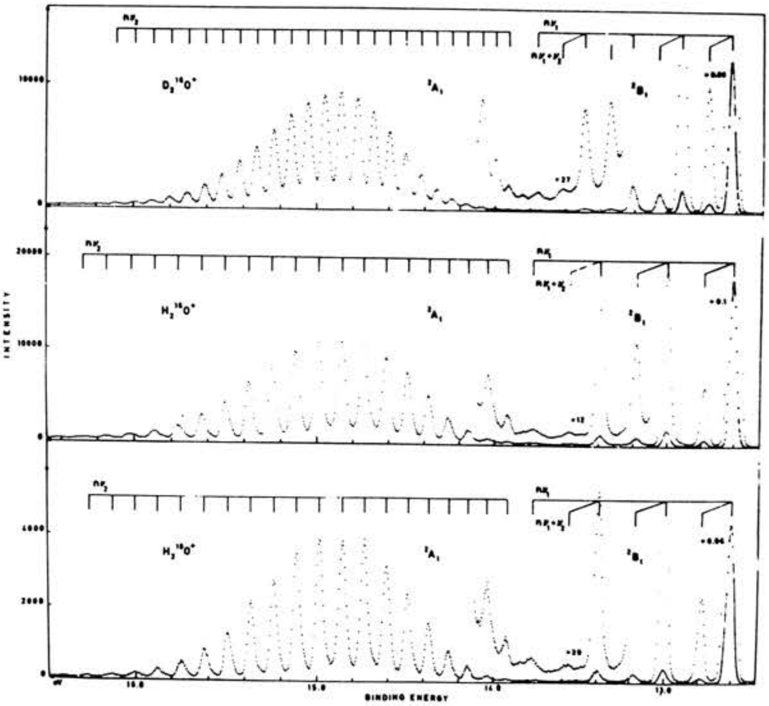

Fig. 41
The electron bands of $D_2{}^{16}O$, $H_2{}^{16}O$ and $H_2{}^{18}O$, corresponding to ionization in the $1b_1$ and $2a_1$ orbitals. For the $^2A_1$ state a vibrational progression of the ν_2 bending mode consists of 20 members. The difference between H_2 and D_2 is obvious. Also, there is a small but measurable difference between O^{16} and O^{18}.

Fig.41 shows the HeI excited valence electron spectrum of H_2O vapour /13/. The resolution in this case was enough to distinguish isotopic differences between H and D and O^{16} and O^{18}. Also rotational structures can be observed in this and some other cases.

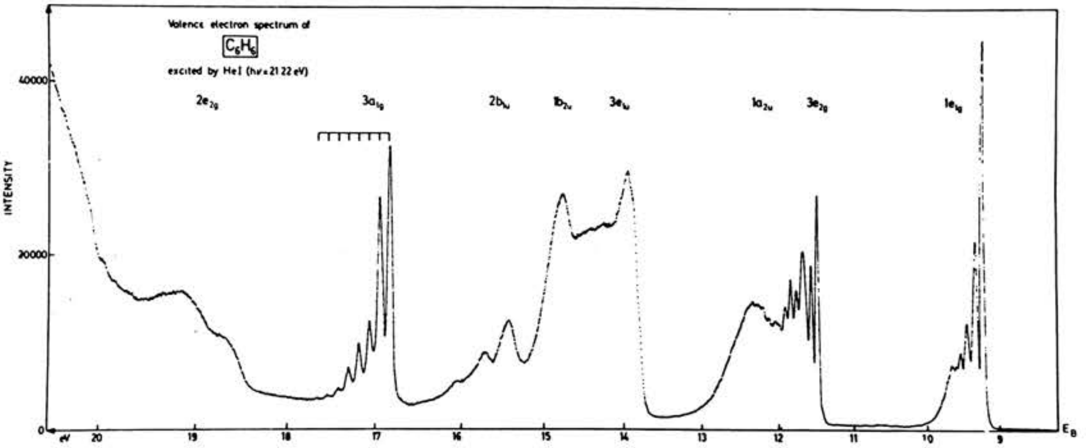

Fig. 42
Valence electron spectrum of benzene, excited by HeI. Scan spectrum.

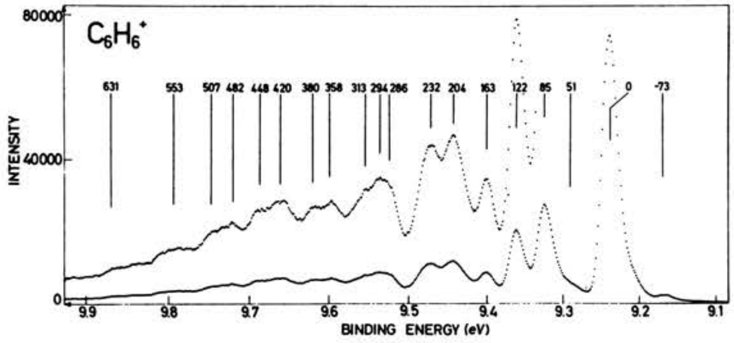

Fig. 43
High resolution spectrum of the outermost orbital $1e_{1g}$ electron lines in benzene. Observe the recorded detailed structures compared to the corresponding scan spectrum in Fig.42. A challenge for future to resolve this structure further.

Fig.42 shows the spectrum of benzene excited by HeI radiation /37/. An expanded, high resolution study of the last band $1e_{1g}$, around 9.5 eV is shown in Fig.43. It is a challenge for future to try to resolve such structures which are presently dominating features in UV excited photoelectron spectroscopy. Improved spectroscopical techniques are required.

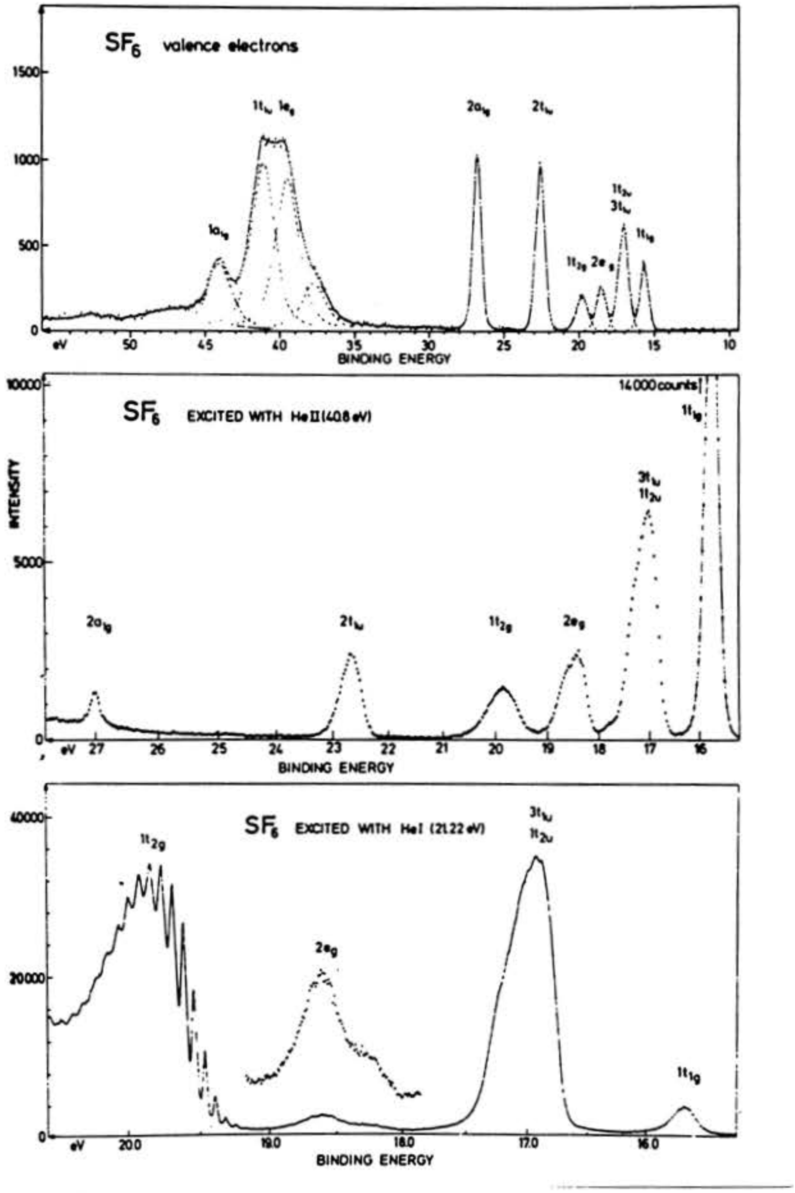

Fig. 44

The valence electron spectrum of sulphur hexafluoride excited by AlKα at 1486.7 eV ($\Delta h\nu=0.2$ eV), HeII at 40.814 eV and HeI at 21.218 eV, respectively.

Observe the large variations of the relative intensities, in particular the $1t_{1g}$ line, showing a resonance.

Finally we show the influence of the energy of the exciting radiation on the appearance of the valence orbital spectrum /37/. Fig.44 is the complete valence spectrum of SF_6 excited by AlKα ($\Delta h\nu$ = 0.2 eV) (upper spectrum). The middle spectrum shows the region 15-28 eV excited by HeII at 40.8 eV. The lower spectrum the region 15-21 eV excited by HeI at 21.22 eV. One observes the large variations of the relative electron line intensities when the energy of the exciting radiation is varied. In particular the $1t_{1g}$ electron line experiences a large increase in intensity going from AlKα to HeII excitation and then a remarkable decrease in intensity going from HeII to HeI excitation. A general rule found in experimental studies of spectra excited by AlKα on one hand and UV on the other is that the former (harder radiation) enhances s-like molecular orbitals, whereas the latter (softer) p-like orbitals. These wavelengths dependent intensity rules can be quantified and are applicable over quite extended energy regions.

8. Vibrational fine structures in core electron and X-ray emission lines

The importance of monochromatization of the exciting radiation and resolution in core electron spectroscopy is further exemplified in Figs.45 and 46. They show the C1s line in CH_4 at modest and high (monochromatized radiation) resolution /15/, respectively. The slightly assymetric 1s line in the first figure splits up at high resolution into three (actually a fourth line can also be seen) well resolved lines. This splitting is caused by the vibration produced when a core electron of the centrally located carbon atom is emitted. The new equilibrium corresponds to a shrinkage of about 0.05 Å, and the Franck-Condon transitions which take place then give rise to the observed vibrational fine structure with intensities given by the Franck-Condon factors.

The existence of vibrational fine structures as a result of electron emission from molecules initiated a series of experiments in our laboratory in 1971 to look for similar effects in ultrasoft X-ray emission /48/. For this purpose a specially designed grazing incidence spectrometer with electron excitation in a differentially pumped gas cell was constructed. The first observation of this vibrational

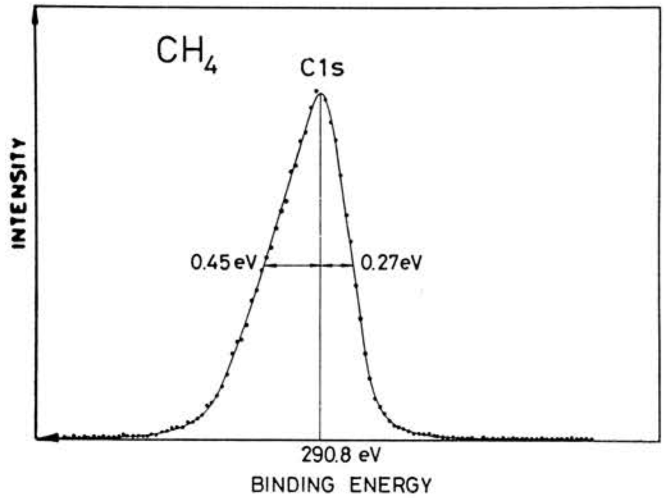

Fig. 45
C1s of gaseous CH_4 with monochromatization of the AlKα radiation but at moderate spectral resolution.
The core line is observed to be slightly asymmetric.

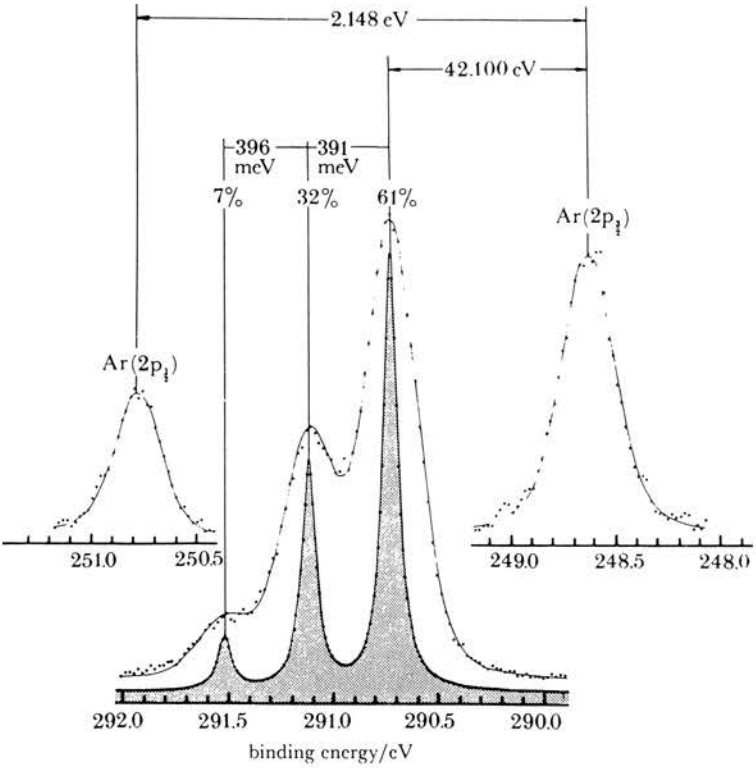

Fig. 46
C1s of gaseous CH_4 with monochromatized ($\Delta h\nu = 0.2$ eV) AlKα-radiation and at high spectral resolution. The line is split up in core vibrational components which now can be subject to a more detailed deconvolution procedure using simultaneously recorded Ar lines as "window curves".

fine structures in X-ray emission spectra for free molecules was found for nitrogen gas /49/. Fig.47 and 48 show a photographic recording and a photometer diagram of this phenomenon.

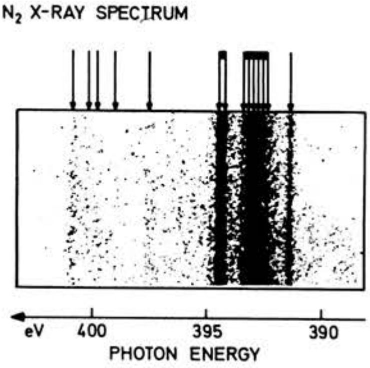

Fig. 47
X-ray emission spectrum of nitrogen gas, showing vibrational structures from resolved valence orbitals.

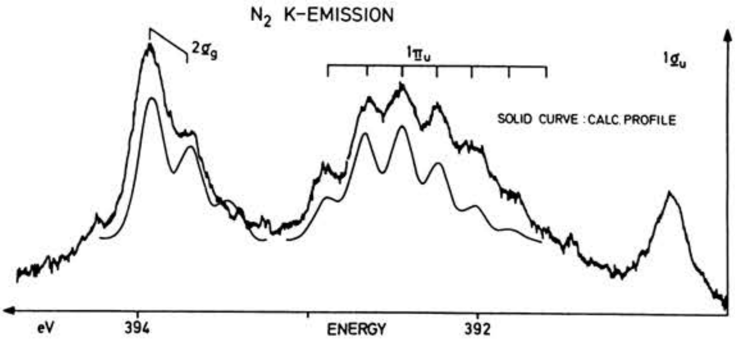

Fig. 48
Photometer curve for the nitrogen X-ray spectrum with calculated line profiles.

Similar investigations were undertaken for a number of other small molecules. Fig.49 can illustrate this in the above mentioned case of CO_2 /50/. An analysis can be performed assuming different atomic distances and the best fit to experimental data yields the new equilibrium for the ion in question. More recently this field has been much developed by J. Nordgren et al. with applications also in new areas of research /51,52/.

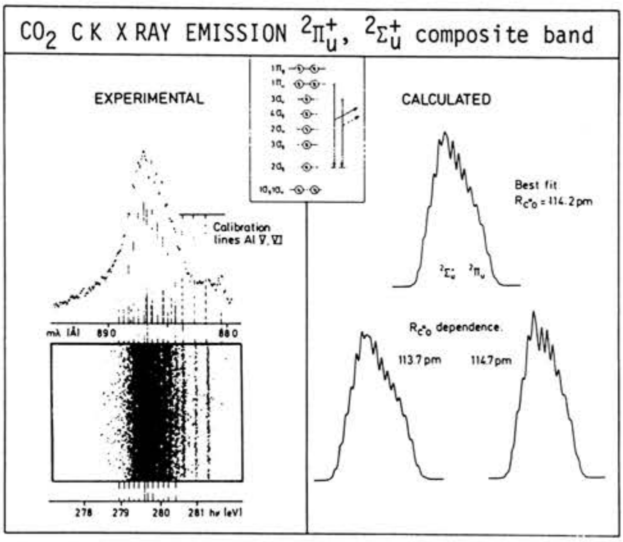

Fig. 49

Vibrational structure of the CK X-ray of CO_2.

9. Angular distributions

The angular distribution of photoelectrons from free molecules or from surfaces are of importance, since these data give information on the symmetry properties of valence orbitals and, in the case of surfaces, on the geometrical arrangements of adsorbed molecules on the crystal substrates.

Fig.50 shows the principle of such an experiment when linearly polarized UV radiation, for example HeI at 21.21 eV, is used for the excitation of the photoelectrons. Photoelectrons from an $n\sigma$ orbital can according to selection rules result in $\varepsilon\pi$ or $\varepsilon\sigma$ final orbitals. If the photons are directed along the axis of the CO molecule, taken as an example, only the $\varepsilon\pi$ alternative is possible. Turning the plane polarized electric vector of the photon beam around and recalling that the $\varepsilon\pi$ orbital has a maximum along the electric vector and a nodal plane perpendicular to this direction one should be able to record a zero amplitude in the photoelectron intensity when the elec-

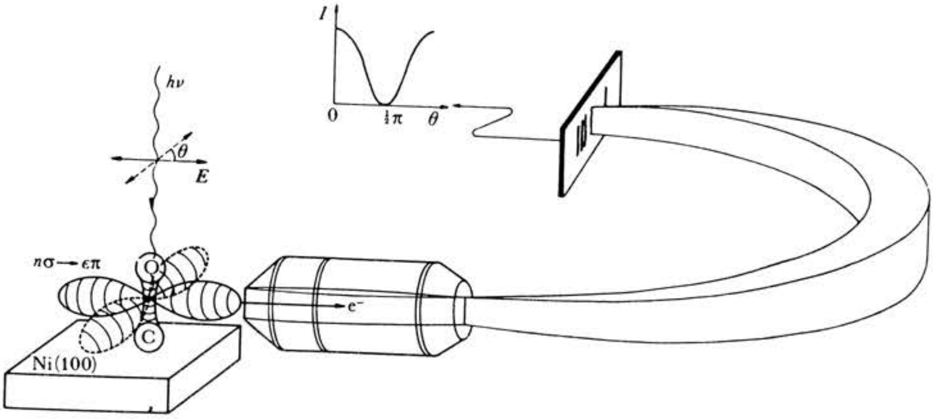

Fig. 50
Principle for using polarized photons to determine the geometry of adsorbed molecules on a single-crystal surface by the photoelectron intensity dependence.

tric vector is perpendicular to the emission direction towards the slit of the electron spectrometer. From such an experiment one can conclude that the CO molecule is actually standing up perpendicularly to the surface in this case.

Experiments of this kind have in general to be combined with extensive calculations concerning continuum wave functions and deformations of molecular shapes at surfaces (e.g. using cluster calculations). Such calculations are known to be difficult to make (very extended basis sets are required) and presently contain great uncertainties. It is likely that new experimental work done for a sufficiently large number of test cases can shed new light on the validity of various such calculations and also eventually lead to semiempirical approaches in somewhat more complicated cases than the simple example discussed here.

The angular distributions of photoelectrons emitted from <u>free</u> molecules can be studied either by varying the angle between the direction of the incoming photons and the emitted photoelectrons <u>or</u> by using plane polarized light in a fixed geometry and observing the intensity variations of the photoelectrons as a function of the angle between the electric vector of the photon beam and the electron emission

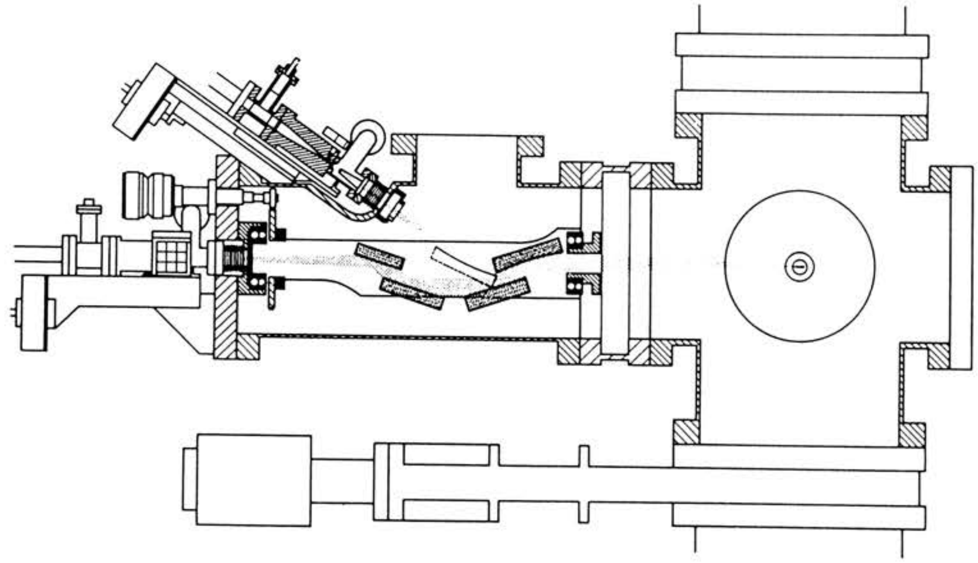

Fig. 51
Ultraviolet monochromator with several toroidal gratings covering the energy range 10 eV<hν<51 eV. Alternatively, the UV radiation is polarized by four succeeding mirrors one of which being a toroidal mirror for focussing, one a plane grating and the other two plane mirrors. The polarizer is automatically turned around its axis, thereby stepwise changing the direction of the electric vector.

direction. This latter scheme is much to be preferred from all points of view provided that a photon polarizer of sufficient intensity and beam quality can be realized /35/.

Fig.51 shows the most recent design (combined with a UV lamp excited by microwaves) from my laboratory which follows up our previous experience. The new design was briefly mentioned in connection with Fig.24. It consists of four optical elements in the following sequence: one plane mirror, one further plane mirror, one plane grating, one toroidal mirror. This device can be automatically rotated around its axis in a programmed fashion by a step motor. The focussing in the toroidal mirror compensates for the reflection losses, and also makes it possible to use a large distance between the light source, polarizer and sample without sacrificing intensity. It is important to minimize the contamination of the reflecting elements, which otherwise makes the polarization to decrease with time. By means of a set of gratings, suitable photon energies can be selected, using different gases in the light source (H_2, He, Ne, Ar, Kr). The photon energy region 10-51 eV can then be covered in small steps.

Some examples illustrate the situation for free molecules. For plane-polarized radiation, the intensity distribution of the photoelectrons is given by

$$I(\theta) = I_o(1+\beta/4(3P\cos 2\theta+1)) \qquad (6)$$

where P is the degree of polarization. The "asymmetry" parameter β can then be calculated from the measured photoelectron intensity parallel and perpendicular to the plane of polarization according to

$$\beta = 4(I_{||}-I_{\perp})/(I_{||}(3P-1)+I_{\perp}(3P+1)) \qquad (7)$$

The good intensity of the polarized radiation makes it possible and meaningful to calculate the asymmetry parameter β point by point, to generate a "β parameter spectrum" (βPS). Fig.52 is a typical βPS showing part of a vibrational sequence of $\tilde{A}\ ^2\Pi_u$ in CO_2 /53/.

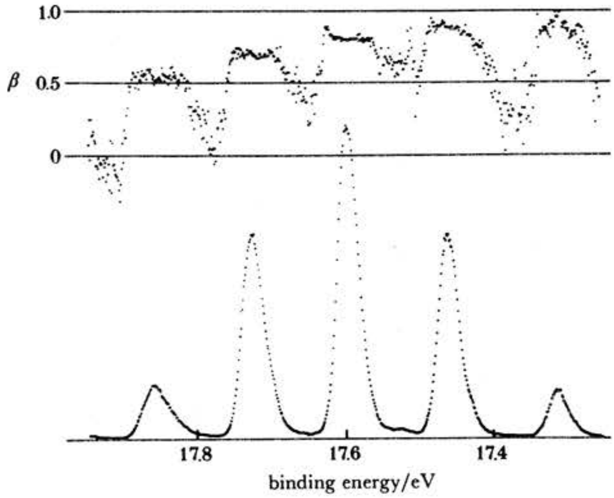

Fig. 52
A β parameter (anisotropy) spectrum of a vibrational sequence of $\tilde{A}\ ^2\Pi_u$ in CO_2.

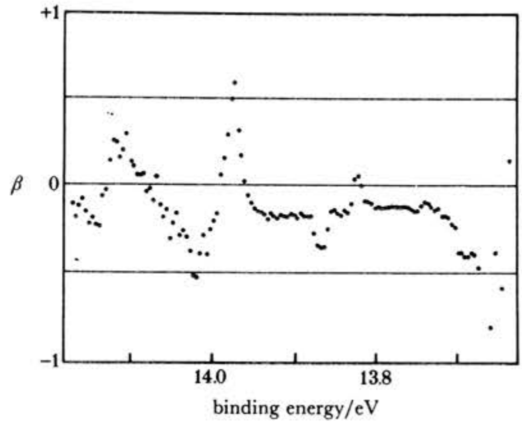

Fig. 53
β parameter spectrum corresponding to the state $\tilde{X}\ ^2\Pi_g$ in CO_2 around a β peak at 13.97 eV. The enhanced β value is due to an interaction with the state $\tilde{A}\ ^2\Pi_u$.

For CO_2, the β parameter was measuared for some 40 vibrational states, several of which had not been observed earlier as ordinary photoelectron lines. The βPS corresponding to the state $\tilde{X}\ ^2\Pi_g$ is shown in Fig.53 /53/. The prominent β peak at 13.97 eV was found to correspond to the excitation of a single quantum of the antisymmetric stretching mode. In the ordinary spectrum, this line is barely visible as a shoulder on a much more intense peak but can be observed here because of its different β value. This excitation is normally forbidden in photoelectron spectra, but it can attain measurable intensity through interaction with the state $\tilde{A}\ ^2\Pi_u$. The large difference in β-value between this line and the allowed lines in the $\tilde{X}$-state is characteristic for peaks that get an enhanced intensity through interaction with another state. The β-value in such cases tends to come closer to that of the perturbing state than to the state to which it belongs.

The $\tilde{X}\ ^2\Pi_g$ state in the CS_2^+ was investigated by means of a number of photon lines between the H Lyα (10.20 eV) and HeIIα (40.8 eV). Besides the more often used lines from NeI (16.84 eV), HeIα and NeII (26.91 eV) a number of lines from discharges in Ar, Kr and Xe were used in the energy region 10.5-13.5 eV. Very rapid oscillations in the β value for the adiabatic transition were observed for kinetic energies of the photoelectron <4 eV. At the same time the intensity of the vibrational excitation varied. Both these phenomena have to be explained by assuming that the ionization occurs at certain photon energies via autoionizing states. In inelastic scattering events (for example in CS_2) one can distinguish between longlived intermediate scattering states, which result in a change from non-zero β to zero β and shortlived intermediate scattering states keeping a non-zero β after scattering /54/.

The energy dependence of β close to the threshold for photoionization shows considerable fluctuations. This was studied in some detail for Ar, Kr and Xe. For Kr a deep dip in β for Kr $4p_{3/2}$ occurred at a photoelectron energy of 581 meV. The β PS could be followed down to a photoelectron energy of 15 meV. Such fluctuations can be ascribed to resonances with series of autoionizing states.

When Xe is excited by means of UV radiation from a discharge in N_2 one can study the β parameter spectrum close to the ionization threshold, in particular in the region between the thresholds for ionization of the $p_{3/2}$ and $p_{1/2}$ states. There is a sufficiently large number of closely spaced UV lines from N_2 in the discharge available for ionization of Xe at all photon energies of interest. As can be seen in Fig.54 the photoelectron spectrum taken parallel to and perpendicular to the electric vector of the N_2 photon beam both reflect the complicated structure of the exciting photon spectrum coming from N_2 in the discharge source, 'scanned' by the p level of Xe in the photoelectron spectrometer. However, from the <u>ratio</u> of the intensities at each photoelectron energy the β parameter spectrum of Xe can be derived, as shown in the upper part of the figure. This β PS contains an interesting sequence of minima, consisting of a converging series of resonances. This can be understood in terms of a series of autoionizing states in Xe, which converges towards the $p_{1/2}$ ionization limit. The figure also shows that the β parameter can be measured down to a few meV above the ionization threshold.

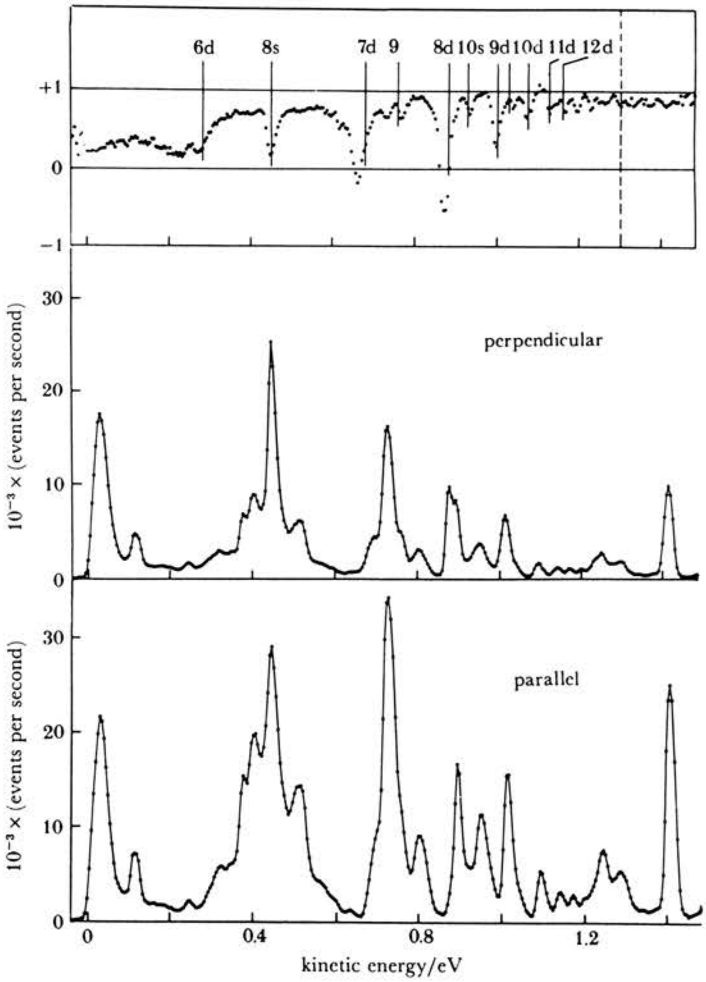

Fig. 54

β parameter spectrum of Xe in the region between the threshold for ionization of the $p_{3/2}$ and $p_{1/2}$ states with the use of N_2 in the light source.

In conclusion one may expect an expanding area of research related to the angular dependence of photoelectrons as a function of energy both close to threshold and at higher energies by means of polarized UV light either from UV lamps or tunable synchrotron radiation. Polarized tunable and laser light and the possibilities of using a Mott detector for the measurements of the emitted photoelectrons spin directions contribute to the interesting developments in this field /56,57/.

10. ESCA diffraction

The angular distributions of photoelectrons from core levels by using photons in the X-ray region (e.g. AlKα or synchrotron radiation) are manifested in the ESCA diffraction patterns. These studies can be made either by recording the angular distributions at a fix X-ray energy (e.g. AlKα) or at a fixed angle and varying the wavelength of the radiation. This latter procedure requires access to the variable synchrotron radiation. Fig.55 shows an early example of an ESCA diffraction pattern from a NaCl single crystal /58/. In this experiment, we noted that core and valence levels in a selected element of a crystal could be studied separately and the corresponding diffraction pattern be recorded. This was also demonstrated for the Auger electron diffraction.

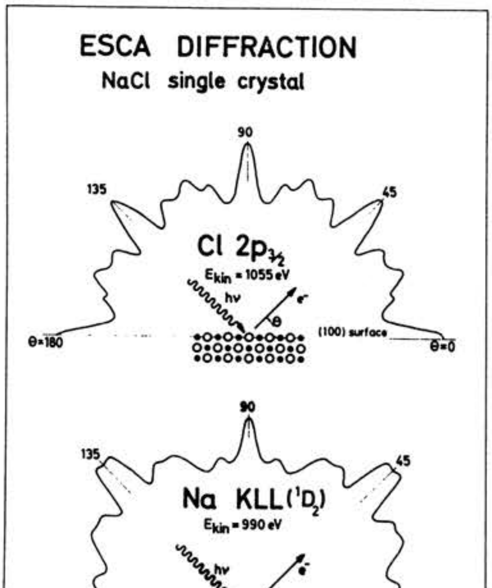

Fig. 55
ESCA diffraction for a NaCl single crystal: (a) $Cl2p_{3/2}$, E_{kin}=1055 eV; (b) NaKLL($^1D_2$), E_{kin}=990 eV.

A number of such studies are now available from several laboratories in which both the polar and the azimuthal angles have been carefully scanned. It has also been found that it is feasible to apply the method to (epitaxially) adsorbed surface species, in which case one gets structural and geometrical information of the adsorbed species related to the substrate lattice /59,60/.

A dominating contribution to the observed patterns is caused by interference through scattering along principal crystal axes. When applied to adsorbed species, e.g. CO on a Ni(001) surface, this constructive interference occurs along the array of atoms. If there are many atoms in the row the first atomic scattering can enhance and focus the intensity but subsequent atoms in the row may deenhance the intensity. The diffraction pattern then saturates when the adsorbed layer is about 3 ML /61,62,63,64/.

Since the photoelectron or the Auger electron line is specific for each element and even for its chemical bonding it is obvious that one is dealing with a new convenient surface diffraction method. Another advantage is that for the energies concerned, say around 500 eV, it turns out that simple single scattering cluster (SSC) theory is sufficient (even for lower energies). The theoretical treatment is similar to the extended X-ray absorption fine structure (EXAFS). Improvements of this simple model have been made based on spherical wave scattering.

In order to make full use of the experimental situation one should arrange for a good angular resolution ($<2^{o}$) /65/. Under these circumstances it seems possible to reach structural information with a resolution of perhaps ±0.1 Å. Using SSC calculations with plane wave (PW) scattering one can conclude, as an example, that in the case of CO on a Ni surface as discussed before the CO molecules are tilted less than 12^{o} from the surface normal. Further improvements in experiments and corrections for multiple scattering may result in better geometrical accuracy.

If Cu is grown epitaxially in successive layers on Ni(001) the diffraction pattern for the CuLMM line is observed /61/, according to Fig.56 which also contains the SSC-PW calculations for comparison. The results for the Cu3p line are similar /66/.

The ESCA diffraction will be much more used as a surface structure tool when the experimental conditions are improved in the future. As an indication of such improvements Fig.57 demonstrates the sharpening of the diffraction pattern for $Ni2p_{3/2}$ when the angular definition is increased from ±3^{o} to ±$1,5^{o}$ in the case of Ni(001) /65/.

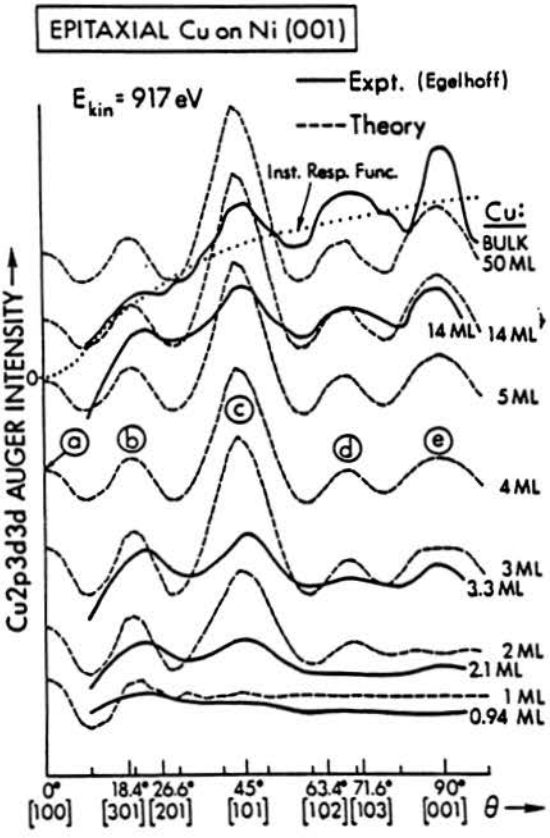

Fig. 56

Experimental Cu 2p3d3d Auger line polar diffraction scan compared to SSC-PW calculations for successive layers of epitaxial growth of Cu on Ni(001). Similar results are obtained for Cu3p.

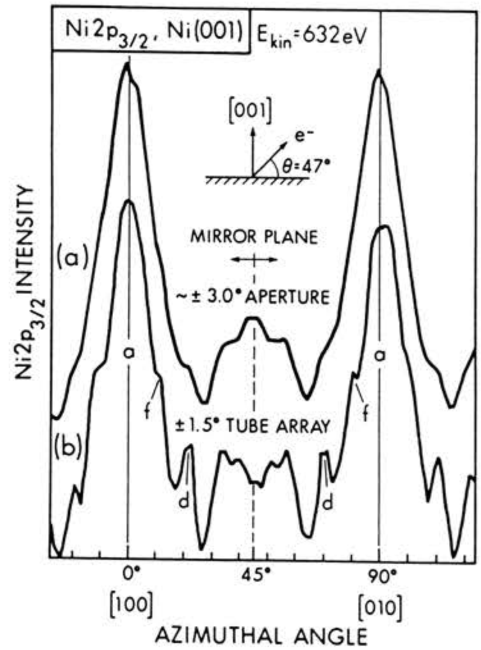

Fig. 57
The effect of improved angular resolution on the diffraction pattern of the AlKα excited Ni $2p_{3/2}$ photoelectron line from Ni(001). Azimuthal scans at $\theta=47^{\circ}$ for an aperture of $\pm 3.0^{\circ}$ and $\pm 1.5^{\circ}$, respectively.

New applications have recently been found in the study of spin-polarized photoelectron diffraction /67/. In this case core level multiplet splitting was used to produce internal spin-polarized sources of photoelectrons which subsequently can scatter from arrays of ordered magnetic moments in magnetic materials. According to findings by C.S. Fadley et al. such spin polarized photoelectron diffraction provides a new tool for probing short-range magnetic order.

Surface structurally informative results have been obtained using synchrotron radiation, in which case the patterns are recorded in the normal direction of the crystal varying the wavelength of the synchrotron radiation. The procedures are described in papers from SSRL (D.A. Shirley et al.) /68,69/ and BESSY (D.P. Woodruff, A.M. Bradshaw et al.) /70,71/. As a recent example a study of the structure of the formate (CO_2H) species on copper surfaces can be quoted /70/.

Fig.58 shows how this species is adsorbed on Cu(100) and (110) surfaces. The results are shown in Fig.59.

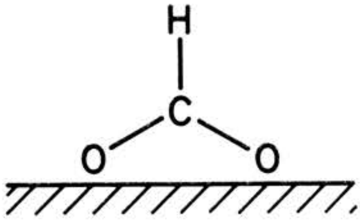

Fig. 58
The perpendicular geometry of the formate species on Cu(100) and (110) surfaces.

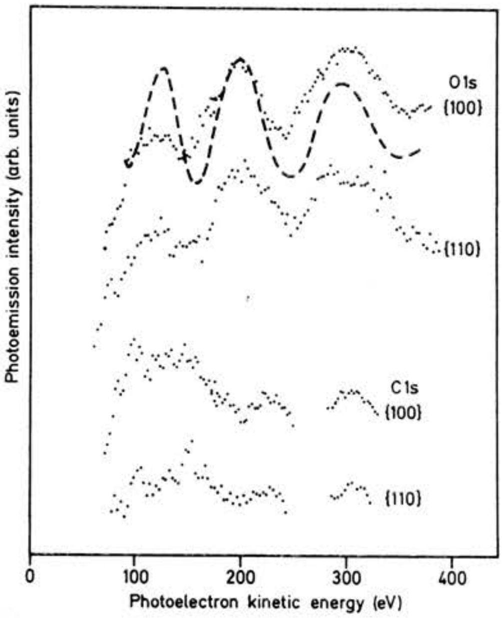

Fig. 59
Diffraction of O1s and C1s at normal emission from formate on Cu(100) and (110) surfaces. The dashed curve corresponds to results of single scattering plane wave calculations from a Cu atom 2.0 Å behind the emitter. The OCO bond angle is evaluated to be 134°.

11. Studies of liquids and ionic solutions

Above I have given a few examples of some current electron spectroscopic studies of free molecules (gases), solids (bulk) and surfaces. The latter state is characterized by so many special features that it deserves the notation as a state of aggregation of its own. The third type of condensed state of aggregation is the liquid state.

The application of ESCA on liquids started in my laboratory in 1971. We made an arrangement for a continuous flow of a thin "liquid beam" in front of the slit in the spectrometer. The liquid beam, subject to differential pumping, was irradiated by X-rays and the resulting spectrum was recorded. Our first study concerned liquid formamide, $HOCNH_2$. We were able to record both the core spectrum and the valence spectrum /72,73/. It has been possible to master the experimental problems to record liquid spectra of sufficiently good quality to enable more reliable conclusions to be drawn. Core line spectra of at least as good quality as previously obtained for solids can now be produced for a great number of different solvents in which chemicals are dissolved. The scope is very wide and most of the applications essentially remain to be done /74/.

The experimental problem is to keep the liquid surface fresh all the time in vacuum and to eliminate the influence of the vapour phase. This is accomplished by renewing the liquid in front of the electron spectrometer slit continuously either by a translational or a rotational movement. In the first case one can form the above mentioned liquid beam in the vacuum in front of and along the slit of the spectrometer. Such a liquid beam or a wetted wire is then continuously subject to X-radiation. The vapour phase is differentially pumped in the same way as gaseous samples are handled.

In this way the expelled photo- or Auger electrons from the liquid can pass the gas phase spending only a short distance before they reach the slit and the analyzer. The liquid surface can also be renewed by the continuous rotation of the liquid exposing the renewed surface layer to the X-ray flux. Again, the expelled photo- and Auger electrons are passing the gas phase at a short distance to the slit before the electrons are being analyzed at high vacuum.

Generally, one obtains two electron lines, a line doublet, for each level, one originating from the liquid phase and the other from the same molecules in the vapour phase. This gives the opportunity to refer the liquid lines to the vacuum level of the free molecules by a suitable calibration procedure in the gas phase. For more complicated structures, e.g. when the structures contain chemical shifts the vapour lines can be removed by a simple trick: A small potential of 10 or 20 V is applied to the metallic substrate of the liquid relative to the first slit. The vapour lines will then be broadened to the extent set by the applied electric field over the vapour volume and will more or less disappear in the continuum whereas the liquid lines which emanate from a well defined potential, will be correspondingly shifted but not broadened.

In order to reduce the intensity of the vapour line the exciting radiation should preferably be directed from the side towards the liquid. Very efficient differential pumping on the gas phase is particularly important for liquids like water solutions with high vapour pressures.

Fig.60 shows a spectrum of liquid ethanol /75/, showing the chemically split C1s line from the ethyl group, the O1s line and the orbital valence electron spectrum of the molecule.

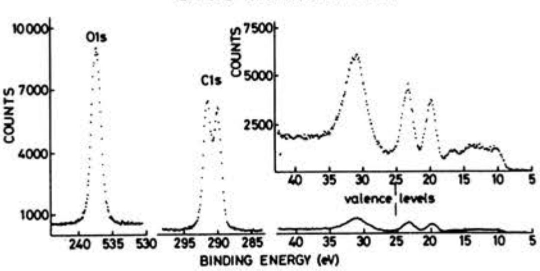

Fig. 60
Liquid spectrum of ethanol; core and valence electron spectrum.

Fig.61 shows a core- and Auger electron spectrum of a solution of Na^+I^-(5M) in glycol /76/. The shifts of the Na^+ lines with respect to the gas phase (solvation shifts) were obtained from separate photoelectron spectroscopical atomic gas phase data combined with calculated atom-ion shifts (using scf techniques).

Fig.62 shows the liquid ESCA spectrum of $SrBr_2$(1M) /77/. The Br^--gas value was likewise obtained from a molecular photoelectron spectroscopical value coupled with a calculated molecule-atom shift and an atom-ion shift.

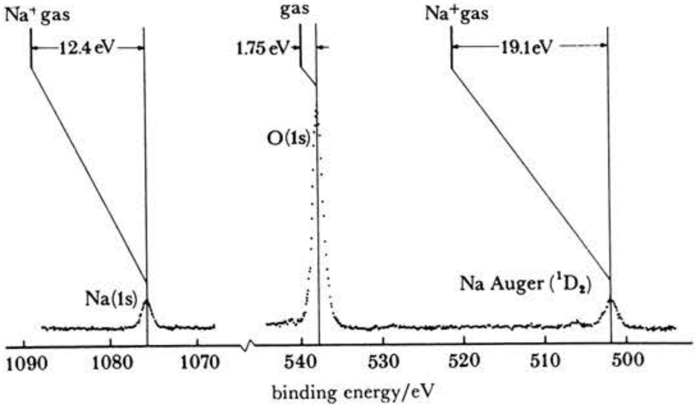

Fig. 61
Core and Auger electron spectrum of a solution of Na^+I^-(5M) in glycol.

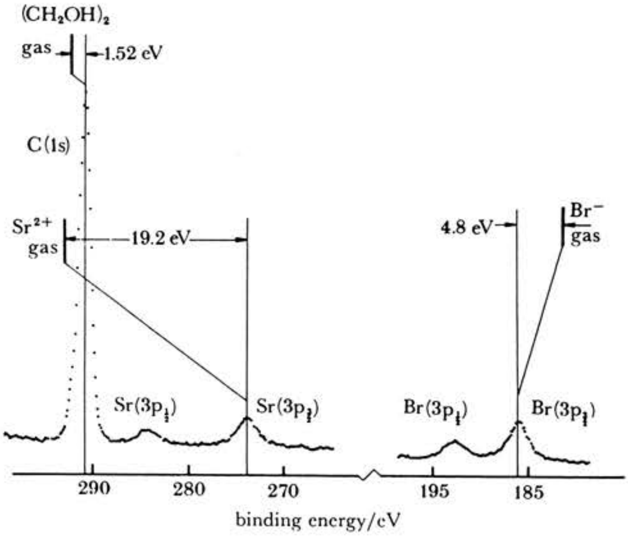

Fig. 62
Liquid spectrum of $SrBr_2$ in glycol (1M).

Fig.63 is the ESCA spectrum of $HgCl_2$(0.2 M) in C_2H_5OH /77/. Observe again the ESCA chemical shift between the two carbon atoms in the ethyl group.

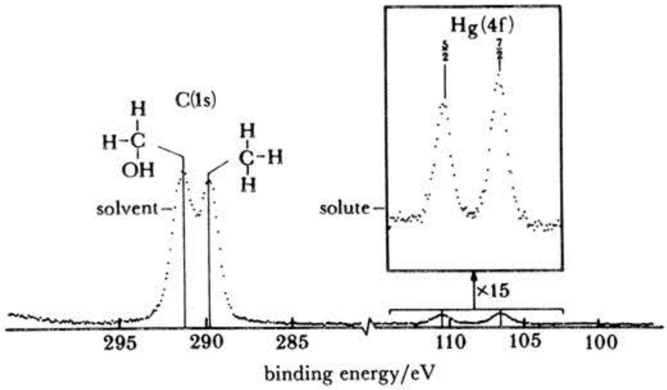

Fig. 63
Liquid spectrum of $HgCl_2$(0.2M) in ethanol at -85°C.

As previously discussed electron spectroscopy gives information about the electric charges around atoms, which change the potential at the formation of different chemical compounds of a given element. The change of charge at the photoelectron emission of one unit for photoelectron lines and two units at the Auger process is followed by a reorganization of the atomic electrons when the hole state is being formed. This is the origin of the reorganization or relaxation energy. One can show that the difference in reorganization energies between two compounds can be determined by measuring both the photoelectron energy shifts and the Auger electron energy shifts. The reorganization energy is on the other hand directly related to the solvation energy of a certain ion in a solution. The solvation energy is defined as the energy difference between charging an ion in vacuum and in the solvent.

It is possible to perform Born-Haber cycles to get relationships between solvation energies and measurable quantities from electron spectroscopy on solutions. Since the solvation energy is essentially the energy associated with the reaction of the solvent against a dissolved ion it corresponds to the previously discussed reorganization or relaxation energy. The molecules of a solvent can react twofold against a dissolved ion: either by a very fast electronic polarization or by a relatively slower reorientation of their electric dipoles. The reorganization energy which is being measured in the fast ESCA process is the electronic part of the order of 10^{-15}sec, whereas the dipolar reorientation takes much longer time to be included in the ESCA process. Therefore, the two contributions to the chemically measurable solvation energy can be separated into independent parts. Recent systematic studies by ESCA shows that at low valence states of the ion the two contributions are about equal, whereas at higher valence states the electronic polarization contribution is becoming the more important part.

The experimental ESCA studies of liquids can be complemented by model calculations of the solvation shifts of core levels. It is reasonable to assume that solvation binding energies and Auger energy shifts of ion energy levels are to be described by a model that combines the long-range continuum-like behaviour of the solvent with a short-range molecular interaction between the ion and first solvation shell of molecules.

In particular, to study the latter part and also to investigate the importance of the long-range interaction, ab initio calculations have been made on Na^+ solvated clusters surrounded by an increasing number of molecule /78/. For a proper comparison with experimental data in solution it is desirable to perform calculations up to and including a fully solvated cluster with six solvent molecules. This is practically possible only for water ligands and carefully chosen basis sets. Calculations for other solvent molecules (such as methanol) must then be made for a more limited number of molecules and results extrapolated to full clusters. The main results of the calculations show that the experimental cluster solvation energies for $Na^+(H_2O)$ are reproduced with good accuracy by using a basis set of moderate size including polarization functions of p-type on ligand molecules. The calculated binding and Auger energy solvation shifts for the cluster are smaller by at least 20% compared with experimental values obtained in solution. The discrepancy is substantially larger for the Auger shift. This reflects the importance of long-range electronic polarization in the description of the solvent environment of small cations in solution. This electronic polarization becomes increasingly important for higher charge states of the ion. A cluster model is generally insufficient to reach the values obtained in ionic solutions by electron spectroscopical means. Replacing H_2O as ligand with CH_3OH results in an increase of the binding energy and Auger shifts of ~ 20%. This may be explained as an effect of the increasing number of polarizable valence electrons in the cluster. The methanol cluster (with the same number of molecules as the water cluster) can be considered as a structure with more than one solvation shell.

Of particular interest is the study of <u>water</u> solutions /79/ in which case the high vapour pressure is an experimental obstacle. Fig.64 is the first example showing the liquid and the gas oxygen 1s lines from water in a saturated LiCl solution. The vapour phase line has been removed in the upper spectrum by applying a small potential on the liquid water backing as discussed above.

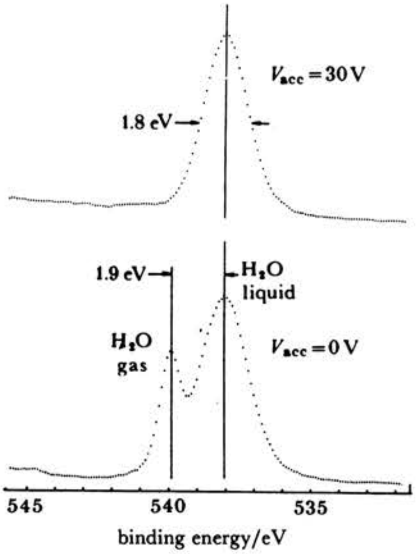

Fig. 64

Spectrum of liquid water at 254 K. The O(1s) water-gas line is removed by applying a potential on the backing of the liquid sample. The remaining O(1s) is from liquid water alone.

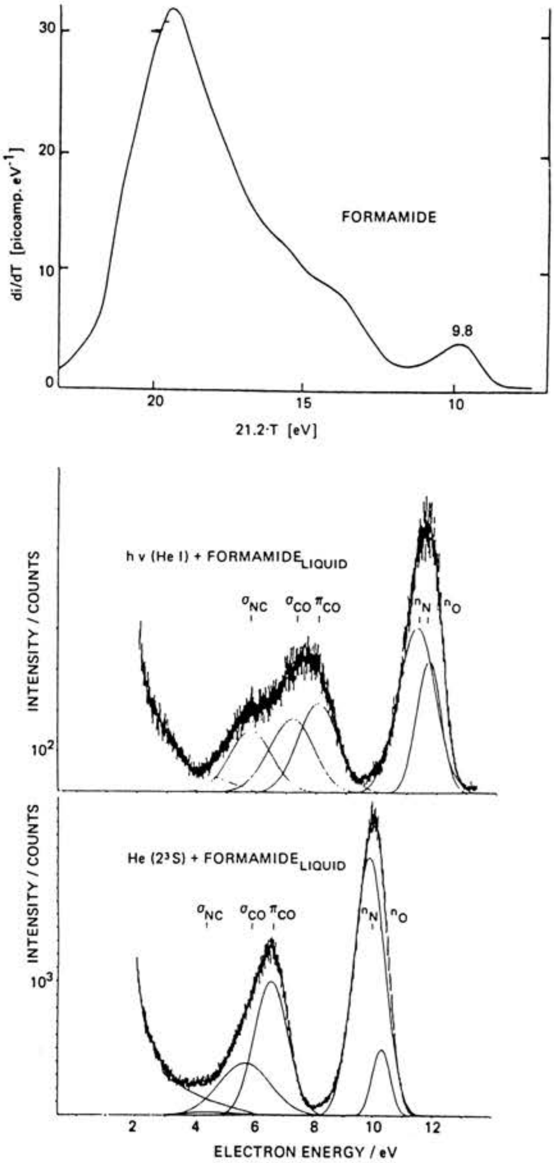

Fig. 65
Valence electron spectrum of liquid formamide excited by HeI and by metastable thermal He* impact (MIES). The upper curve is the previously obtained spectrum by HeI.

The valence region is within reach also by means of the He radiation. There have been problems here for liquids for some time with respect to line shapes and signal:background ratio, which so far have complicated the applicability of this approach. These experimental problems now seem to have been removed. In a new attempt using HeI radiation on formamide (which previously /72,73/ was the first spectrum which

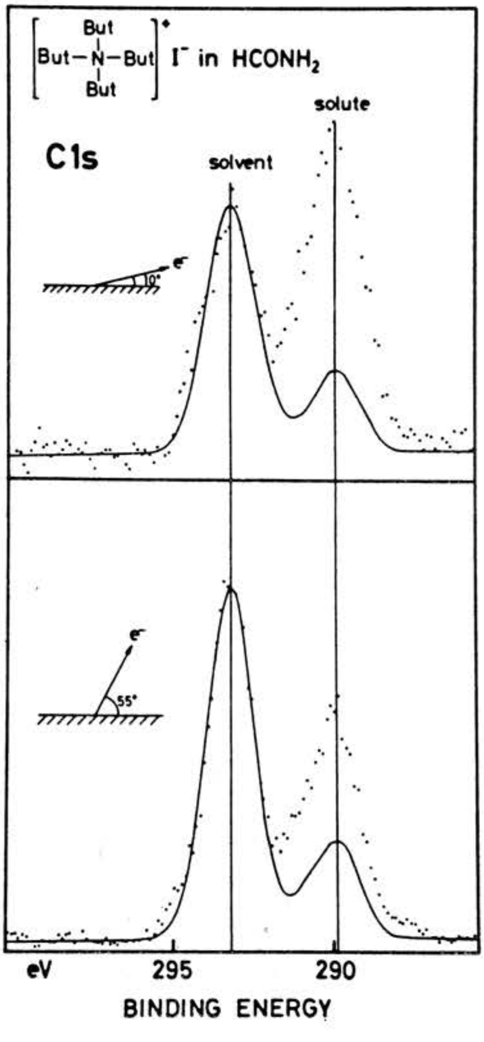

Fig. 66
C(1s) spectra for two different take-off angles ($\theta=55^{\circ}$ and $\theta=10^{\circ}$) for the system $(But_4N)^+I^-$ in $HCONH_2$(0.2M). The full-drawn curves represent in both spectra the profile expected for the bulk concentration relation between the two components (peak area 1:3). The spectra show a very pronounced surface segregation of the solute within the sampling depth of the photoelectrons.

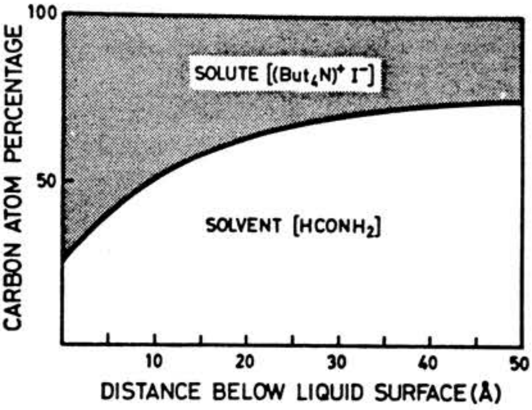

Fig. 67

Depth concentration profile in the system $(But_4N)^+I^-/HCONH_2$ deduced from the spectra in Fig.66. The profile is based on the assumption of an exponential decrease of the solute concentrations with increasing depth in the solution. The data give a mean segregation depth of 15 Å and a ratio between surface and bulk solute concentration of 3:1.

was recorded with X-ray excitation by means of the above mentioned liquid beam technique) Keller et al. /80/ have shown that in addition to X-radiation also UV radiation can produce valence electron spectra of quite good quality (see Fig.65). They furthermore used a beam of thermal metastable He atoms from the same He discharge lamp to excite electron spectra (MIES) at the uppermost surface of the liquid, shown at the bottom of the figure. The upper spectrum was a previously obtained spectrum by means of HeI radiation. From a comparison between their two differently excited spectra Keller et al. draw additional conclusions about the position of the formamide compound in the surface.

An interesting further pathway would now be to try using polarized XUV radiation and perhaps laser radiation for excitation. Auger electron spectra excited by an electron beam also remain to be done and so do electron scattering experiments.

The technique of a variable take-off angle for the emitted electrons which was discussed before (e.g. Figs.9 and 10) can be applied to liquids in order to scan the ionic concentrations as a function of the distance from the surface. This was done in an experiment on the system on $(\mathrm{ButN})_4^+ I^-$ desolved in $HCONH_2$ (0.5 M) /81/. Fig.66 shows the Cls lines for the solvent and solute at two different take-off angles, 10° and 55°. The full-drawn curves represent the expected line profiles for the bulk concentration relation between the two components (peak area 1:3). As one can see the spectra instead show pronounced surface segregation. The results can be put on a quantitative basis by making some reasonable approximate assumptions anticipating an exponential decrease of the solute concentration with increasing depth in the solution. The result is shown in Fig.67. One notices the strong change of concentrations over a depth of some 15 Å, being the mean segregation depth in this case.

12. New extensions of electron spectroscopy by means of laser excitation

More recently the modes of excitation by means of X and UV photons have been complemented by the use of laser radiation. There are two ways to proceed here: The first one is to use various non-linear optical media to achieve frequency doubling or higher harmonics of the laser radiation in order to reach wavelengths far down into the VUV region. These possibilities are getting gradually more promising because of improvements in laser technology. There are now available much more efficient crystals for frequency doubling than before, e.g. the BBO crystal. Furthermore, some gases have turned out to be quite efficient for frequency tripling e.g. Hg, Xe, Kr, Ar and Ne (see Fig.68) /82/. Although the pathway towards higher frequencies can proceed only at a great loss of intensity the starting point with a pulsed laser is so good that the final result after frequency multiplication (tripling or even more) still yields tunable laser intensities decent for excitation of photoelectron spectra in the wavelength region around 1000 Å and even far below. This technique has already been used in some preliminary studies. The number of extremely monochromatic and tunable photons can be in the region of 10^{10} per pulse. This alternative obviously opens up interesting new possibilities and offers opportunities for very high resolution, both for molecular studies and for band studies, e.g. in the semiconductor field.

According to Fig.68 the penetration into the VUV proceeds quite well by using e.g. a mercury cell until one reaches the region ~105 nm when it is hindered by the cut-off of the LiF window. Already this extended wavelength region in the VUV is of great interest for optical molecular studies, since this wavelength region has been much less explored than at longer wavelengths. Furthermore the extremely narrow bandwidth and the tunability of the laser represents no doubt a new and most powerful tool as a UV monochromator in optical spectroscopy. It can also be used for photoelectron spectroscopy at very high resolution. Fig.69 shows an experimental arrangement due to U. Heinzmann et al. for photoionization yield measurements using a mercury cell for resonant sum- and difference-frequency mixing /83/. Two tunable lasers are used and the two beams are merged via a dichroic mirror into the mercury cell. The vapour pressure is 1.5 mbar Hg mixed with 4 mbar Ne. The bandwidth is $4.5\cdot10^{-4}$ nm.

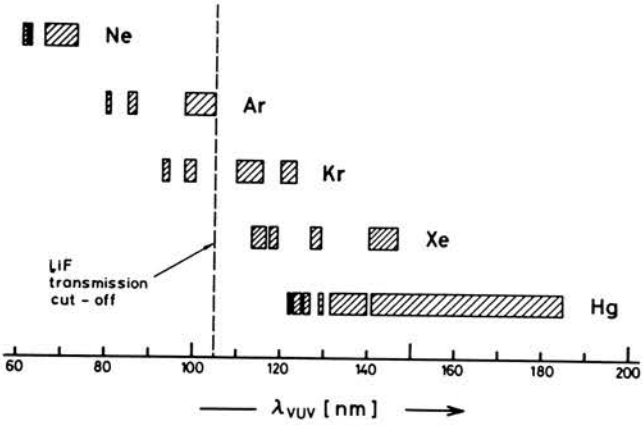

Fig. 68
Spectral regions for frequency tripling in rare gases and in mercury.

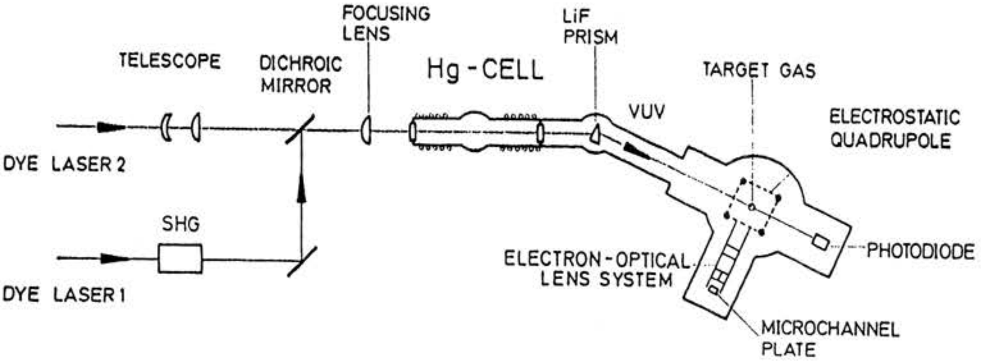

Fig. 69
Scheme for a tunable laser source for photoionization measurements using a mercury cell for resonant frequency mixing according to U. Heinzman et al.

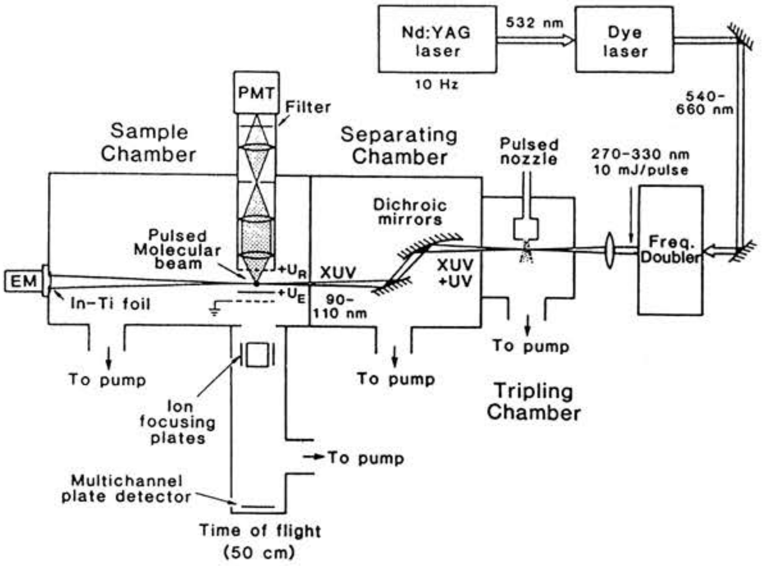

Fig. 70
Scheme for frequency tripling by means of a pulsed rare gas jet and differential pumping according to D. Zare et al.

A second arrangement due to R. Zare et al. is shown in Fig.70 /84/. In this case the the frequency-doubled dye laser beam is traversing the non linear optical rare gas medium in the form of a jet beam (produced by a pulsed nozzle). In this way windows can be avoided since a strong differential pumping on this pulsed nozzle chamber can be arranged.

One may anticipate that arrangements of these types will be further developed. Already, wavelength regions around 50 nm have provisionally been reached. The photon intensities are quite good in the upper part of this VUV wavelength region even for photoelectron spectroscopy but decreases rapidly towards the lower part of the region. Still, the prospects are good to eventually achieving sufficient photon intensities to enable the work with tunable laser photon beams in photoelectron spectroscopy far down in the XUV region as powerful alternatives to the presently available discharge lamps and synchrotron radiation sources.

The second way to proceed is to use multiphoton ionization (MPI) or, preferably, resonance enhanced multiphoton ionization (REMPI). These processes are now sufficiently well understood to be applicable in electron spectroscopy. Although the field is new and far from being maturized there exist already a few comprehensive survey articles based on recent developments by e.g. K. Kimura /85/ and R. Compton and J. Miller /86/. The experiments are performed by means of pulsed lasers in the optical region. The laser power usually needed is in the region of 10^6-10^{10} watts/cm^2.

The best way to proceed is to use two tunable lasers pumped by an excimer or YAG laser. The first laser is tuned to hit a resonance in the molecule (in a supersonic jet beam). The power is adjusted so that few if any events lead to further photon absorption from this laser pulse which would result in photoionization and dissociation in a fairly complicated pattern. The second laser is tuned to ionize the excited molecule in one step. The resulting electron spectrum (around a few eV in extension) is recorded either in a time of flight (TOF) fashion or by means of an ordinary electron spectrometer. Provisions can be made to record also the molecular ion mass spectrum.

An early study of the resonance enhanced multiphoton ionization of chlorobenzene was made by R. Zare et al. /87/. In his paper one finds

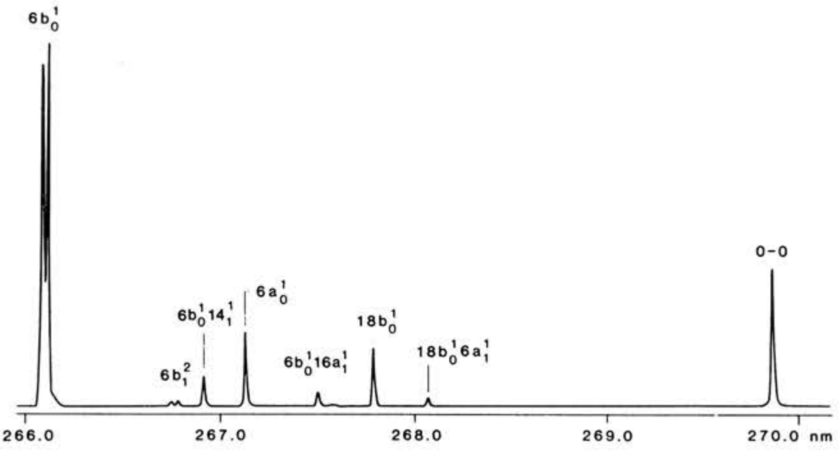

Fig. 71
Multiphoton ionization (MPI) spectrum of jet-cooled chlorobenzene. The ion current is recorded as a function of laser wavelength.

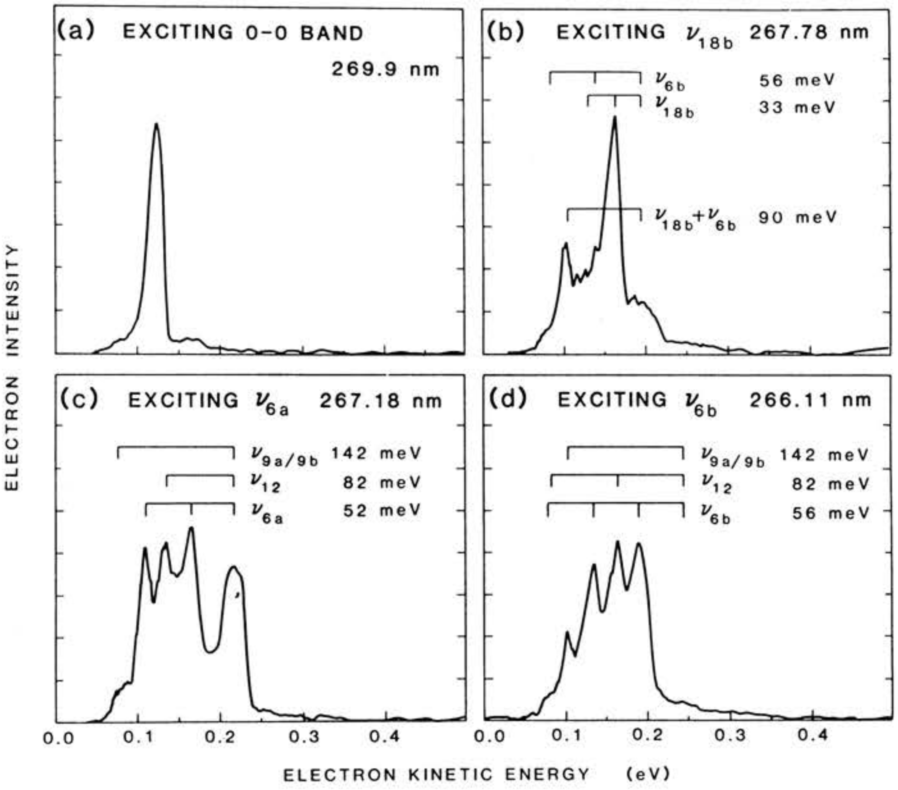

Fig. 72
REMPI electron spectra from four selected resonances in chlorobenzene according to Fig.71. Vibrational progressions and energy spacings are listed.

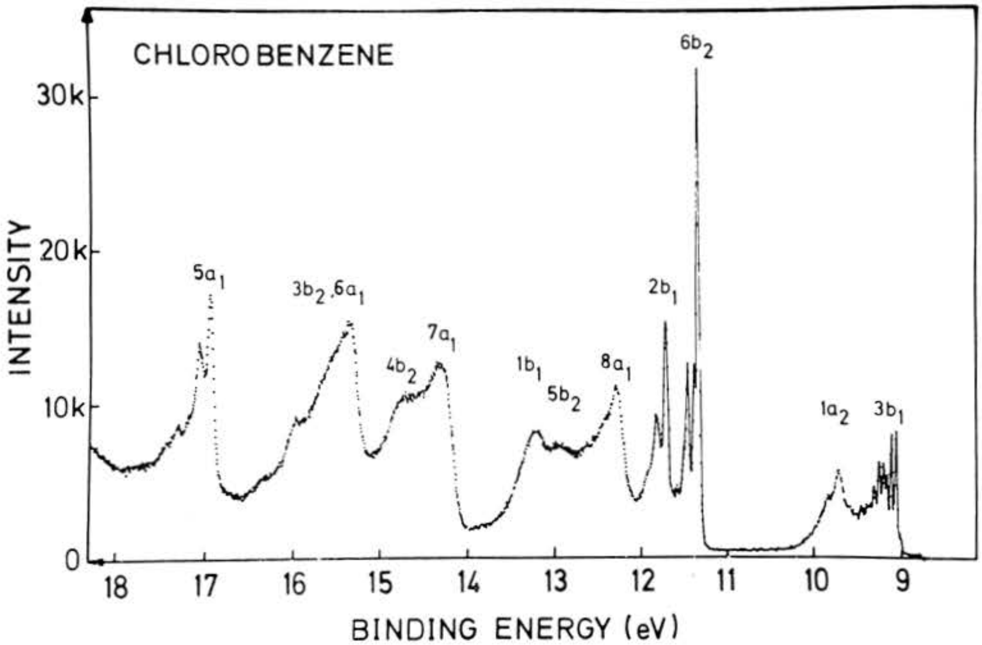

Fig. 73
Valence electron spectrum of chlorobenzene excited by HeI.

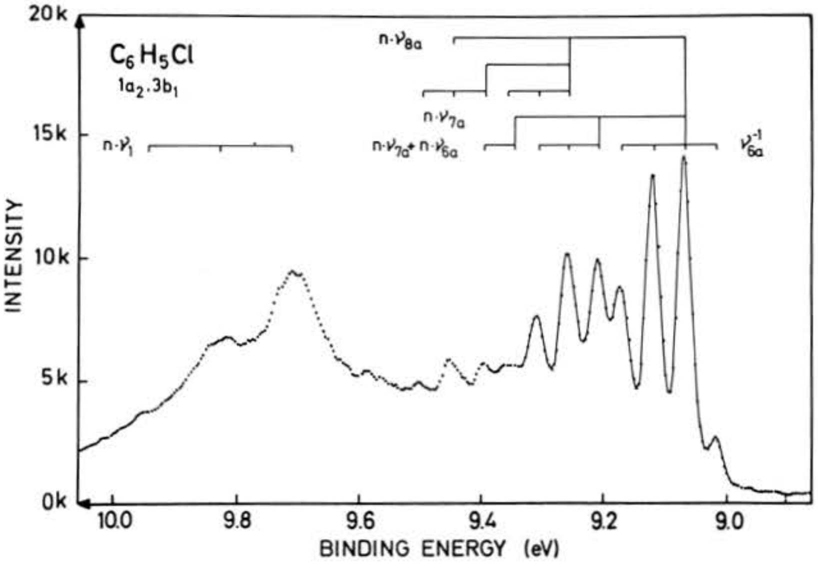

Fig. 74
The $1a_2$ and $3b_1$ bands of chlorobenzene with vibrational assignments to be compared to the results in Fig.72.

references to some early works by other groups, e.g. Compton and Miller; Meek, Jones and Reilly; Kimman, Kruit and van der Wiel and Achiba, Sato, Shobatake and Kimura etc. Fig.71 shows the ion current as a function of laser wavelength for chlorobenzene as obtained by R. Zare. The procedure is to select one of the resonances and then to record the corresponding photoelectron spectrum. There are several advantages to use this highly controllable method of excitation to get the correct vibrational assignments, which are often difficult to make, using ordinary UV photoelectron spectroscopy. Fig.72 shows some of the recorded photoelectron spectra for chlorobenzene obtained by TOF techniques at different laser wavelengths when the laser was tuned to fulfil the conditions for REMPI. For comparison Fig.73 shows the complete HeI excited valence orbital electron spectrum of chlorobenzene /88/. The band near the binding energy 9 eV is shown in more detail in Fig.74. The different orbital vibrational modes with their assignments and vibrational energies can be extracted from these data and be compared to the REMPI results.

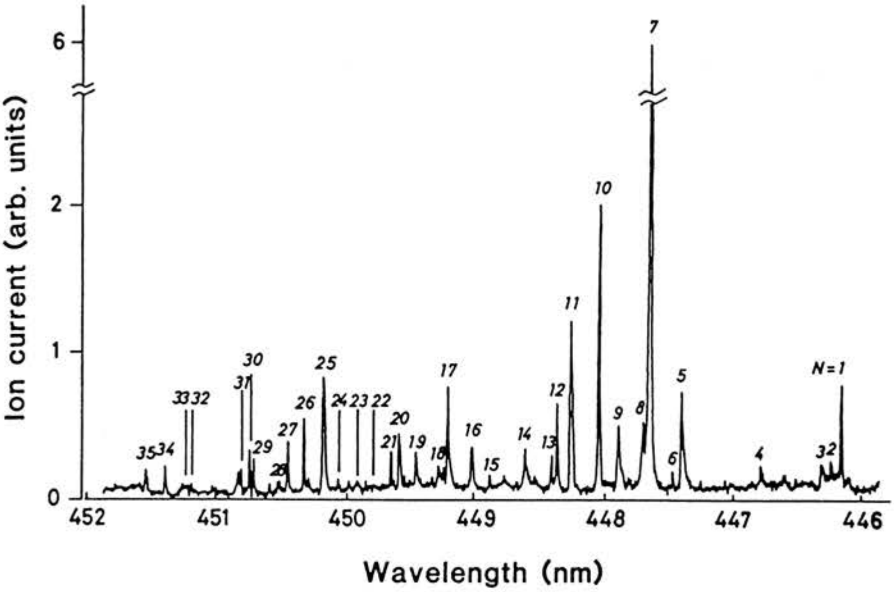

Fig. 75
Ion current as a function of wavelength for $Fe(CO)_5$.

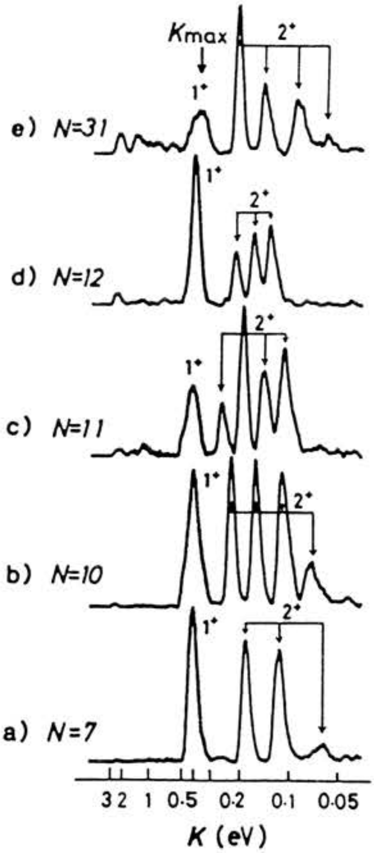

Fig. 76
Some selected REMPI electron spectra for $Fe(CO)_5$ corresponding to resonances in Fig.75.

Another case studied by Kimura and Achiba et al. /89/ is shown in Fig.75 and Fig.76 and concerns $Fe(CO)_5$. Fig.75 shows the ion current produced by the laser as a function of wavelength. One can then select any of the peaks and take the associated photoelectron spectrum. Some of these are shown in Fig.76.

In order to collect a substantial fraction, ~50%, of the produced photoelectrons in REMPI a magnetic bottle reflector has been devised /90/. A recent study concerning (2+1) REMPI photoelectron spectroscopy on Rydberg states of molecular bromine is an illustration of this method /91/.

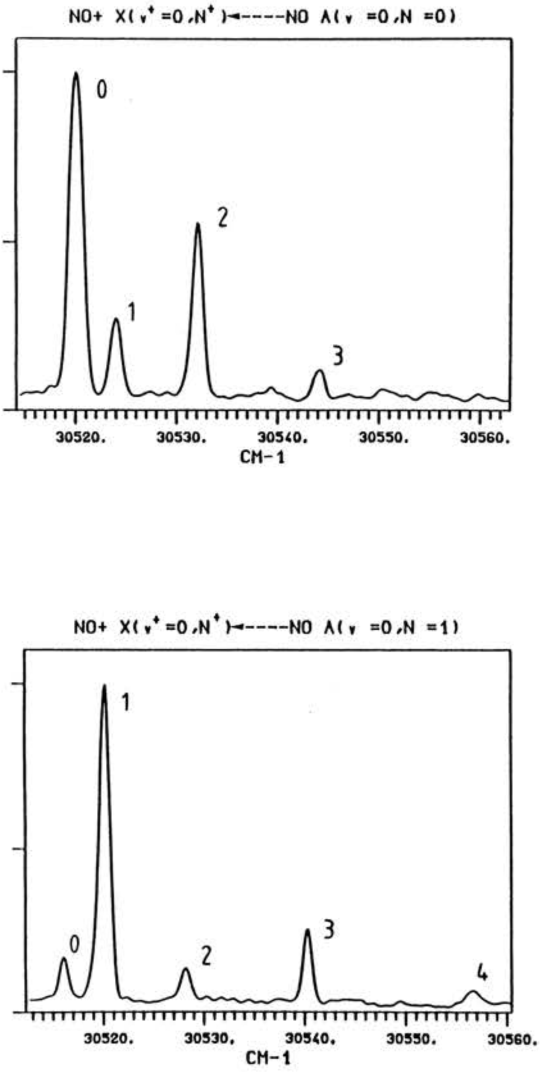

Fig. 77
Two-colour laser induced zero kinetic energy (ZKE) photoelectron spectra in the (NO$^+$) X ← NO A photoionization process. The rotationa lines are fully resolved.

A particularly interesting possibility is offered when the second laser is tuned to produce zero kinetic energy electrons. After a small time delay (a few μ sec) the still remaining zero energy electrons are swept out from the production volume by an electric pulse into the electron spectrometer. The collection efficiency can approach

100% /92/. In this case the time-of-flight alternative is suitable. For high resolution it is important to produce only a few electron-ion pairs per pulse, otherwise the Coulomb forces will broaden the linewidths. Without this and other precautions the attainable resolution will be equal or worse than for ordinary XUV photoelectron spectroscopy (>10 meV). The ideal laser arrangement is a high repetition rate and short pulses $\lesssim$1 nsec, even psec. In favourable cases the electron linewidths in such ionization studies can approach those set by the laser linewidths. The attainable resolution under optimum conditions using zero energy (threshold) photoelectrons can in fact be so much increased that the rotational sublevels of the intermediate resonance level can be studied in detail. This has been achieved by K. Müller-Dethlefs et al. who report a resolution of ~1 cm^{-1} (~0.1 meV) in the case of NO /92/ and benzene /93/. Fig.77 shows a NO spectrum where rotational components have been completely resolved /94/.

A new and very promising development of the above techniques has recently been introduced by E.W. Schlag et al. which is a combined resonance enhanced multiphoton dissociation spectroscopy (RE-MPDS) and multiphoton ionization /95/. This technique has been applied to the benzene cation /96/.

Laser-photoelectron spectroscopy can be arranged in several different ways. As an example one variant is to study mass-selected negative cluster ions using the tunable laser for photodetachment. This has been done for negative cluster ions of silicon and germanium in the 3-12-atom range by R.E. Smalley and coworkers /97/ with interesting results.

J.V. Coe et al. /98/ have studied the photoelectron spectra of negative cluster ions $NO^-(H_2O)_n$ by laser induced photodetachment (n=1,2) with 2.54 eV photons. The spectra resemble that of free NO^- but are shifted to successively lower electron kinetic energies.

Since intermediate levels can be reached in REMPI by two or several photon absorptions such levels can be excited and observed by the following ionization either through the electrons or ions, which are forbidden optical transitions in ordinary fluorescence spectroscopy because of selection rules. Thus a very wide spectroscopical area is now available for study, as an extension to previous optical molecular spectroscopy.

The recording of the dissociated molecular fragments by TOF technique yields further information about molecular dynamics. These latter phenomena have been reviewed by D.A. Gobeli et al. /99/ and by U. Boesl /17/. The interplay between the observed ionization and successive fragmentation can be described by and compared to different models, one of the most useful being the so called "ladder" model /17/. This model gives a reasonable account for many of the successively observed ions in the mass spectra under laser irradiation.

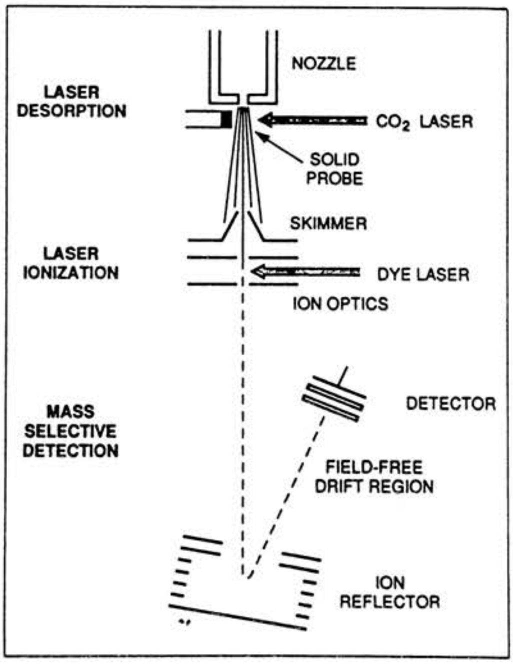

Fig. 78

Two-step arrangement for high resolution TOF mass spectroscopy using an ion reflector. Molecular desorption takes place in the first step by an IR laser. The desorbed complete molecules are cooled in the jet beam. They are ionized by the pulsed tunable laser in a 'soft' fashion, i.e. at low power. This mode produces pure molecular ions. Gradually the laser intensity is increased to achieve 'hard' ionization, producing fragmented molecular ions in a controlled fashion.

A powerful "soft" ionization laser technique using an ion reflector for energy focussing to record mass spectra even of biomolecules at high resolution (R=10000) and under controlled ionization conditions has been developed by E.W. Schlag and coworkers /100/ (see Fig.78). Fig.79 shows a recent example of such spectra. This is a state selective technique with extreme sensitivity in the femtogram class. For surface desorption studies /101/ for example it is an ideal tool which no doubt will be widely used in the next future. This scheme has been adopted in the instrument shown in Fig.23.

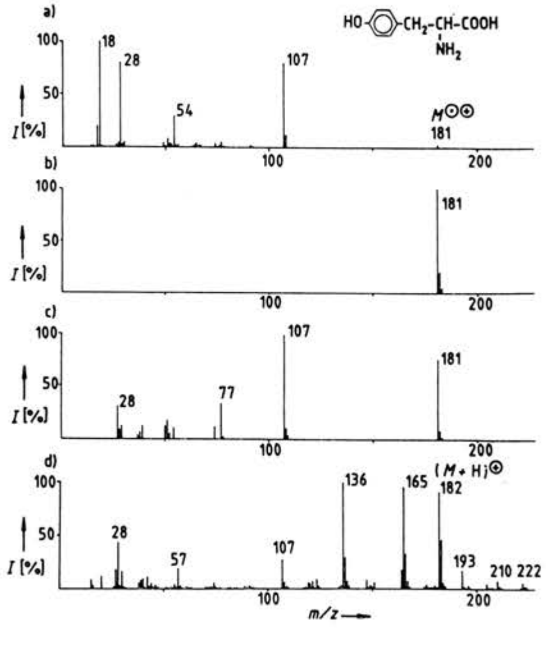

Fig. 79
Comparison of mass spectra of L-tyrosine by different method of ionization. a) Electron beam induced mass spectrum. The pure molecular ion peak at m=181 is quite weak. b) 'Soft' laser induced mass spectrum according to the scheme in Fig.78. The pure molecular ion is the only one being formed. c) 'Partially hard' laser ionization at λ=272 nm producing characteristic ion fragments in a controlled fashion. d) Chemical ionization (CI) using methane, corrected for the methane background.

Mo Yang and J. Reilly /102/ have proposed a scheme for very high resolution mass spectroscopy of desorbed molecules, e.g. aniline. They compare the different conditions when the laser beam is striking the surface directly or is being internally reflected against the surface

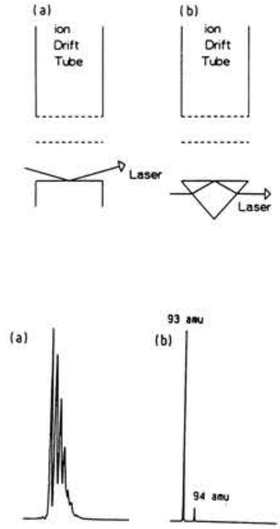

Fig. 80
UV laser induced surface ionization (anilin) with prisma internal reflexion using TOF mass spectroscopy. a) shows the result when the laser beam is reflected against the surface and b) when it is internally reflected. In the latter case very high mass resolution can be achieved by a TOF arrangement with reflector.

according to Fig.80. In the first case the desorbed species are ionized in the gaseous phase after desorption, in the second case directly at the welldefined surface. The first mass spectrum gets more complicated than the second one. In particular, the second alternative provides a very precisely defined geometry for starting the time of flight measurement. Using the reflector method and picosecond techniques they suggest that it might be possible to achieve higher resolution than before, 10^5 or perhaps even higher.

It is interesting to consider the combination of laser excitation and various simultaneous excitation by other means. Such studies have been performed on sodium atoms under the simultaneous excitation by laser and synchrotron radiation /103-105/.

The experimental arrangement previously shown in Fig.23 and 24, is designed for the purpose of exciting from various directions a molecular beam (or a surface) by two-coulour polarized laser radiation in addition with excitations of Auger electron spectra by means of a focussed electron gun, polarized VUV photons of different wavelengths from the previously mentioned VUV polarizer. Furthermore, highly monochromatic electrons with variable energy from 1 eV up to 5 keV are produced by the electron monochromator with the electron beam directed to the slit of the electrostatic lens system with the subsequent high resolution electron energy analyzer provided with a multidetector system or a Mott detector for the determination of the electron spin polarization. This electron analyzer is in common for all the different modes of excitation.

Apart from the separate modes of excitation the arrangement might enable combinations of the different excitation sources. For example, energy loss spectra by means of the electron monochromator and the following electron spectrometer can, in principle, be combined with laser excitation or Auger electron spectra studied under simultaneous laser excitation etc. Intensity problems will be encountered due to the reduced detection efficiency inherent in such double modes of excitations. Still, such experiments are particularly interesting to consider for the future.

Finally, a recent experiment will be briefly discussed here where picosecond double excitation techniques have been applied to study shortlived interface states in the band gap between the valence and the conduction bands in a time resolved fashion due to R. Haight et al. /106/. The laser system provides tunable picosecond pulses by means of a NdYAG laser and an excimer laser according to Fig.81. After passing a KDP crystal the laser pulses are frequency doubled and one "probe" signal is further frequency multiplied by passing a tube filled with one of the noble gases shown in Fig.68. Another laser pulse passes a variable time delay and is reflected colinearly with the probe pulse into the UHV sample chamber. The two picosecond pulses so produced are impinging on a GaAs crystal.

According to Fig.82 the first pulse is used as an optical pump to populate the shortlived interface states by electrons from the valence band. Before these states decay, i.e. within the picosecond region,

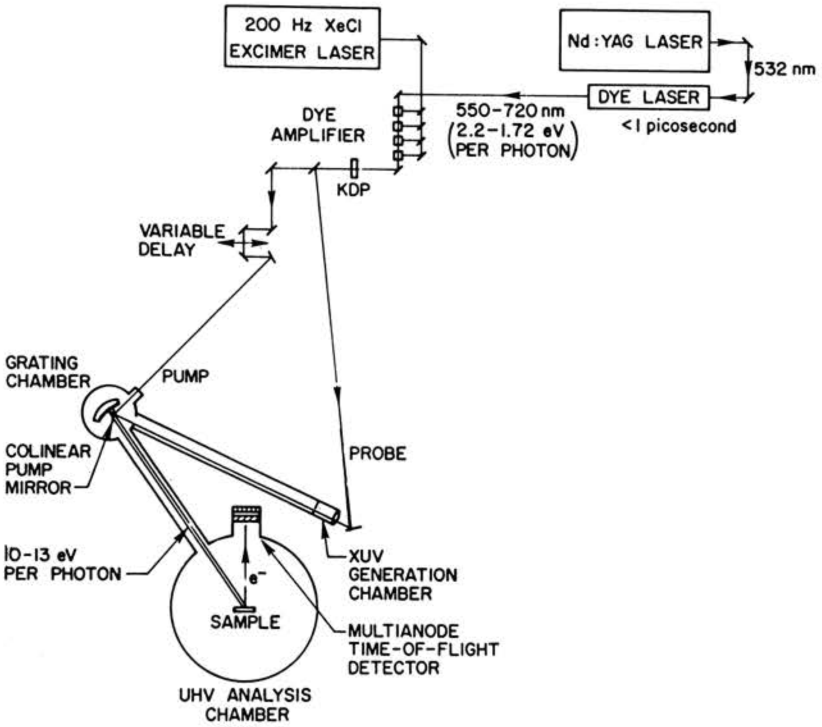

Fig. 81
Layout for a tunable picosecond laser system, yielding one 'pump' signal in the optical region and one 'probe' signal, after frequency tripling in a rare gas non linear medium. This signal is tunable up to an energy of 13 eV. This system offers the opportunities to study time resolved photoelectron spectra from laser excited interfaces and surfaces. System due to R. Haight et al.

they are ionized into the vacuum by the "probe" XUV pulses with energies up to 13 eV. This results in an electron spectrum which is recorded in a TOF arrangement which is capable of recording also the angular distribution. This and similar schemes are of considerable interest for the future to explore the region of shortlived interface states by means of tunable two-photon ionization.

The two-photon excited electron emission from semiconductors has been reviewed by J.M. Moison /107/.

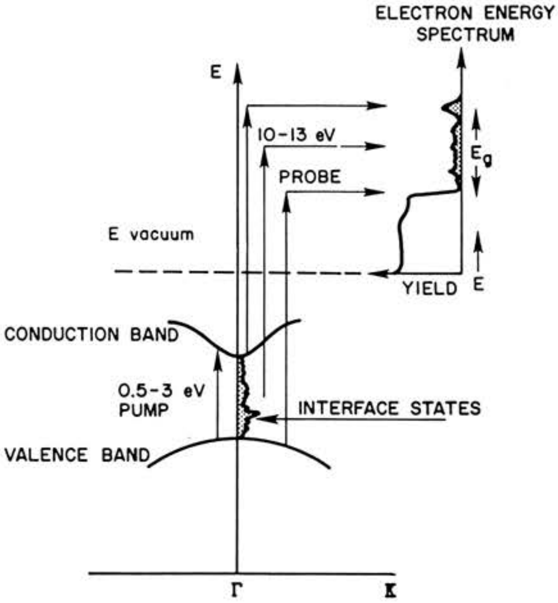

Fig. 82
Photoelectron spectroscopy of two-colour picosecond laser excited and ionized interface states (see Fig.81). The short arrow corresponds to optical transitions by the pump pulse. The longer arrows show the photoelectron transitions induced by the XUV probe.

13. Electron scattering spectroscopy

Electrons of a few keV energy as a primary source of excitation are mostly used to produce Auger electron spectra from surfaces. The scattered electron background is a dominating feature. Because of the very high intensity of electrons available from an electron gun the Auger line structures can be visualized thanks to the good statistics simply by differentiating the electron energy distribution once or twice. One advantage by using an electron beam for excitation is the fact that it can easily be focussed onto a small spot on the specimen and therefore it gives a very good lateral resolution. There are certain limitations encountered with this technique due to the radiation damage caused by the electron beam. For materials like metals etc. this circumstance is of minor importance, but for organic and other materials the situation is different. Gases again are not

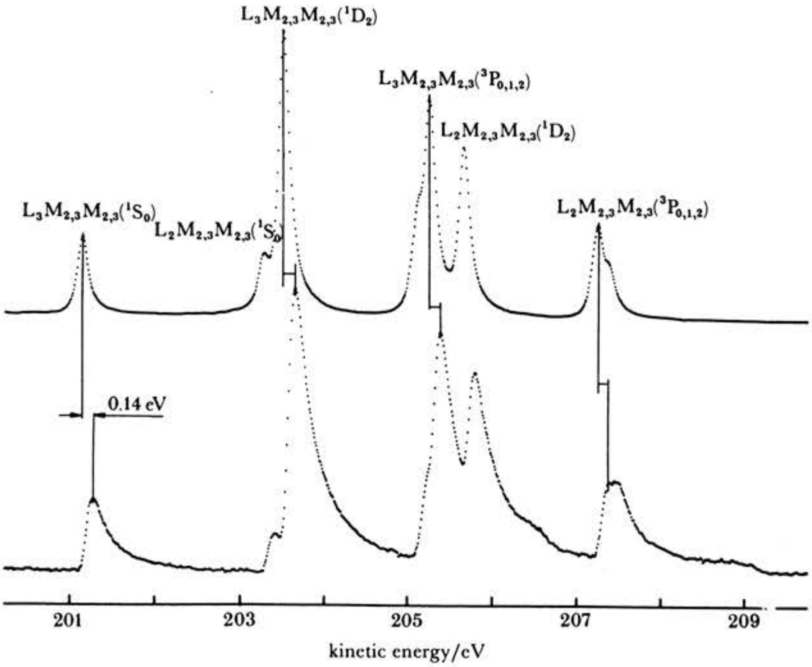

Fig. 83
Argon $L_{2,3}M_{2,3}M_{2,3}$ Auger electron spectrum, excited by electrons at two different excess energies (2750 eV for top spectrum and 30 eV for bottom) above threshold. The shifts and asymmetries of the lines are caused by the 'post-collision' interaction (PCI) effect.

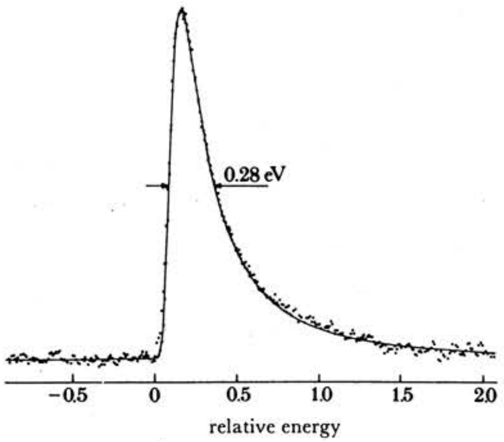

Fig. 84
Comparison between the experimentally obtained and a calculated line shape according to an assumed dynamics of the PCI effect on a time scale of femto-sec.

subject to this limitation and Auger and autoionization spectra from gaseous samples are therefore convenient to study /5/. In these cases the signal:background is quite good and no differentiation is necessary.

Fig.83 shows a highly resolved Auger electron spectrum for ArLMM transitions /108,109/. At sufficiently high resolution and with exciting energy just above the threshold for Auger electron emission one can notice typically asymmetric line profiles (Fig.84). This is due to 'post-collisional' effects during the electron emission. The phenomenon is now well understood in terms of an interaction between the two slow remaining electrons after the excitation of the shell in question. Under the above conditions this results in an expelled low energy electron from that shell. The primary electron loses most of its energy and the ejected fast Auger electron leaves the molecular ion which is screened by the two mentioned remaining slow electrons. Depending on the details of the dynamics one can calculate the time behaviour of the screening and this gives rise to the asymmetric line shape /110,111/. Conversely, the above study of the Auger electron line shape gives information about the dynamics on a time scale of $\sim 10^{-15}$ sec.

Chemical shift investigations of electron excited Auger electron spectra for free molecules are fairly scarce compared to those for solid materials. As was mentioned before a combination of such shift data from both the photoelectron and the Auger spectra provides the information to determine the relaxation energies. As an example /112/ Fig.85a shows the KLL Auger electron spectrum of SO_2 and Fig.85b the chemical shifts for the S $KL_{2,3}^2$ Auger lines and the S $2p_{1/2,3/2}$ photoelectron lines for a gas mixture of SF_6, SO_2 and COS. The Auger lines were excited by electrons, the photo lines by monochromatic AlKα radiation. Such spectra can be evaluated with high accuracy at good experimental conditions, by the use of efficient differential pumping, molecular gas beams or low pressure gas cells /113,114/.

Electron energy loss spectroscopy has developed into a very useful technique to record excited states of species irradiated by an electron monochromator. A recent comprehensive review of the applications

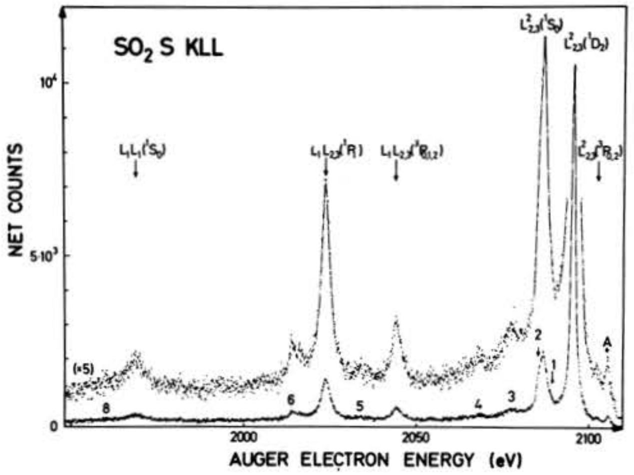

Fig. 85a

Sulphur KLL Auger electron spectrum of SO_2, excited by an electron beam (5 kV, 5 μA).

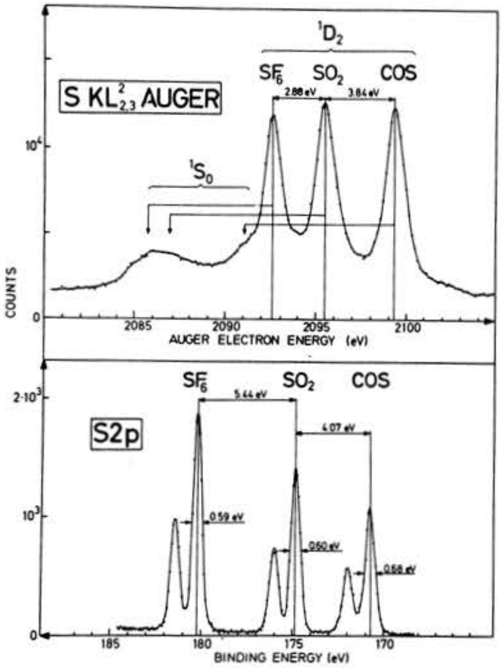

Fig. 85b

Auger electron lines, $SKL_{II}L_{III}(^1D_2)$ obtained from a gas mixture of SF_6, SO_2 and COS (top figure). For comparison the S2p photoelectron spectrum (AlKα, Δhν = 0.2 eV) is shown in the bottom figure. The chemical shifts are in this case larger for the photoelectron lines than for the Auger electron lines. In other cases it may be the opposite. Relaxation energies are extractable from such studies.

in surface science is given by G. Ertl and J. Küppers /115/. Low electron energy loss spectroscopy gives direct information on e.g. vibrational modes of surfaces and of adsorbates on substrates, in particular developed by H.Ibach and coworkers /116/. High resolution can be achieved by monochromatization to around 5-10 meV (HREES).

HREES is a frequently used alternative to IR or Raman spectroscopy for surfaces. It is interesting to note that more recently it has become possible to overcome the previous limitation in this techniqu to study surfaces of insulators, e.g. thick polymers or oxides. P.A. Thiry et al. /117/ found that if such a surface was simultaneously irradiated with unfocussed ~1 keV electrons the charging problem was elliminated and the electron loss spectra at specular reflection and at a primary electron beam energy around 6 eV approached the previou resolution for conductors. Fig.86 shows the loss spectrum for MgO(001 and Fig.87 for polyethylene. A comparison with the corresponding results from IR and Raman spectroscopy showed that not all the bands visible in HREES were excited in the optical modes due to selection rules. Otherwise the agreement was good.

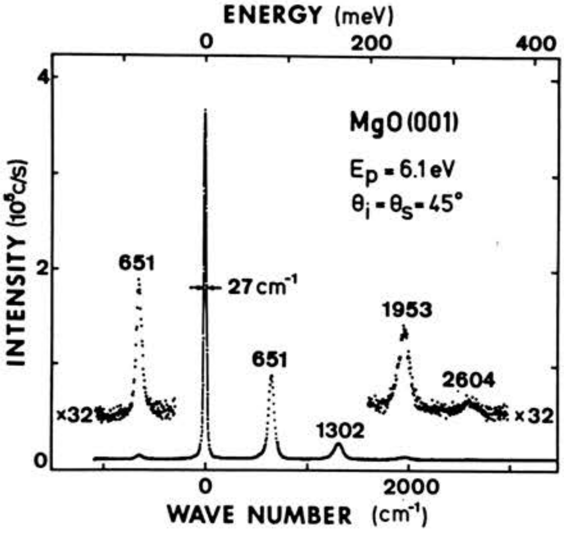

Fig. 86
Electron energy-loss spectrum (HREES) of 6.1 eV electrons after reflection on a MgO(001) surface (insulator). The charging problem has been eliminated by means of an auxiliary unfocussed electron flood gun at 2.8 keV and 1 µA.

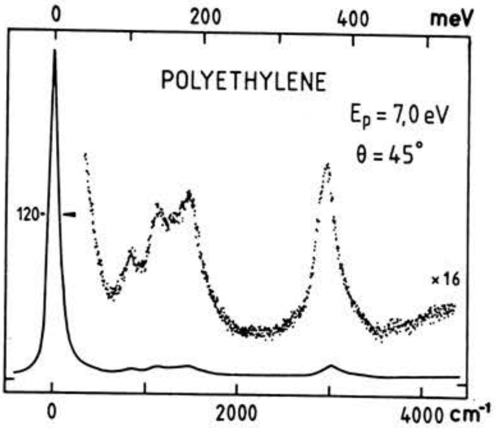

Fig. 87
Electron-loss spectrum (HREES) of a massive sample of the insulato polyethylene using an electron flood gun in the keV region.

Although HREES is normally used as a particularly surface sensitive technique it has more recently been found that at low electron ener <10 eV and at specular reflection, also interfaces in the important case of semiconductors can be reached. This is due to the long rang of the electric fields of the scattered electrons and the polarizati of the material. The resultant dipolar interaction excites or annihilates long wavelength optical phonons, called Fuchs-Kliever modes. By increasing the electron energies and using non-specular geometr the conditions favour instead short range scattering. This extensio of HREES towards the studies of interfaces of layered semiconductor compounds in a superlattice of GaAs-$Al_{0.3}Ga_{0.7}$, such as for optoelectronics devices, has been demonstrated by P.A. Thiry et al. /118/.

Another field of interest in the very low energy electron scattering region around 5 eV is VLEED fine structure. Such structures occur only at these low energies and disappear after showing up a few components. At the same time the lines decrease in linewidth according to a $1/n^3$ ratio which applies to the Rydberg series. The spectroscopic techniques to observe these phenomena requires high resolution (bett than 50 meV) and an angular resolution of $<0.5^{\circ}$. To describe this fine structure a model can be used where the electrons in the surfa region experience an image barrier potential. The barrier structure for metals are now understood but it remains to study the surface barriers for semiconductors and insulators with high resolution VLE techniques. This field has recently been reviewed by R.O. Jones and P.J. Jennings /119/.

When the beam from the electron monochromator traverses a gas follo by an electron analyzer (as in Fig.23) the molecular excitations car be recorded both in the valence region and in the core region. Fig.8 shows a typical electron impact energy loss spectrum in the valence region for H_2 /120/. The excitation energy in this case is 30 eV. This is a well recognized field for studying electron molecular int- actions which is under continuous development. Basic problems are e.g. related to accurate cross section measurements /121,122/.

Improved molecular beam methods and combinations with laser techniqu are promising pathways. With further increased spectral resolution one may hope to be able to resolve and investigate rotational and other fine structures and to discover resonance states etc.

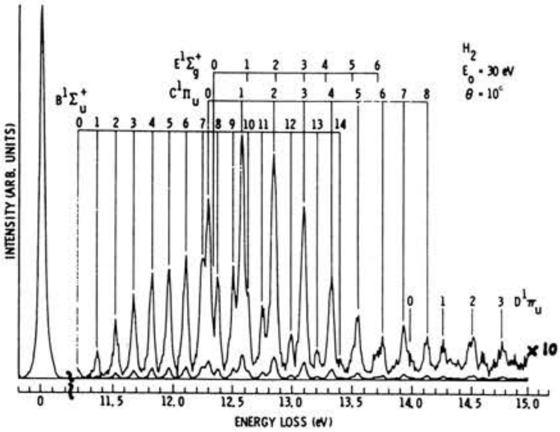

Fig. 88

Electron energy loss spectrum for H_2 gas. The strong singlet state excitations and the elastic peak are shown.

In the core region the energy loss spectroscopy corresponds to X-ray absorption spectroscopy and has developed during recent years to become an interesting complement to this. Fig.89 shows a typical example in the case of ammonia and the metyl amines around the absorption edges of N1s /123/. Fig.90 is a similar recording of the valence region, which concerns tetrametylsilane /124/.

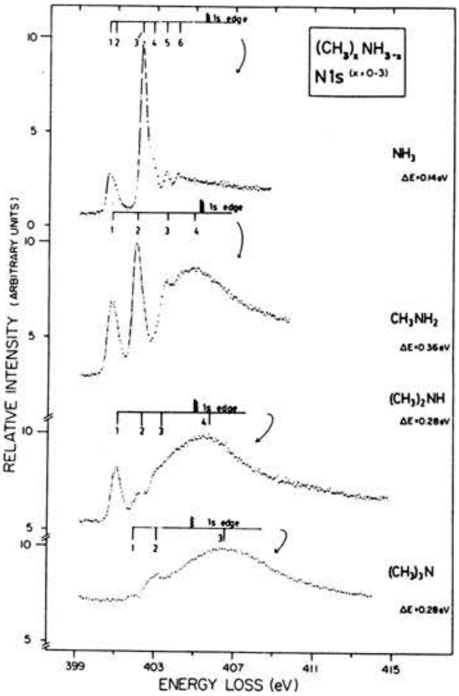

Fig. 89
Short range electron energy loss spectra of the N1s region of ammonia and the methyl amines.

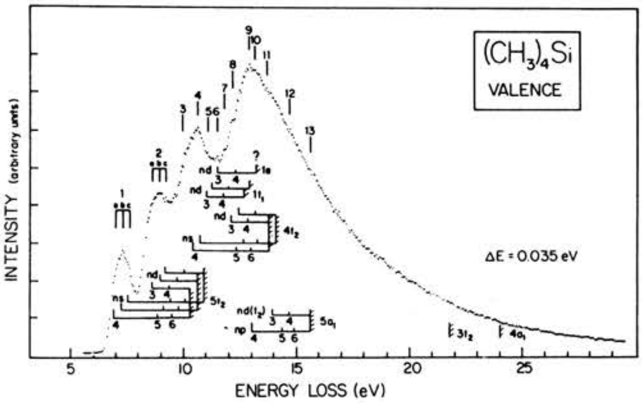

Fig. 90
Valence shell electron energy-loss spectrum of tetramethylsilane. Estimated positions of the first members of the Rydberg series are shown below the spectrum.

Extended absorption fine structures in X-ray absorption spectroscopy, EXAFS, has been a useful technique for geometrical structure information for several years thanks to the availability of tunable synchrotron beams. More recently, the possibilities to make use of electron beams for similar purposes as a complement to X-rays have been investigated in the electron reflexion mode.

Fig.91 is an overview of the various parts which can be distinguished in a scattered electron spectrum from a surface with the primary electron energy E_p. Close to the elastically scattered electrons forming the E_p peak one finds the mentioned EELS spectrum, containing e.g. vibrational information etc. Next structure, EELFS, is the region of core electron excitation and ionization with its fine structure which is the equivalent to the X-ray absorption edge and its near and extended fine structures, XANES and EXAFS (there are also other alternative acronyms for those structures).

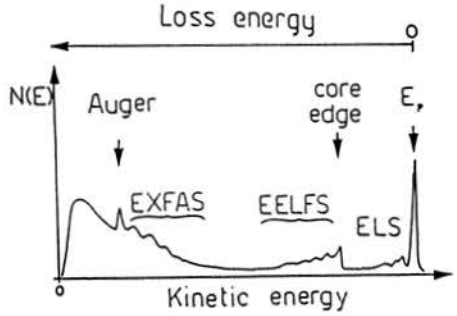

Fig. 91
Energy distribution of electrons scattered from a sample with primary electrons E_p.

A more recent interest is concerned with the fine structures in the neighbourhood of Auger lines, denoted by J. Derrien et al. /125,126/ by EXFAS, (extended fine structure of the Auger spectral lines). Also from this structure one can extract geometrical information similar to EXAFS and EELFS. Figs.92 and 93 exemplify these findings. Fig.92 shows the Cr Auger spectrum containing the LVV, LMM and MVV (V are valence levels) Auger transitions. The lower part of the figure is a magnified part of the MVV Auger spectrum in which one observes several extended Auger fine structure components (EXFAS).

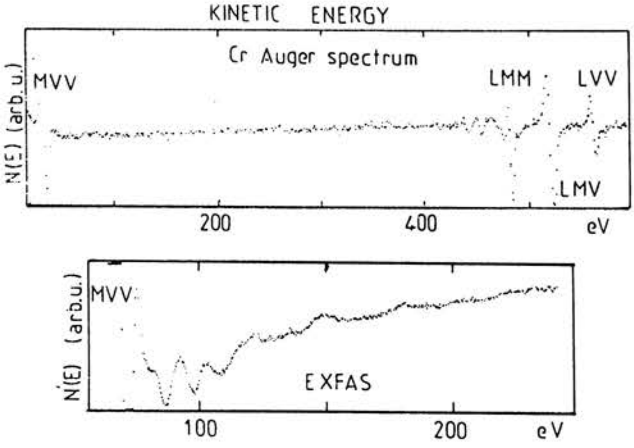

Fig. 92
Auger electron spectrum of a clean Cr film (upper figure). Magnification of the MVV Auger electron line region shows several extended fine Auger electron structures (lower figure).

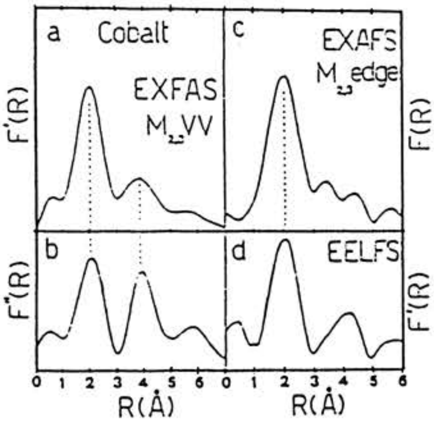

Fig. 93
Fourier transforms of EXFAS recorded on cobolt above the $M_{2,3}VV$ transition detected in both the first-derivative (a) and second-derivative mode (b). The EXAFS Fourier transform of the same edge is shown in (c) and the EELFS in (d). All three techniques (EXFAS, EXAFS and EELFS) give the same nearest-neighbour distance.

Fig.93 demonstrates the close relationship between EXFAS, EXAFS and EELFS. It shows the Fourier transforms of the $M_{2,3}VV$ transition in cobolt (first and second derivatives) for EXFAS, EXAFS (the M_{23} edge) and EELFS. All three techniques yield the same nearest-neighbour distances. The connection between the various fine structures and their appropriate evaluations in terms of near neighbour distances are discussed by G. Ertl and J. Küppers in their above mentioned book on low energy electrons and surface chemistry /115/.

The "appearance potential" techniques (APS) is complementary to the just mentioned ones to get geometrical distances. One can either record the changes in soft X-ray emission SXAPS or the changes (disappearance) of the elastically reflected electrons (DAPS).

Another possibility is to record the appearance of Auger electrons (AEAPS). Extended fine structures have been observed in SXAPS but due to the low fluorescence yield of X-rays AEAPS and DAPS are somewhat more efficient.

Electron scattering spectroscopy is an interesting and powerful alternative which supplements other approaches which are presently being made by means of synchrotron radiation, e.g. XANES and EXAFS etc. It also offers great potentialities for surface studies, complementary to optical methods.

14. References

1. M. Siegbahn: Spektroskopie der Röntgenstrahlen, Springer, Berlin 1931.

2. K. Siegbahn: Beta- and Gamma-Ray Spectroscopy, North Holl. Publ. Co, Amsterdam 1955; Alpha-, Beta and Gamma-Ray Spectroscopy, North Holl. Publ. Co, Amsterdam 1965.

3. H . Robinson, Phil. Mag. 50, 241, 1925.

4. K. Siegbahn, C. Nordling, A. Fahlman, R. Nordberg, K. Hamrin, J. Hedman, G. Johansson, T. Bergmark, S.-E. Karlsson, I. Lindgren, B. Lindberg: ESCA, Atomic, Molecular and Solid State Structure Studied by Means of Electron Spectroscopy. Nova Acta Regiae Societatis Scientiarum Upsaliensis, Uppsala 1967.

5. K. Siegbahn, C. Nordling, G. Johansson, J. Hedman, P.F. Hedén, K. Hamrin, U. Gelius, T. Bergmark, L.O. Werme, R. Manne, Y. Baer: ESCA Applied to Free Molecules, North Holland Publ. Co., Amsterdam 1971.

6. J.G. Jenkin, R.C. Leekey and J. Liesegang, J. Electron Spectr. Rel. Phen. 12, 1, 1977.

7. T.A. Carlson (ed.): Benchmark Papers in Phys. Chem. and Chem. Phys. 2, Dowden, Hutchinson and Ross 1978.

8. H. Siegbahn and L. Karlsson: Photoelectron Spectroscopy, Handbuch der Physik XXXI, W. Mehlhorn (ed.), Springer, Berlin Heidelberg 1982.

9. K. Siegbahn, Les Prix Nobel, Stockholm, 1981; Rev. Mod. Phys. 54, 709; Science 217, 111, 1982.

10. R. Maripuu, Thesis, Acta Universitatis Upsaliensis no. 696, 1983.

11. T.D. Bussing, P.H. Holloway, Y.X. Wang, J.F. Moulder and J.S. Hammond, J. Vacuum Science and Techn. B6, no. 5, 1514, 1988.

12. U. Gelius, L. Asplund, E. Basilier, S. Hedman, K. Helenelund and K. Siegbahn, Nucl. Instr. and Meth. B1, 85, 1983.

13. K. Siegbahn: Electron Spectroscopy - An Outlook, J. Electron Spectr. Rel. Phen. 5, 3, 1974.

14. M. Kelley, SSI, (private communication) 1988.

15. K. Siegbahn: Some Current Problems in Electron Spectroscopy and references therein, Atomic Physics 8 (ed. I. Lindgren, A. Rosén and S. Svanberg), Plenum Press, 1983.

16. E.F. Ritz Jr., Recent Advances in Electron Beam Deflection, Advances in Electronics and Electron Physics 49, 299, 1979.

17. U. Boesl, Habilitationsschrift: "Resonante Laseranregung und Massenspektrometrie", Technischen Universität München, Garching, 1987.

18. F.C. Tang, X. Zhang, F.B. Dunning and G.K. Walters, Rev. Sci. Instr. 59, 504, 1988.

19. A. Nilsson, N. Mårtensson, J. Hedman, B. Eriksson, R. Bergman and U. Gelius, Proc. of ECOSS-7, Surf. Sci. 1985.

20. N. Mårtensson, Thesis, Uppsala 1980.

21. B. Johansson and N. Mårtensson, Phys. Rev. B21, 4427, 1980.

22. J.S. Jen and T.D. Thomas, Phys. Rev. B13, 5284, 1976.

23. J.Q. Broughton and D.C. Perry, J. Electron Spectr. Rel. Phen. 16, 45, 1979.

24. R. Nyholm, Thesis, Uppsala 1980.

25. P. Steiner, S. Hüfner, N. Mårtensson and B. Johansson, Solid State Commun. 37, 73, 1981.

26. N. Mårtensson, B. Reihl and O. Vogt, Phys. Rev. 25, 824, 1982.

27. N. Mårtensson, A. Stenborg, O. Björneholm, A. Nilsson and J.N. Andersen, Phys. Rev. Lett. 60, 1731, 1988.

28. A. Nilsson and N. Mårtensson, Solid State Comm. in press.

29. J.R. Waldrop, S.P. Kovalczyk and R.W. Grant, J. Vac. Sci. Technol. 21, 607, 1982.

30. R.S. Bauer, Phys. Rev. Lett. 43, 663, 1983.

31. G. Margaritondo, Surf. Sci. 132, 469, 1983.

32. R. Purtell, G. Hollinger, G.W. Rubloff and P.S. Ho, J. Vac. Sci. Technol. A1, 566, 1983.

33. U. Gelius, K. Helenelund, L. Asplund, S. Hedman, P.A. Tove, K. Magnusson and I.P. Jain, Inst. of Physics Rep. UUIP-1101, 1984.

34. B. Lindberg, R. Maripuu, K. Siegbahn, R. Larsson, C.G. Gölander and J.C. Eriksson, Inst. of Phys. Rep. UUIP-1066, 1982.

35. N. Larsson, P. Steiner, J.C. Eriksson, R. Maripuu and B. Lindberg, J. Colloid Interface Sci. 75, 1982.

36. W.F. Egelhoff Jr., Core-Level Binding-Energy Shifts at Surfaces and in Solids, Surface Science Reports 6, no. 6-8, 1987.

37. K. Siegbahn, Electron Spectroscopy for Solids, Surfaces, Liquids and Free Molecules, Ch. 15 in Molecular Spectroscopy (ed. A.R. West), Heyden and Son Ltd., London 1977.

38. S. Svensson, B. Eriksson, N. Mårtensson, G. Wendin and U. Gelius, J. Electron Spectr. Rel. Phen. 47, 327, 1988.

39. G.V. Hansson and R.I.G. Uhrberg, Proc. 8th Int. COnf. on Vac. UV Rad. Phys., Physica Scripta T17, 1987.

40. G.V. Hansson and R.I.G. Uhrberg, Photoelectron Spectroscopy of Surface States on Semiconductor Surfaces, Surface Science Reports 9, no. 5-6, 1988.

41. D.E. Eastman and Y. Farge (ed.), Handbook on Synchrotron Radiation, North Holl. Publ. Co., Amsterdam 1983 and further on.

42. H. Winnik and S: Doniach, Synchrotron Radiation Research, Plenum Press, New York, 1980.

43. N. Mårtensson, R. Nyholm, H. Calén, J. Hedman, Phys. Rev. B24, 1725, 1981.

44. J. Verbist, J. Riga, J.J. Pireaux and R. Caudano, J. Electron Spectr. 5, 193, 1974.

45. V. Dose, Momentum-Resolved Inverse Photoemission, Surface Science Reports 5, no. 8, 1986.

46. F.J. Himpsel in Semiconductor Interfaces: Formation and Properties (ed. G. LeLay, J. Derrien and N. Boccara), 196, Springer, Berlin-Heidelberg, 1989.

47. D.W. Turner, C. Baker, A.D. Baker and C.R. Brundle, Molecular Photoelectron Spectroscopy, Wiley-Interscience, London, 1970.

48. K. Siegbahn, Perspectives and Problems in Electron Spectroscopy, Proc. of Asilomar Conf., 1971 (ed. D.A. Shirley), North Holl. Publ. Co, Amsterdam 1972.

49. L.O. Werme, B. Grennberg, J. Nordgren, C. Nordling and K. Siegbahn, Phys. Rev. Lett. 30, 523, 1973; Nature 242, 453, 1973.

50. J. Nordgren, L. Selander, L. Pettersson, C. Nordling, K. Siegbahn and H. Ågren, J. Chem. Phys. 76, no. 8, 3928, 1982.

51. J. Nordgren, J. de Physique 48, Colloque C9, suppl. 12, 1987

52. J.-E. Rubensson, N. Wassdahl, R. Brammer and J. Nordgren, J. Electron Spectr. Rel. Phen. 47, 131, 1988.

53. H. Veenhuizen, B. Wannberg, L. Mattsson, K.-E. Norell, C. Nohre, L. Karlsson adn K. Siegbahn, UUIP-1107, Inst. of Phys. Reports 1984.

54. K.-E. Norell, B. Wannberg, H. Veenhuizen, C. Nohre, L. Karlsson, L. Mattsson and K. Siegbahn, UUIP-1109, Inst. of Phys. Reports 1984.

55. B. Wannberg, H. Veenhuizen, K.-E. Norell, L. Karlsson, L. Mattsson and K. Siegbahn, UUIP-1110, Inst. of Phys. Reports, 1984.

56. U. Heinzmann, Physica Scripta T17, 77, 1987.

57. G. Schönhense, Appl. Phys. A41, 39, 1986.

58. K. Siegbahn, U. Gelius, H. Siegbahn and E. Olson, Phys. Lett. A32, 221, 1970; Physica Scripta 1, 272, 1970.

59. C.S. Fadley: Angle-Resolved X-ray Photoelectron Spectroscopy, Progress in Surface Science 16, no. 3, 275, 1984.

60. C.S. Fadley, Physica Scripta T17, 39, 1987.

61. W.F. Egelhoff Jr., Phys. Rev. B30, 1052, 1984; J. Vac. Sci. Technol. A2, 350, 1984.

62. H.C. Poon and S.Y. Tong, Phys. Rev. B30, 6211, 1984.

63. W.F. Egelhoff Jr., J. Vac. Technol. A4, 758, 1986.

64. W.F. Egelhoff Jr., Vac. Technol. A6, no. 3, 730, 1988.

65. R.C. White, C.S. Fadley and R. Trehan, J. Electron Spectr. 41, 95, 1986.

66. E.L. Bullock and C.S. Fadley, Phys. Rev. B31, 1212, 1985.

67. B. Sinkovic and C.S. Fadley, Phys. Rev. B31, no. 7, 4665, 1985; J. Vac. Sci. Technol. A4, no. 3, 1477, 1986.

68. J.J. Barton, S.W. Robey and D.A. Shirley, Phys. Rev. B34, 778, 1986.

69. C.C. Bahr, J.J. Barton, Z. Hussain, S.W. Robey, J.G. Tobin and D.A. Shirley, Phys. Rev. B35, 3773, 1987.

70. D.P. Woodruff, C.F. McConville, A.L.D. Kilcoyne; Th. Lindner, J. Somers, M. Surman, G. Paolucci and A.M. Bradshaw, Surface Science 201, 228, 1988.

71. Th. Lindner, J. Somers, A.M. Bradshaw, A.L.D. Kilcoyne and D.P. Woodruff, Surface Science 203, 333, 1988.

72. H. Siegbahn and K. Siegbahn, J. Electron Spectr. 2, 319, 1973.

73. H. Siegbahn, L. Asplund, P. Kelfve, K. Hamrin, L. Karlsson and K. Siegbahn, J. Electron Spectr. 5, 1059, 1974; Ibid, 7, 411, 1975.

74. H. Siegbahn, J. Phys. Chem. 89, 897, 1985.

75. H. Siegbahn, S. Svensson and M. Lundholm, J. Electron Spectr. 24, 205, 1981.

76. H. Siegbahn, M. Lundholm, S. Holmberg and M. Arbman, Physica Scripta 27, 431, 1983.

77. H. Siegbahn, M. Lundholm, S. Holmberg and M. Arbman, Chem. Phys. Lett. 110, no. 4, 425, 1984.

78. M. Arbman, H. Siegbahn, L. Pettersson and P. Siegbahn, Mol. Physics 54, no. 5, 1149, 1985.

79. M. Lundholm, H. Siegbahn, S. Holmberg and M. Arbman, J. Electron Spectr. 40, 165, 1986.

80. W. Keller, H. Morgner and W.A. Müller, XIV Int. Conf. on the Physics of Electronic and Atomic Collisions, 605, 1985 (eds. D.C. Lorents, W. Mayerhof and J. Petterson), North Holl. Co., Amsterdam, 1986.

81. S. Holmberg, R. Moberg, Zhong Cai Yuan and H. Siegbahn, J. Electron Spectr. 41, 337, 1986.

82. R. Hilbig, G. Hilber and R. Wallenstein, Applied Physics B41, 225, 1986.

83. T.Huth, A. Mank, N. Böwering, G. Schönhense, R. Wallenstein and U. Heinzmann, personal communication.

84. T.P. Softly, W.E. Ernst, L.M. Tashiro and R.N. Zare, Chem. Phys. 116, 299, 1987.

85. K. Kimura: Molecular Dynamic Photoelectron Spectroscopy using Resonant Multiphoton Ionization for Photophysics and Photochemistry, International Reviews in Physical Chemistry, 1986.

86. R.N. Compton and J.C. Miller: Multiphoton Ionization Photoelectron Spectroscopy, Oak Ridge, Tennessee, 1986.

87. S.L. Anderson, D.M. Rider and R.N. Zare, Chem. Phys. Letters 93, no. 1, 11, 1982.

88. I. Reineck, C. Nohre, R. Maripuu, P. Lodin, K.E. Norell, H. Veenhuizen, L. Karlsson and K. Siegbahn, UUIP-1084, Uppsala Inst. Phys. Reports, 1983.

89. Y. Nagano, Y. Achiba and K. Kimura, J. Chem. Phys. 84, no. 3, 1063, 1986.

90. P. Kruit and F.H. Read, J. Phys. E16, 313, 1983.

91. B.G. Koenders, G.J. Kuik, Karel E. Drabe and C.A. de Lange, Chem. Phys. Lett. 147, no.4, 310, 1988.

92. K. Müller-Dethlefs, M. Sander and E.W. Schlag, Z. Naturforsch. 39a, 1089, 1984.

93. L.A. Chewter, M. Sander, K. Müller-Dethlefs and E.W. Schlag, J. Chem. Phys. 86, no 9, 4737, 1987.

94. M. Sander, L.A. Chewter, K. Müller-Dethlefs and E.W. Schlag, Phys. Rev. A36, no. 9, 4543, 1987.

95. R. Weinkauf, K. Walter, U. Boesl, E.W. Schlag, Chem. Phys. Lett. 141, 267, 1987.

96. K. Walter, R. Weinkauf, U. Boesl and E.W. Schlag, personal communication.

97. O. Chesknovsky, S.H. Yang, C.L. Pettiette, M.J. Craycraft, Y. Liu and R.E. Smalley, Chem. Phys. Lett. B8, nr. 23, 119, 1987.

98. J.V. Coe, J.T. Snodgrass, C.B. Freidhoff, K.M. McHugh and K.H. Bowen, J. Chem. Phys. 87 (8), 4302, 1987.

99. D.A. Gobeli, J.J. Yang and M.A. El-Sayed, Chem. Rev. 85, 529, 1985.

100. J. Grotemeyer and E.W. Schlag, Angew. Chemie 27, no. 4, 447, 1988.

101. Liang Li and D.M. Lubman, Rev. Sci. Instr. 59, 557, 1988.

102. Mo Yang and J.P. Reilly, Anal. Instr. 16, 133, 1987.

103. J.M. Bizau, F. Wuilleumier, D.L. Ederer, J.C. Keller, J.L. LeGouit, J.L. Picqué, B. Carré and P.M. Koch, Phys. Rev. Lett. 55, 1281, 1985.

104. J.M. Bizau, D. Cubaynes, P. Gerard, F.J. Wuilleimier, J.L. Picqué, D.L. Ederer, B. Carré and G. Wendin, Phys. Rev. Lett. 57, no. 3, 306, 1986.

105. M. Ferray, F. G^unand, P. D'Oliveira, P.R. Fournier, D. Cubaynes, J.M. Bizau, T.J. Morgan and F.J. Wuilleumier, Phys. Rev. Lett. 59, no. 18, 2040, 1987.

106. R. Haight, J.A. Silberman and M.I. Lilie, Rev. Sci. Instr. 59, no. 9, 1941, 1971.

107. J.M. Moison, Semiconductor Interfaces: Formation and Properties (ed. G. LeLay, J. Derrien and N. Boccara), Proc. in Physics 22, Springer, Berlin-Heidelberg, 1987.

108. K. Helenelund, S. Hedman, L. Asplund, U. Gelius and K. Siegbahn, Physica Scripta 27, 245, 1983.

109. K. Helenelund, Thesis, Acta Universitatis Upsaliensis no. 757, 1984.

110. W. Sandner, J. Phys. B, At. Mol. Phys. 19, L863, 1986.

111. R. Huster, W. Sandner and W. Mehlhorn, J. Phys. B, At. Mol. Phys. 20, L, 1987.

112. L. Asplund, P. Kelfve, B. Blomster, H . Siegbahn, K. Siegbahn, R.L. Lozes and U.I. Wahlgren, Physica Scripta 16, 273, 1977.

113. L. Asplund, Thesis, Acta Universitatis Upsaliensis no 479, 1977

114. P. Kelfve, Thesis, Acta Universitatis Upsaliensis no 483, 1978

115. G. Ertl and J. Küppers, Low Energy Electrons and Surface Chemistry, VCH Verlagsgesellschaft, Weinheim, 1985.

116. H. Ibach and D.L. Mills, Electron Energy Loss Spectroscopy and Surface Vibrations, Academic Press, New York, 1982.

117. P.A. Thiry, J.J. Pireaux, M. Leihr and R. Caudano, J. Physique 47, 103, 1986.

118. P.A. Thiry, M. Liehr, J.J. Pireaux and R. Caudano, Ph. Lambin, J.P. Vigneon, A.A. Lucas and T. Kuech, J. Vac. Sci. Technol. B4, no.4, 1028, 1986.

119. R.O. Jones and P.J. Jennings, Surface Science Rep. 9, 165, 1988.

120. S. Trajmar, XIV Int. Conf. on the Phys. of Electronic and Atomic Collision, 77, 1985 (ed. D.C. Lorents, W.E. Meyerhof and J.R. Petersson), North Holland, Amsterdam, 1986.

121. E.N. Lassettre and A. Skerbele, Methods of Experimental Physics 3, 868, 1974.

122. E.N. Lassettre, Chem. Spectr. and Photochem. in the Vac. Ultr. Viol., 43, (ed. C. Sandorfy, P.J. Ansloos and M.B. Robin, Reidel Publ. Co., Boston, 1974.

123. R.N.S. Sodhi and C.E. Brion, J. Electr. Spectr. 36, 187, 1985.

124. R.N.S. Sodhi, S. Daviel, C.E. Brion and G.G.B. de Souza, J. Electr. Spectr. 35, 45, 1985.

125. J. Derrien, E. Chaînet, M. de Crescenzi and C. Noguera, Surface Science 189/190, 590, 1987.

126. J. Derrien, Semiconductor Interfaces: Formation and Properties (ed. G. LeLay, J. Derrien and N. Boccara), 102, Springer, Berlin-Heidelberg, 1987.